DESIGN AND DEVELOPMENT OF WIRELESS ACOUSTIC EMISSION SENSOR SYSTEM FOR STRUCTURAL HEALTH MONITORING APPLICATIONS

By

CHANDAN KUMAR BHAGAT
(Enrollment No: ENGG02201204005)

Indira Gandhi Centre for Atomic Research, Kalpakkam

A thesis submitted to the
Board of Studies in Engineering Sciences

In partial fulfillment of requirements
for the Degree of

DOCTOR OF PHILOSOPHY

of

HOMI BHABHA NATIONAL INSTITUTE

June, 2020

Homi Bhabha National Institute

Recommendations of the Viva Voce Committee

As members of the Viva Voce Board, we certify that we have read the dissertation prepared by **Chandan Kumar Bhagat** entitled **"Design and development of wireless acoustic emission sensor system for structural health monitoring applications"** and recommend that it may be accepted as fulfilling the dissertation requirement for the Degree of Doctor of Philosophy.

Chairman - **Dr. B. K. Panigrahi**	**Date:** 12/06/20
Guide / Convener – **Dr. C. K. Mukhopadhyay**	**Date:** 12/06/2020
Co-Guide - **Dr. B. P. C. Rao**	**Date:** 12/6/2020
Member 1 - **Dr. K. Velusamy**	**Date:**
Member 2- **Dr. V. S. Srinivasan**	**Date:**
External Examiner- **Dr. Seshan Srirangarajan**	**Date:** 12/06/2020

Final approval and acceptance of this dissertation is contingent upon the candidate's submission of the final copies of the dissertation to HBNI.

I hereby certify that I have read this dissertation prepared under my direction and recommend that it may be accepted as fulfilling the dissertation requirement.

Date: 12/06/2020

Place: Kalpakkam

(Dr. C. K. Mukhopadhyay)
Guide / Convener

STATEMENT BY AUTHOR

This dissertation has been submitted in partial fulfilment of requirements for an advanced degree at Homi Bhabha National Institute (HBNI) and is deposited in the library to be made available to borrowers under rules of the HBNI.

Brief quotations from this dissertation are allowable without special permission, provided that accurate acknowledgement of source is made. Requests for permission for extended quotation from or reproduction of this manuscript in whole or in part may be granted by the competent authority of HBNI when in his or her judgment the proposed use of the material is in the interests of scholarship. In all other instances, however, permission must be obtained from the author.

Chandan Kumar Bhagat

Date: 12/06/2020

Place: Kalpakkam

(CHANDAN KUMAR BHAGAT)

DECLARATION

I, hereby declare that the investigation presented in the thesis entitled **“Design and development of wireless acoustic emission sensor system for structural health monitoring applications”** submitted to Homi Bhabha National Institute (HBNI), Mumbai, India, for the award of **Doctor of Philosophy in Engineering Sciences**, is the record of work carried out by me under the guidance of **Dr. C. K. Mukhopadhyay**, Professor, HBNI and former Head, Non Destructive Evaluation Division, Metallurgy and Materials Group, Indira Gandhi Centre for Atomic Research, Kalpakkam. The work is original and has not been submitted earlier as a whole or in part for a degree / diploma at this or any other Institution/University.

Chandan Kumar Bhagat

Date: 12/06/2020

Place: Kalpakkam

(CHANDAN KUMAR BHAGAT)

LIST OF PUBLICATIONS ARISING FROM THE THESIS

Journal

a) Published

1. **Chandan K. Bhagat**, Nilangshu K. Das, C. K. Mukhopadhyay and B. Purna Chandra Rao, "Hardware-based parameter extraction of acoustic emission burst signal for structural health monitoring applications", IETE Journal of Research, Vol. 65, pp. 157-163, May 2018. https://doi.org/10.1080/03772063.2017.1417753.
2. **Chandan K. Bhagat**, C. K. Mukhopadhyay and B. Purna Chandra Rao, "Design and development of signal conditioning unit for acquisition of acoustic emission signal for metallic materials", Transactions of the Indian Institute of Metals, Vol. 71, pp. 1913-1918, August 2018. https://doi.org/10.1007/s12666-018-1326-8.

b) Under Review

1. **Chandan K. Bhagat**, C. K. Mukhopadhyay and B. Purna Chandra Rao, "Design and development of wireless acoustic emission sensor system for structural health monitoring of concrete", Journal of IETE Technical Review.
2. **Chandan K. Bhagat** and C. K. Mukhopadhyay, "Design development and validation of data acquisition for acoustic emission signals using programmable system on chip", IET Science, Measurement & Technology.

Conferences

1. **Chandan K. Bhagat**, Nilangshu K. Das, C. K. Mukhopadhyay and B. Purna Chandra Rao, "Acoustic emission signal conditioning and analysis using digital storage oscilloscope", IEEE Conference Proceedings (ICCES), pp. 1–4, 2016. DOI:10.1109/CESYS.2016.7889941.
2. **Chandan K. Bhagat,** C. K. Mukhopadhyay and B. Purna Chandra Rao, "Design scheme of wireless acoustic emission sensor system", National Conference on Condition Monitoring (NCCM-2017), October 26-27, 2017, Kalpakkam, India.
3. **Chandan K. Bhagat,** C. K. Mukhopadhyay and B. Purna Chandra Rao, "Parameter analysis of acoustic emission signals for characterizing damage and crack growth in concrete", Conference & Exhibition on Non-destructive Evaluation (NDE-2017), December 14-16, 2017, Chennai.
4. **Chandan K. Bhagat** and C. K. Mukhopadhyay, "Parameter analysis of acoustic emission signals for characterizing corrosion damage in concrete", Second International Conference on Structural Integrity (ICONS), December 14-17, 2018, Chennai.

Chandan Kumar Bhagat

(CHANDAN KUMAR BHAGAT)

DEDICATIONS

TO MY FAMILY MEMBERS AND MENTORS

ACKNOWLEDGEMENT

This thesis would not have been possible without the support and encouragement of many people who contributed and extended their valuable co-operation for the completion of the research work. I fell short of words in expressing my appreciation for their help at various stages of this work.

First and foremost, I would like to express my sincere gratitude to my guide **Dr. C. K. Mukhopadhyay**, Professor, HBNI and former Head, Non Destructive Evaluation Division (NDED), Metallurgy and Materials Group (MMG), Indira Gandhi Centre for Atomic Research (IGCAR), Kalpakkam for his continuous support, encouragement, enthusiasm and immense knowledge. His intellectual ideas and guidance helped me in my research work and writing this thesis. He has always been a source of motivation for me in difficult times during the research work. I express my deep sense of appreciation for his support and for energizing me to overcome all the hurdles.

I am thankful to my doctoral committee members **Dr. B. K. Panigrahi** (Chairman), **Dr. B. P. C. Rao** (Co-Guide), **Dr. K. Velusamy** (Member) and **Dr. V. S. Srinivasan** (Member) for their encouragement, insightful comments and suggestions. I thank all the **Professors of HBNI** who taught me various subjects during my course work.

I express my sincere gratitude to **Dr. A. K. Bhaduri**, Director, IGCAR and **Dr. G. Amarendra**, former Director, MMG, IGCAR, for their inspiration and encouragement. I express sincere gratitude to **Dr. Shaju K. Albert**, Director, MMG, IGCAR for inspiration and encouragement. Furthermore, I sincerely thank the **Department of Atomic Energy** (DAE), India, for providing the necessary financial support. I would like to thank **Dr. M. Saibaba** (former Dean, Student Affairs), **Dr. Lakshmi Narasimhan** (Dean, Student Affairs), **Dr. G. Sasikala** (former Dean, Engineering Sciences), **Dr. Anish Kumar** (Dean, Engineering Sciences) and authorities of **GSO, Kalpakkam** for providing a pleasant accommodation in the enclave.

I would like to express my sincere gratitude to **Dr. N. K. Das** (former Scientific Officer, NDED, IGCAR) for his help and support. I would like to express my gratitude to **Mr. T. K. Haneef,** NDED, IGCAR, for help in carrying out the experimental work. I am grateful to **Dr. S. Thirunavukkarasu**, NDED, IGCAR, for his invaluable inputs, constant encouragement and support in preparing this thesis.

I express my gratitude to IGCAR colleagues, especially, **Mr. V. Arjun, Dr. B. Sasi**, **Dr. W. Sharatchandra Singh**, **Dr. T. Saravanan** and **Dr. G. K. Sharma**, for their support and help in carrying out the experiments. I thank my colleagues **Dr. Varun Hasija**, **Mr. Manoj Kumar Parida**, **Dr. Vikas Kumar**, **Mr. Shivang Triphati**, **Mr. T. S. Nidhin**, **Dr. Anil Kumar Soni**, **Dr. S. Shuaib Ahmed**, **Dr. Sambasiva Rao Kambala**, **Mr. Santosh Kumar**, **Mr. K. Thirukkumaran, Dr. K. Prajna**, **Ms. Vijayachandrika**, **Ms. Sumana** and other NDED members and Research scholars for their suggestions and moral support.

Apart from the intellectual support, emotional support is always needed to conquer the hardship. For this, I would like to thank, from the bottom of my heart, **Mr. A. Viswanath, Mr. G. V. K. Kishore**, **Mr. G. M. S. K. Chaitanya**, **Mr. Manoj Kumar Raja**, **Mr. M.**

M. Narayanan, **Mr. A. Ravi Gopal**, **Mr. S. Ponseenivasan** and **Ms. S. Sosamma** for their help and support.

I thank **all the members of Enclave cricket and badminton team** for the funny, entertaining and exciting moments we shared during cricket and badminton matches. I would also like to express my heartfelt thanks to the **Mess Cook**, **Hostel in charge**, and especially **cleaning staff** for making the stay at the enclave very pleasant and lovely one.

Finally, I would like to express my heartfelt gratitude to most important persons in my life that is my beloved parents **Mr. Mahendra Kumar Bhagat** and **Ms. Kunti Devi** along with my father-in-law **Mr. Ramjee Bhagat** and mother-in-law **Ms. Anita Devi** who have been so caring and supportive of me all the time. I would like to thank and share this achievement with my beloved wife **Ms. Kumari Rashmi**, who has always been with me creating a cheerful world filled with love, affection, and support.

Above all, I thank the **Almighty,** for granting me wisdom, health and strength to undertake this research work and enabling me to take it to completion. He is the one who knows all the hardships, all my hard works and he is the one whose satisfaction and acceptance I seek the most.

Chandan Kumar Bhagat

(CHANDAN KUMAR BHAGAT)

Table of Contents

Abstract i

List of figures iii

List of tables ix

List of abbreviations xi

1 Introduction 1

1.1 Preamble 1

1.2 Non-destructive testing 1

1.3 Structural health monitoring (SHM) 3

1.4 Acoustic emission testing (AET) 6

1.4.1 Acoustic emission (AE) source mechanism 9

1.4.2 Background noise 12

1.5 Advantages and limitations of AET 14

1.5.1 Advantages 14

1.5.2 Limitations 15

1.6 Applications of AET 16

1.7 Instrument of AET 19

1.7.1 Acoustic emission sensor 20

1.7.1.1 Calibration of sensor 21

1.7.2 Amplification 23

1.7.3 Filter 23

1.7.4 Cable 24

1.7.5 Couplant 24

2 Literature Survey 27

2.1 Preamble 27

2.2 Acoustic emission signal 27

2.3 AET for damage detection of concrete 32

2.4 Acoustic emission system 35

2.4.1 Wireless structural health monitoring 37

2.4.1.1 Signal conditioning unit (SCU) 40

2.4.1.2 Parameter processing of AE signal 43

2.4.1.3 Data Acquisition (DAQ) 44

2.4.1.4 PSoC based DAQ device and computational core unit (CCU) 45

2.4.1.5 PSoC family 48

2.5 Motivation and objective 51

2.6 Organization of the thesis 53

3 Design development and validation of the signal conditioning unit 55

3.1 Preamble 55

3.2 Introduction 55

3.3 Sensor with integral pre-amplifier ... 56

3.3.1 Sensor ... 56

3.4 Signal conditioning unit ... 59

3.4.1 Sensing interface circuit ... 60

3.4.2 Gain control amplifier ... 62

3.4.3 Filter design ... 63

3.5 Design validation of the SCU ... 66

3.5.1 Metallic material ... 66

3.5.2 Concrete ... 72

3.6 Summary ... 76

4 Simulation study for parameters extraction of burst type AE signals ... 79

4.1 Preamble ... 79

4.2 Hardware design for parameter extraction ... 79

4.2.1 Processing board (AE Board) ... 82

4.2.1.1 Analog circuit block ... 84

4.2.1.2 Digital circuit block ... 88

4.2.2 Results and discussion ... 93

4.3 Summary ... 97

5 Design development and validation of data acquisition device ... 99

5.1 Preamble ... 99

5.2 Introduction 99

5.3 Description of PSoC family and its selection 100

5.4 Data acquisition system 105

5.4.1 Design of data acquisition hardware 107

5.4.2 Data acquisition software design 109

5.5 Signal generator device 110

5.6 Communication interface 113

5.7 Experimental, results and discussion 115

5.8 Summary 118

6 Design development and validation of wireless AE sensor system 119

6.1 Preamble 119

6.2 Wireless sensing hardware design and architecture 119

6.2.1 Redesign of the signal conditioning unit 121

6.2.2 Design of the computational core unit 123

6.2.3 Wireless communication unit 126

6.3 Assembled prototype wireless sensor unit 127

6.4 Performance validation of the wireless sensor unit 130

6.4.1 Signal validation using artificial AE signal 130

6.4.2 Signal validation using pencil lead break 132

6.4.3 Application of the wireless AE sensor system to concrete compression test ………………………………………………………………………….134

6.4.4 Application of the wireless AE sensor system to concrete corrosion test.. 142

6.5 Summary 146

7 Conclusion, contribution and scope for future work 149

7.1 Conclusion 149

7.2 Contribution 151

7.3 Scope of future work 153

Appendix 155

A 155

B 159

C 163

References 169

Abstract

Acoustic emission (AE) testing plays a significant role in structural health monitoring (SHM) applications. Acoustic emissions are high frequency (20 kHz – 1 MHz) stress waves, which are generated due to crack initiation and fracture growth behaviour of a material/structure by the rapid release of transient energy from the confined sources. AE testing involves the recording of these waves using piezoelectric sensors attached to the surface of structures under test and then analyzing the signals to extract information about the nature of the sources. There are different parameters associated with acoustic emission signals such as peak amplitude, RMS, counts, cumulative counts, rise time, and event duration. These parameters are beneficial for assessing the AE activity obtained during SHM applications and provide vital information about the integrity of components. A few commercial AE systems are available for these applications, the cost of which is very high, and details of instrumentation development proprietary in nature. For continuous monitoring of structures, typical AE sensing systems demand compact, portable and battery-operated devices. Distributed AE sensing also demands less wiring complexities for the ease of deployment and maintenance. In this context, the present thesis presents a first of its kind details about the design and development of a wireless acoustic emission sensor system (AE-SS) for structural health monitoring applications using the programmable system on chip (PSoC). The design challenges and validation of different sub-modules of AE-SS, such as signal conditioning unit (SCU), data acquisition (DAQ) device, and computational core unit (CCU) have been realized towards achieving the objectives of the thesis:

A signal conditioning unit has been designed and developed for amplifying weak AE signals enabling their further processing. The performance of the developed SCU has been validated

using artificial AE events generated by pencil lead break (PLB) test. A novel hardware design approach has been proposed for the extraction of the parameters of AE signals. A data acquisition device has been designed and developed on the programmable system on chip. The developed DAQ device has also been validated by using an artificial burst type AE signal. Zigbee based wireless communication unit is interfaced with the CCU for transmission of AE parameters and their analysis. Different sub-modules of the wireless AE sensor system have been fabricated and assembled in a compact single two-layer printed circuit board (PCB).

Finally, the AE results obtained from compression and corrosion tests of concrete using the developed wireless system have been compared with those obtained by using a commercially available wired system for validation. The results of compression and corrosion tests of concrete have been verified with scanning electron microscopy and X-ray radiography methods. The developed wireless system offers several unique advantages such as it is cost-effective, compact in size (85 mm x 56 mm), easy to install on structures, portable, low power consumption (50 mA) capability to ensure long term monitoring in a single charge battery supply and remote operational capability. The developed AE system can be effectively utilized for condition monitoring and health monitoring of structures and components such as nuclear power plant (NPP) containments, bridges, tanks, and components in petrochemical industries where corrosion is a potential issue, with utmost ease and efficiency.

List of figures

Figure No.	Caption	Page No.

Figure 1.1 Block diagram representation of the SHM system... 5

Figure 1.2 Process block diagram of the acoustic emission testing.................................. 7

Figure 1.3 Basic of acoustic emission activity shows the Kaiser effect (BCB), Felicity effect (DEF) and emission during hold (GH) [45]... 11

Figure 1.4 AET applications: (a) pressure vessel, (b) pipeline leakage inspection, (c) inspection of weld quality and (d) integrity monitoring of bridge [48]. 17

Figure 1.5 Hsu-Nielson source.. 22

Figure 2.1 (a) Burst type AE signal and (b) Continuous type AE signal [56]................... 28

Figure 2.2 Cumulative counts (CC) by compression tests in (a) plain concrete and (b) fly ash concrete for different periods of curing [83]. 35

Figure 2.3 Block diagram architecture of acoustic emission sensor system. 36

Figure 2.4 Block diagram of signal conditioning... 41

Figure 2.5 Block diagram of typical MCU [139]... 47

Figure 2.6 Block diagram of PSoC 5LP [139]... 47

Figure 2.7 Comparison of PSoC family. 49

Figure 3.1 Block diagram of the acoustic emission system.. 56

Figure 3.2 Block diagram of the signal conditioning unit..59

Figure 3.3 Sensing interface circuit design. 62

Figure 3.4 Circuit design for the digital gain control amplifier..63

Figure 3.5 Schematic design and simulation results of the bandpass filter........................65

Figure 3.6 Photograph of prototype signal conditioning unit...66

Figure 3.7 Photograph of experimental setup used for acoustic emission testing on a metallic plate using (a) developed signal conditioning unit and (b) commercially available PAC system. 68

Figure 3.8 Result of pencil lead break test of AE signals for the plate received from sensor one and sensor two respectively by the developed conditioning unit. 69

Figure 3.9 Result of pencil lead break test of AE signals for the plate received from sensor one and sensor two respectively by the PAC system...69

Figure 3.10 FFT of PLB test signals acquired using the developed SCU..........................71

Figure 3.11 FFT of PLB test signals acquired using the PAC system...............................71

Figure 3.12 Photograph of the experimental setup used for acoustic emission testing in concrete. 72

Figure 3.13 PLB signals and corresponding FFT for distances of 10 cm (a), 20 cm (b) and 30 cm (c) from the sensor. 75

Figure 3.14 Peak amplitude of the AE signal versus distance from the sensor. 76

Figure 4.1 Schematic design of a hardware system for parameter extraction of the AE signal. 81

Figure 4.2 Flow diagram representation of the hardware system functionality................ 82

Figure 4.3 Block diagram of AE Board with the components used in the design. 83

Figure 4.4 AE Board design........ 84

Figure 4.5 AnalogCircuit (Analog circuit) block design. 84

Figure 4.6 Peak detect circuit along with peak reset. 86

Figure 4.7 RMS circuit design. 87

Figure 4.8 Differentiator circuit design. 87

Figure 4.9 Rise time clock circuit design. 88

Figure 4.10 Digital circuits (DigitalCircuit) block design. 89

Figure 4.11 Monoshot circuit design. 90

Figure 4.12 Retriggerable monoshot circuit design. 90

Figure 4.13 Short pulse circuit design. 90

Figure 4.14 Simulation results of (a) AnalogCircuit block and (b) DigitalCircuit block... 94

Figure 5.1 Block diagram representation of PSoC 5LP kit [108]. 104

Figure 5.2 Data acquisition system block diagram. 106

Figure 5.3 Block diagram representation of components used for the DAQ. 107

Figure 5.4 Schematic design of the DAQ in PSoC creator 4.0 IDE. 108

Figure 5.5 Software design flow chart for the acquisition of AE signals. 109

Figure 5.6 Schematic design of the signal generator device in PSoC creator 4.0 IDE.....111

Figure 5.7 Block diagram of signal validation test. 112

Figure 5.8 Photograph of the experimental setup for validation of the AE signal generator. 112

Figure 5.9 (a) Burst type AE signal generated and it's (b) FFT received from signal generator device. 113

Figure 5.10 Photograph of the experimental setup for the data acquisition system. 116

Figure 5.11 Burst type AE signal received from DAQ displayed using LabVIEW. 116

Figure 5.12 AE signal received from the (a) DAQ and its (b) FFT. 117

Figure 6.1 System architecture block diagram for the wireless AE sensor system. 120

Figure 6.2 Multisim simulation result for the bandpass filter. 122

Figure 6.3 Optimized circuit diagram of SCU in a single IC. 122

Figure 6.4 Design of computational core unit in a PSoC creator 4.0 IDE. 123

Figure 6.5 Front and rare views of integrated prototype wireless AE sensor unit. 128

Figure 6.6 Voltage and current are measured by USB meter. 129

Figure 6.7 Block diagram representation of test setup for signal validation test. 131

Figure 6.8 Photograph of the test setup made in the laboratory for validation of wireless AE sensor system. 131

Figure 6.9 FFT of the signal received from the wireless sensor system. 132

Figure 6.10 Photograph of the experimental setup of the wired based PAC system along with the wireless AE sensor system in the Lab.. 133

Figure 6.11 Pencil lead break test signal and it's FFT from (a) wireless AE system and (b) wired PAC system. 134

Figure 6.12 Photograph of an experimental setup for the compression test of concrete specimen. 136

Figure 6.13 Counts and applied load as a function of time from (a) developed wireless AE system and (b) wired PAC system. 139

Figure 6.14 Cumulative counts and applied load as a function of time from (a) developed wireless AE system and (b) wired PAC system.. 139

Figure 6.15 RMS and applied load as a function of time from (a) developed wireless AE system and (b) wired PAC system. 140

Figure 6.16 Peak amplitude and applied load as a function of time from (a) developed wireless AE system and (b) wired PAC system.. 140

Figure 6.17 Rise time and applied load as a function of time from (a) developed wireless AE system and (b) wired PAC system. 141

Figure 6.18 Event duration and applied load as a function of time from (a) developed wireless AE system and (b) wired PAC system.. 141

Figure 6.19 SEM images of the fracture surface of a concrete specimen. 142

Figure 6.20 Photograph of an experimental setup for the concrete corrosion test in the Lab. 143

Figure 6.21 Cumulative count as a function of time in days from (a) developed wireless AE system and (b) wired PAC system. 144

Figure 6.22 X-ray radiography image of concrete block (a) without corrosion (b) after accelerated corrosion.. 145

List of tables

Table No. **Caption** **Page No.**

Table 3.1 Specifications of the sensors used for metallic material 57

Table 3.2 Specifications of the sensor used for concrete specimen. 58

Table 4.1 AE parameters measurement values (Figure 4.14a and Figure 4.14b) 95

Table 4.2 Event duration measurement values taken from the simulation data (Figure 4.14b) 97

Table 4.3 Rise time measurement values taken from the simulation data (Figure 4.14 b) 97

Table 5.1 PSoC types and specifications 101

Table 5.2 The UART parameters configuration for DAQ and the PC. 115

Table 6.1 Key characteristics of the ZigBee wireless transceiver.................................. 127

Table 6.2 Approximate current consumption of different components. 129

Table 6.3 Details of specimens used for compression tests... 135

Table 6.4 Specifications of the sensor used with the wired PAC, USA system 137

List of abbreviations

ADC	Analog to digital converter
AE-SS	Acoustic emission sensor system
AET	Acoustic emission testing
API	Application programmer interface
ARM	Advanced RISC Machine
ASCII	American standard code for information interchange
ASIC	Application specific integrated circuit
BW	Bandwidth
CAN	Controlled area network
CCU	Computational core unit
CMRR	Common mode rejection ratio
CPU	Central processing unit
CRC	Cyclic redundancy check
DAC	Digital to analog converter
DAQ	Data acquisition
DC	Direct current
DMA	Direct memory access
DSO	Digital storage oscilloscope
ECT	Eddy current testing
EMI	Electromagnetic interference
FFT	Fast Fourier Transform
FPGA	Field programmable gate array
FRC	Fiber reinforced concrete
GUI	Graphical user interface
I^2C	Inter Integrated Circuit
IC	Integrated circuit
IDE	Integrated development environment
IRT	Infrared testing
ISR	Interrupt Service routine
JTAG	Joint test action group
kHz	Kilo Hertz
kSPS	Kilo sample per second
LED	Light emitting diode
LPT	Liquid penetrant testing
MCU	Microcontroller
MHz	Mega Hertz
MOS	Metal oxide semiconductor
MPT	Magnetic particle testing

MSPS	Mega sample per second
NDE	Non-destructive evaluation
NPP	Nuclear power plant
OPAMP	Operational amplifier
PAC	Physical Acoustic Corporation
PC	Personal computer
PCB	Printed circuit board
PGA	Programmable gain amplifier
PRS	Pseudo random sequence
PSoC	Programmable system on chip
RAM	Random access memory
RMS	Root mean square
ROM	Read only memory
RT	Radiography testing
SAR	Successive approximation register
SCU	System control unit
SEM	Scanning electron microscope
SHM	Structural health monitoring
SNR	Signal to noise ratio
SoC	System on chip
SPI	Serial peripheral interface
SS	Stainless steel
UART	Universal asynchronous receiver and transmitter
USB	Universal synchronous Bus
UT	Ultrasonic testing
VREF	Reference voltage
VS	Visual studio
VT	Visual testing

1 Introduction

1.1 Preamble

This chapter provides a brief introduction to non-destructive evaluation (NDE), structural health monitoring (SHM), principles of acoustic emission testing (AET), and acoustic emission instrument. As the thesis is concerned with the development of an instrument for SHM applications using acoustic emission method, a brief description of the method, and signal analysis is discussed.

1.2 Non-destructive testing

Non-destructive testing (NDT) is an interdisciplinary technology that plays a vital role in ensuring the quality and structural integrity of components and systems **[1]**. The NDT is defined as the identification of the physical condition of materials/structures without affecting their intended functions **[2]**. NDT technologies are essential in various industries, including petrochemical, nuclear, aerospace, construction, automotive, and defence **[3]**. Several NDT methods are available based on a particular physical principle **[4-9]**. There exist different NDT methods which are used for inspection of materials/structures such as visual testing (VT), magnetic particle testing (MPT), radiography testing (RT), liquid penetrant testing (LPT), ultrasonic testing (UT), vibration testing (VT), eddy current testing

(ECT), infrared thermography testing (IRT) and acoustic emission testing (AET). These methods are further subdivided into various techniques. These methods and techniques lend themselves well to specific applications such as structural integrity assessment, online monitoring, etc. through detection and characterization of damage and defects, e.g., cracks, porosity, inclusions **[10-11]**. Judicious selection of methods and techniques is an essential part according to the area of applications.

NDT methods can be classified into offline and online. The methods such as VT, LPT, MPT, RT, UT and ECT are offline while the vibration testing, AET and IRT are online. NDT methods generally use some form of energy such as x-ray radiation, ultrasonic waves and electromagnetic waves, to interrogate a material/structure. The interaction of this energy with the material/structure is sensed to detect the presence of flaws. AET is an exception to this, wherein the material/structure under test acts as a source for the emission of acoustic waves which are associated with dynamic events such as the growth of cracks and microstructural degradation **[12]**. Thus, AET is useful for the continuous monitoring of large structures such as pressure vessels, aircraft and concrete bridges in real-time. The AE method is distinct in two main aspects from other traditional NDT methods. Firstly, in the AE method, an external stimulus is present to aid the dynamic events. Secondly, the AE method detects the internal changes in materials subject to loading. AET is widely used for early fault detection and diagnosis compared to other NDT methods for monitoring materials/structures **[13-14]**. The details of structural health monitoring are discussed subsequently.

1.3 Structural health monitoring (SHM)

SHM is adopted to assess the healthiness/condition of structures through their monitoring and any damage sensing before failure. SHM is vital for monitoring the health of any structure to ensure the safety of working personnel and has economic implications **[15]**. SHM is a new concept in the field of engineering. It is intended for continuous monitoring of structures in real-time. It also evaluates the structural performance under various external stimulus to identify damage or deterioration, in order to ensure the healthiness of the structures/components. Towards the advancement in SHM, many non-destructive testing methods have been developed over the past three decades **[16-17]**. NDT including proof loading, coring, radar methods and conductivity mapping have all been used for enhancement of the visual inspection method for concrete and sandstone based civil structures **[18-19]**. Many researchers have gone about trying to determine the best methods of damage prognosis in mechanical, civil and aerospace structures for SHM applications.

Structural health monitoring is applied to monitor the operational loads and to the components/structures which are prone to accidental impairment **[20]**.

The structural health monitoring on a continuous real-time basis is essential for manufacturing, end-users and maintenance teams. SHM system allows optimal use of the structure, avoidance of catastrophic failure and a minimized downtime. The SHM system, once correctly implemented, shows improvement in a product and drastically changes maintenance service. The drastic changes in maintenance philosophy are described in several publications, particularly for civil infrastructure **[21]**, military air vehicle **[22]**, army systems **[23]** and civil aircraft **[24]**. In civil infrastructure, wireless SHM is a potential tool for condition monitoring applications **[20]**. SHM system involves the integration of structures, sensors, computational core, data transmission, computational power, and PC/Server/Base station. The typical block diagram representation of the SHM system is given in **Figure 1.1**.

In an SHM application, the sensor is mounted on the monitoring material or structure for the detection of signals generated by crack growth or fracture. The signals are acquired and processed using the computational core. Finally, the processed signals are transmitted through wired/wireless mode to the personal computer/server/Base station for data collection, data analysis and diagnostics towards structures/materials condition assessment. The power management is taken care of by the computational power of the individual system used in the design of SHM systems. The current trend and widely accepted methods for monitoring large structures are based on sensor network technology where multiple sensors are mounted on the structures.

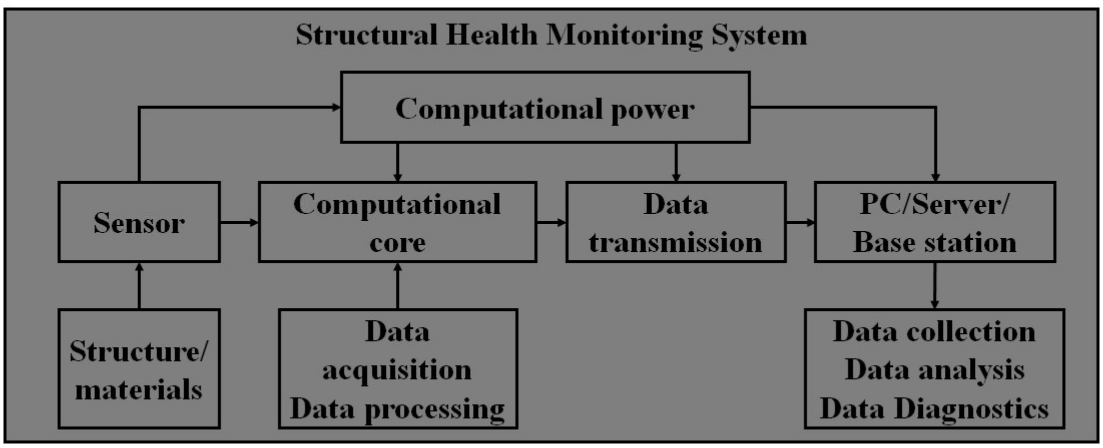

Figure 1.1 Block diagram representation of the SHM system

Traditionally SHM uses wired technology for collecting AE data. SHM has advantages in its anti-interference ability. Also, the wired system requires a large number of cables, and increases workforce, wiring complexity and cost of maintenance as the number of sensor node increases. Also, in some situations, it may not be possible to install cables for such monitoring. The technological improvement in wireless technology has enabled the wireless system to overcome the constraints of the wired system. AET plays a significant role in structural health monitoring. The details of AET, including its applications and instrumentation, are explained subsequently.

1.4 Acoustic emission testing (AET)

Acoustic emission is generated by a release of transient energy from the localized source when materials are subjected to an external stimulus like pressure, load and temprature **[25]**. Acoustic emission is one of the structural health monitoring techniques to monitor the performance and integrity of the structure when subjected to a stimulus. AET has emerged as a potential and reliable NDT method that can provide an estimate of the source location, severity and type of damage in the material/structure **[26-27]**. The frequency range of interest in AET is from 20 kHz to 1 MHz. AET is useful in the detection of initial stage failure and onset of cracking during monitoring of structures under loading condition. There are different structures such as bridges, buildings and aircraft which are vital for modern society. While these structures are designed to provide sustainable functionality under reasonable operating condition, it is also often necessary to re-examine their integrity in the presence of any structural deterioration **[28]** or after extreme loading scenarios **[29-30]**.

When a load is applied to a material, it results in the transient energy/stress wave release from the material. The transient energy released travels in the form of a spherical wavefront in the material. These stress waves undergo distortion and attenuation while travelling through the material. The part of the wave reaching the material surface is highly distorted and attenuated concerning to the original wave. With the help of a suitable piezoelectric transducer or sensor mounted on the surface of the material using couplant, these stress waves are converted into electrical signals. The stress waves undergo multiple distortions through material, couplant and transducer, and it depends upon characteristics of the transfer function. The strength of the AE signal can be increased by interfacing a pre-amplifier with the transducer and making it compatible with the analog to digital convertor. The amplified signals applied to the filter along with the threshold levels are used to filter ambient noise and unwanted frequency components from the signals. The process involved during acoustic emission testing is shown in **Figure 1.2**.

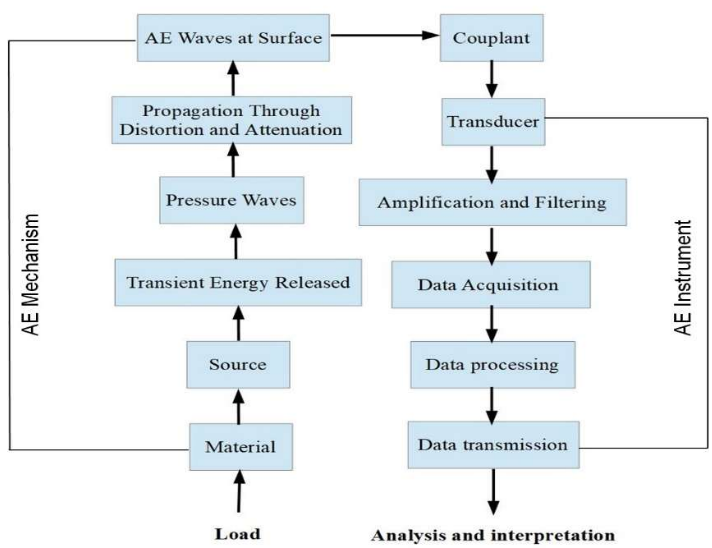

Figure 1.2 Process block diagram of the acoustic emission testing.

The dynamic events such as dislocation movement, slip, twinning, phase transformation, initiation and propagation of cracks, and fusion (welding) are typical examples of mechanisms giving rise to AE. The magnitude and characteristics of the acoustic emission generated from the material are dependent on the source characteristics such as the severity of source, the metallurgical structure of the material and environment. Acoustic emission technique is used to investigate the micro-mechanisms of deformation and fracture in materials **[31]**. The sources of AE are related to the damage and growth of defects and is used to predict the failure of materials or structures **[32]**. Partial discharge localization of power transformers uses the method of acoustic emission **[33]**.

Acoustic emission testing is widely used for integrity assessment or health monitoring of structures/systems like pressure vessels, pipelines, reactor vessels, concrete structures, etc. **[34-37]**. Fundamental studies on AE are directed at clarifying the mechanisms of AE generation, correlation of AE signals to physical or mechanical processes, and evaluation of the interaction of stress waves with the material/structure through which it passes **[38]**. Since practical applications of AE have become more demanding, more understanding of the AE phenomena is required. An understanding of the acoustic emission signals generated during various deformation and fracture processes is essential for successful monitoring of the integrity of structural components. Fundamentals of AET are discussed subsequently.

1.4.1 Acoustic emission (AE) source mechanism

Different mechanisms responsible for the generation of AE are given below **[39]**:

a) Naturally occurring sources

1. Earthquake
2. Rock bursts in mines

b) Sources in metals

1. Crack propagation
2. Grain boundaries and dislocations movement
3. Slip formation
4. Twins growth
5. Realignment or growth of magnetic domains
6. Grain boundary sliding

c) Secondary sources

1. Leaks and cavitations
2. Friction
3. Solid-solid phase transformation

When a certain magnitude of stress is applied to a material, then strain induces in the material. During application of stress to the material, it is possible that the material may get back to its original state (elastic deformation) or may get permanently deformed (plastic deformation) which depends upon the magnitude of stress during loading and unloading condition **[40]**. The maximum AE activity is observed when the material is under plastic deformation **[40]**. The occurrence of plastic deformation at a microscopic level causes the slip of atomic planes past each other through the movement of dislocations **[41]**. These movements of dislocations produce energy called as elastic waves. The elastic wave thus produced can be conceived as naturally generated AE signal, travelling through the material. When cracks exist in a material, the stress level present at the crack tip can be several times higher than the surrounding area. Hence, AE activity will also be observed when the material with a crack undergoes plastic deformation **[42]**. Fatigue cracks also cause acoustic emission in two different ways. The first is emissive particles (e.g. non-metallic inclusions or second phase precipitates) at the origin of the crack tip. The other source is crack growth through the movement of dislocations and small-scale cleavage produced by tri-axial stresses at the crack tip **[43]**. The maximum amplitude and amount of energy released during emission depend upon the source mechanism. The magnitude of acoustic emission is proportional to the velocity of crack propagation and size of the surface area created during crack growth of the material. Large and discrete crack jumps will produce larger AE signals than cracks that propagate slowly over the same distance **[44]**. Hence, the elastic signal detection and its transformation into an electrical signal is the basis of AE testing. Analysis of these signals yields valuable information regarding the origin and severity of flaws/cracks in a material.

The acoustic emission signals generated at different loading conditions can provide vital information concerning the structural integrity of a material/structure. The levels of load that have been previously exerted on a metallic material do not produce AE activity during further loading and emit AE when the load is exceeded beyond the previous loading, is known as Kaiser effect **[45].** The cumulative emission versus load plot for the metallic material is shown in **Figure 1.3**.

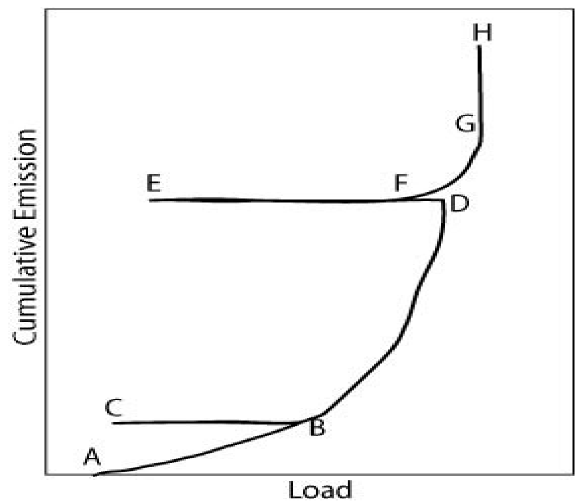

Figure 1.3 Basic of acoustic emission activity shows the Kaiser effect (BCB), Felicity effect (DEF) and emission during hold (GH) **[45]**.

The AE activity starts accumulating, as shown in the segment AB during continuous loading of the material. The segment BCB corresponds to unloading and then reloading. The AE activity starts generating only when the load is exceeded from point B. As the load increases, AE activity also increases shown by BD and AE activity stops when the load is removed.

At point F, the applied load is high enough to cause significant AE generation even though the previous maximum load (D) is not reached, and it is known as Felicity effect [**45]**. The Felicity effect is quantified by using Felicity Ratio, which is defined as the load where considerable AE activity resumes divided by the maximum applied load (F/D). This felicity effect is used for the study of composite materials **[45]**.

1.4.2 Background noise

The amount of background noise often limits the sensitivity of an acoustic emission system. Acoustic emission testing noise refers to the undesired signals detected by the transducer. The noise from background in most of the situations where AET is performed is high. It is essential to understand the types of noise sources and to ensure the elimination of their influence on AE testing and analysis. It is required to take a survey on the influences of noise which helps in identifying the amplitude/frequency, selecting sensor, setting threshold and finalizing test procedure before AE testing. It has to be also noted that whether AE signals during testing is detected above the background noise. The frequency response of the noise helps in the selection of optimum operating frequency band (sensor frequency, filtering, etc.) to avoid noise. Before AET, it is crucial to study the effect of background noise and suggest ways to nullify it.

Different types of noise are (1) Mechanical noise, (2) Hydraulic noise, (3) Cyclic noise, (4) Electrical (Electro-Magnetic Noise). The types of mechanical noise are due to the following reasons:

1. Mechanical part movement,
2. Fretting noise which gives a broad frequency spectrum,
3. Roller bearings with spalled races,
4. Riveted, pinned, or bolted structures usually are noisy due to their loose-fitting.

The mechanical noise is used for the detection of mechanical failures such as turbines, blades, bearings, etc. Different types of hydraulic noise consist of a) Boiling of liquid, b) Leaks in hydraulic system, c) Leaking airlines and d) Turbulence and cavitation. The cyclic noise is periodic, which is bursty, e.g. electrode positioning during spot-welding and during a specific time for every rotation in rotating machinery. It is possible to eliminate the uniform noise generation having a low repetition rate by blocking the AE recording periodically. Electromagnetic interference (EMI) is the noise associated with AE instrumentation due to electrical conduction and radiation. There are different sources of EMI which include noise from welding machines, fluorescent lamps, turning relay power on/off with inductive load, and electric motor circuits. The electromagnetic noise can be eliminated by providing better shielding to the sensor, pre-amplifier and main amplifier in high conductivity metal cases and by grounding the cases at a common point. Use of isolation to the transformer on the power supply side can also reduce EMI. A significant problem may arise if the test structure has a ground system that is different from the AE system. The difference in potential between the structure and AE system can be substantial and may produce high-frequency noise spikes which is much higher than the valid signals detected by the sensors. Even a sensor is insulated from the structure, can influence capacitively coupled noise. A differential type AE transducer will provide substantial relief from such noise types. Auspiciously, researchers have developed viable techniques in order to filter or discriminate the noisy test environments **[12]**.

1.5 Advantages and limitations of AET

1.5.1 Advantages

AET is found to be most advantageous in source location and evaluation of dynamic discontinuities in an entire structure in one stroke compared to other NDT techniques which selectively test the localized area. The superiority of the AE technique over other NDT techniques lies in its monitoring capability of the entire structure in real-time without disturbing its operation **[46]**.

The advantages of AET are listed as follows:

i) AET gives dynamic characteristics of active defects.

ii) It is a global volume technique, i.e. structures such as bridges, pressure vessels and storage tanks can be monitored in one stroke by mounting several sensors on it from where the source of an acoustic event can be realized.

iii) The AE data provides real-time detection of cracks/damage.

iv) AET is used for source location in components such as active flaws.

v) It can distinguish different types of active defects, i.e. source characterization is possible.

vi) Though the initial cost is comparable with other NDTs, operational cost is minimum for AET.

1.5.2 Limitations

The limitations of AET are as follows:

i) The limited accuracy of source localization.

ii) The structure should be loaded to get the AE signals.

iii) It has very limited information on the size of a flaw.

iv) Usually, the transducer has to be placed on the structure under test.

v) Test object has to be stimulated to make the defects active.

vi) Extraneous noise is a severe problem in AE testing.

1.6 Applications of AET

Acoustic emission technique can always be an aspirant when testing is associated with dynamic changes of an object. Firstly, the AET is helpful for researchers in the laboratory. Recorded AE data can provide useful information to a researcher for a better understanding of test object properties. Secondly, AE testing assists in quality control during different metal joining and metal forming operations such as brazing, welding, thermo-compression bonding, punch press operating, shaft straightening etc. At last, AET helps to ascertain the structural integrity of the dam, components in power plants, storage tanks, aircraft, pressure vessels and bridges [**34-38**]. Partial discharge localization of power transformer uses the method of acoustic emission **[47]**. A few of the applications of AET are shown in **Figure 1.4**. The detailed applications of AET are as follows **[48]**:

1) Testing of material: It involves different testing methods such as fatigue testing, crack detection testing, detection of corrosion, hydrogen embrittlement detection, ceramic material testing, integrity testing of composite materials, tribology testing of materials, and reinforced plastics testing.

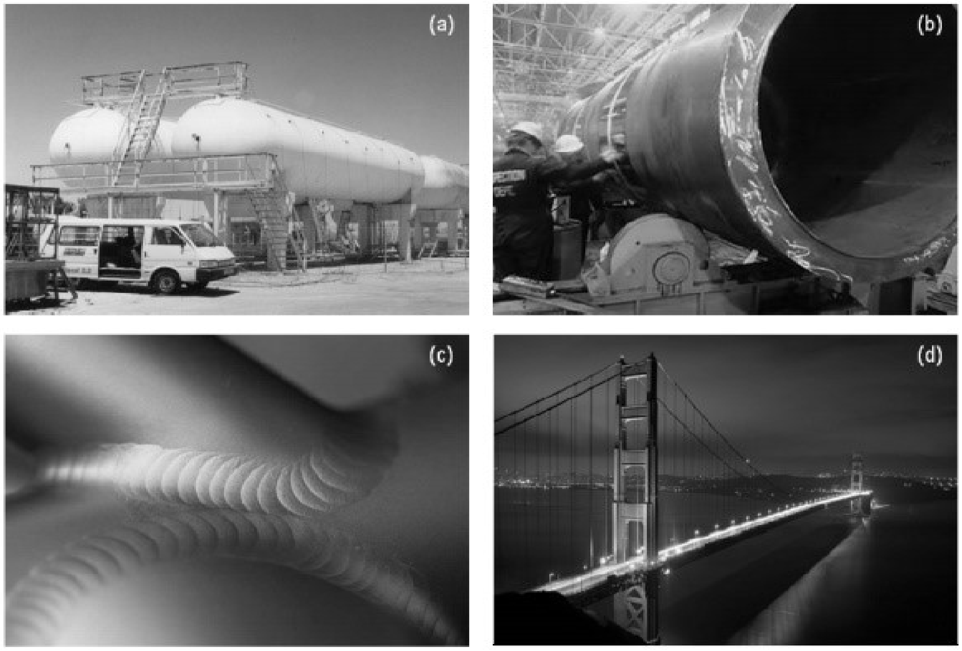

Figure 1.4 AET applications: (a) pressure vessel, (b) pipeline leakage inspection, (c) inspection of weld quality and (d) integrity monitoring of bridge **[48]**.

2) Petroleum and chemical industries: It involves several applications such as integrity monitoring of spherical tanks, pressure vessel testing, testing of cryogenic tanks, towers, columns, hot piping systems and cool down for boiling reactors, tank bottom testing, real-time corrosion monitoring, pipeline and FRP tank testing, gas valves leak detection, buried pipes leak detection, offshore pipelines sand detection, and monitoring the integrity of the maritime platform.

3) Power plant and electric industries: It involves the applications such as monitoring and diagnosis of power plant components and high-pressure vessels, testing of steam chests, testing of steam line and its continuous monitoring, testing of partial discharge in transformers, evaluation of valves for quantitative steam loss, testing of bucket trucks, furnace monitoring, monitoring of leak detection in reheat pipelines, leak detection in the boiler, testing and condition monitoring of turbine blade, and condition monitoring of turbine bearing.

4) Aerospace and aircraft industries: It involves different applications such as proof testing of aircraft, testing of aged aircraft, structures/aircrafts fatigue testing, monitoring landing gear, wind turbine blade testing and testing of helicopter blade, continuous monitoring of on-board aircraft, fuselage crack detection, skin lap joints and pivot bearing testing, in-process tracking of helicopter gearbox transmission, composite fuel tanks testing and examination of explosive bolt, aerospace launcher proof testing.

5) Metalworking industries: Applications such as detection of wear and breakage in the cutting tool, grinding wheel/dresser touch detection and dressing verification, quality control during metalworking processes, testing of forging press, detection of chatter, crash detection and prevention during the manufacturing processes.

6) Civil structure: Applications such as testing of the concrete building, testing of the bridge, testing of the tunnel, testing of the dam, continuous monitoring of crack propagation in structures made of concrete and testing of the crane.

7) Applications in transportation: Applications used for detection and location of flaws in tube trailers, tank trucks and railroad cars, detection of a crack in railway materials and structures, integrity testing of tunnels and bridges, flaw detection in train and truck ball bearing, detection of cracks in components of the train such as shafts and wheels.

8) Other applications: Applications such as integrity testing of flasks, testing of wear and friction, testing of pinpoint trouble spots in welds, detection of head disk interference, rock detection, drought stress monitoring of woods and crops, seismological and geological applications, monitoring of engine status, steel roller crack detection, monitoring of automobile shaft strengthening process, monitoring of investment casting process and monitoring of operations in rotating machinery.

1.7 Instrument of AET

AET instrument consists of a sensor, cable, amplifier, filter, acquisition system and personal computer. AET can be performed in the field or the laboratory. The acquisition system and personal computer are used for the measurement, storage and display of the AE data. A description of the equipment used in AE testing is provided in the subsequent sections.

1.7.1 Acoustic emission sensor

Acoustic emission transducer is a device that transforms local material displacements produced by a stress wave to an electrical signal. The piezoelectric (PZT) type sensor is commonly used for the detection of AE signal. A piezoelectric sensor is based on the principle of piezoelectricity which converts the changes in temperature, pressure, vibration, acceleration, and strain into electrical charges. PZT sensor is used for the measurement of various processes such as process control, quality assurance, research and production industries. The sensor is made of lead zirconate titanate, which is an inorganic compound called PZT. It is a ceramic material that shows marked piezoelectricity effect, meaning that the compound changes shape when an electric field is applied. The sensor is attached to the material/structure by using couplant and measures the change in electrical impedance during any damage in the material/structure **[49].** Selection of a specific sensor depends on the application, type of damage/flaw to be revealed, background noise characteristics and other factors. AE sensors are classified into two categories based on their frequency response: (a) resonant and (b) wideband or broadband. Resonant type sensors are most sensitive at resonant frequencies, and the ranges of operating frequencies are a decisive factor for their applications. The resonant type AE sensors are used where different AE parameters such as RMS, amplitude, count, event duration and rise time are required for analysis **[50]**. Broadband sensors are used where one is interested in finding the dominant frequency in the received signal **[51]**. AE sensors with in-build pre-amplifiers are called active sensors, whereas sensors without pre-amplifiers are known as passive sensors. A passive sensor requires an external pre-amplifier. In general, the active sensor is more cost-effective compared to the passive sensor. The resonant type AE sensors are used for applications related to concrete which has high attenuation characteristics. The resonant type sensors have higher sensitivity, but the range of frequency is lower than the broadband type AE sensors.

1.7.1.1 Calibration of sensor

There is a possibility for the variation in sensor characteristics with time, operating environment etc. Therefore, the calibration of sensors should be checked periodically for frequency response and sensitivity before using. A reproducible artificial reference AE source should be used for testing the sensors. Following the work of Hsu and Nielsen **[52],** AE source is also called Hsu-Nielsen source. The Hsu-Nielsen source is most widely used to simulate an AE event through pencil lead break test where the lead is pressed against a workpiece or object **[53]**. The standard method of Hsu Nielsen pencil lead break test is shown in **Figure 1.5.**

The Nielsen-Hsu Pencil aids to simulate an event of AE by graphite lead break in an appropriate fitting. The 2H pencil lead of 0.5 mm diameter is pressed to break at the surface of the object with an approximate tip length of 3 mm (+/-0.5 mm). The pencil lead breaking (PLB) against the surface generates intense signal similar to the natural source of acoustic emission **[54]**. The signal generated during the rapture process from a material is the same as the signal produced by the PLB test. The application of force to the pencil lead against a structure produces a local deformation which suddenly relieves during the lead break.

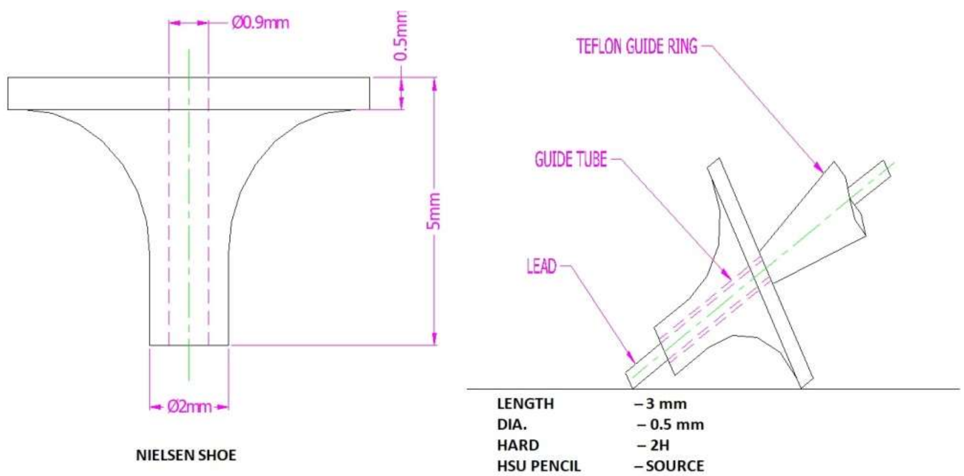

Figure 1.5 Hsu-Nielson source.

Nielsen-Hsu Pencil and Nielsen shoe play a significant role in practical acoustic emission testing applications. The pencil lead break creates a very short-duration source of signal similar to the natural signal source of AE, e.g. crack.

Moreover, the amplitude range of the generated signal by the PLB test lies within that of the actual source generated from cracks. The Hsu pencil breaking is a well-known procedure to simulate the sources of AE in different applications, including source location techniques.

It is widely used for finding the maximum possible distance among different sensors for detection of the source. For the development of a graph, the amplitude values of signals at different distances from the sensor are recorded through the PLB test. The average values of amplitudes for different distances can be plotted against the distances from the sensors.

1.7.2 Amplification

The amplitude of the AE signal received from a sensor is very low, usually in the range of microvolt. The amplification and filtering are required in order to process the signal further. The amplification of the signal is performed by using an electronic amplifier circuit which increases the power of the signal. Quantitatively the amount of amplification provided by an amplifier is measured by amplification factor or gain. The amplifier circuit has the power to gain greater than one. The gain of the amplifier is defined as the ratio of output power (P_{out}) to input power (P_{in}) and is usually measured in decibel (dB). When measured in decibel, it is logarithmically related to the power ratio:

$$(\text{Gain})\text{dB} = 10 * \log\left(\frac{\text{Pout}}{\text{Pin}}\right) \text{-------------------------------} \quad \textbf{(1.1)}$$

1.7.3 Filter

The sources of noise during AE testing may be due to impact loading, friction, liquid flow and electromagnetic. The recorded AE signals during a test contaminated by background noise will affect the reliability and accuracy of the test results. As the noise has always been an issue for acoustic emission testing, it is required to handle carefully and appropriately during either practical AE application or laboratory testing. The undesired frequency can be avoided by implementing the proper frequency range in a bandpass filter for the AE application.

1.7.4 Cable

The function of cable is to transmit an electrical signal from source to load. The connecting cables should be chosen to eliminate electromagnetic interference **[55]**. For the application of AET, coaxial cables are used universally because of their proper shielding. These cables are offered with BNC, Microdot, or SMA connectors on the sensor end, and BNC connections are used on the pre-amplifier end.

1.7.5 Couplant

The couplant plays an essential role in the accuracy of AET because of the low amplitude of the AE signal. The couplant is used between the sensor, and the component surface is essential for efficient detection of acoustic emission. A high viscosity fluid or a semi-solid gel will help to transmit the AE waves from the surface of the structure to the sensor. Thus, the purpose of a couplant is to ensure excellent acoustic contact on the microscopic level between the two surfaces. Couplants should have the following characteristics:

1. High wettability

2. Corrosion resistance
3. Sufficient viscosity
4. Easy removal

Some commonly used couplants are:

1. Natural wax
2. Silicone grease
3. Epoxy resin
4. Propylene glycol

Generally, silicone grease is most widely used in AE testing.

2 Literature Survey

2.1 Preamble

This chapter presents the application of AE signal for damage detection of concrete. This chapter also introduces the state-of-the-artwork in both AE testing as well as wireless system design through literature survey, towards setting the motivation and identifying the objective of this research work.

2.2 Acoustic emission signal

The majority of acoustic emission signals lie in the frequency range of 20 kHz - 1 MHz **[28]**. The waveform of the AE signal generated is broadly classified into burst type and continuous type. The waveform of burst type AE signal is detected as single decaying sinusoid due to resonance in the structures and transducers. It is generated during crack growth and fracture in materials/structures **[56]**. The waveform of continuous type emission appears to consist of an overlapping sequence of individual bursts. The continuous type emission is commonly associated with plastic deformation, grain boundary sliding and dislocation movement in a metal or alloy **[56]**. Typical burst and continuous type AE signals are shown in **Figure 2.1 (a)** and **(b)** respectively. The technique used for the analysis of burst type AE signals is known as parameter-based technique. In this technique, several parameters from the received burst type signals are extracted without saving the waveforms. The parameters of the burst type AE signals are peak amplitude, ring down count or AE count, root mean square (RMS), rise time and event duration and these are used to assess the AE activities **[57]**. The pictorial representation of different burst type AE parameters definition is given in **Figure 2.1 (a)**. Each parameter of burst type emission is defined with the mathematical expression and are as follows:

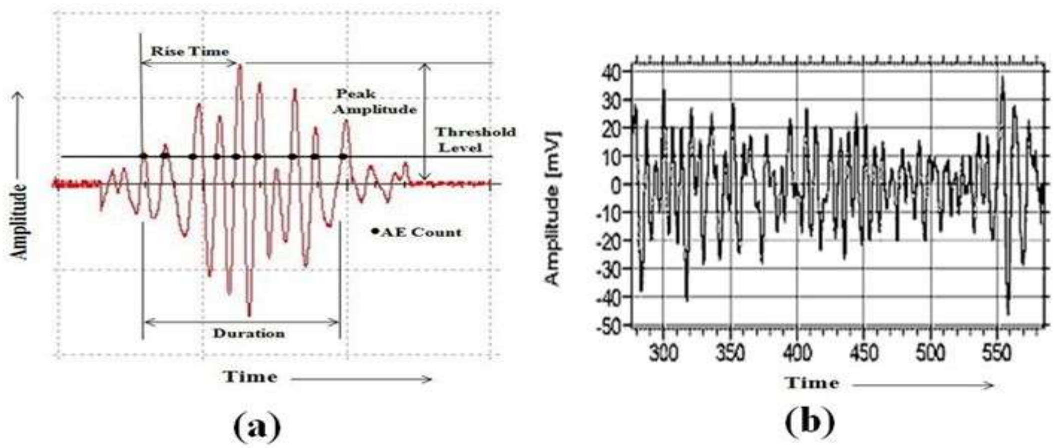

Figure 2.1 (a) Burst type AE signal and (b) Continuous type AE signal **[56]**.

Burst signal: It is oscillatory in shape whose oscillations have a rapid increase in signal amplitude from an initial reference level followed by a decrease gradually to a value close to the initial level. Harris et al. **[58]** expressed the output voltage from a transducer excited by an event of acoustic emission as follows:

V (t)= $Vo\ e^{-\gamma t} \sin \omega t$-----------------------------(2.1) where, V (t) = Output voltage from the transducer, V0 = Initial signal voltage, γ = Decay constant (>0), t = time and ω = Signal frequency.

Threshold: It is a voltage level set in the instrument to eliminate low amplitude noise from the AE signal. An event of the AE signal is detected only when a threshold voltage is set slightly higher than the voltage level of the background noise **[58-59]**. The pencil lead break (PLB) test is carried out to simulate AE events for calibration purpose of checking sensor couplings and of defining threshold **[152]**. The mathematical expression of the threshold is as follows:

$$V_t = Vo\ e^{-\gamma t^*} \text{---------------------------}(2.2)$$

V_t= Fixed threshold voltage or Minimum voltage required to trigger the count or event, V0 = Initial signal voltage, t* = time for amplified acoustic emission signal to ring down or AE count below the trigger level of the count and γ is the decay constant (>0).

Peak amplitude: It is defined as the maximum amplitude attained by an acoustic emission signal. This parameter plays a vital role in the detection of acoustic emission event. The magnitude of the AE signal varies from microvolt to millivolts range. The amplitude of the AE signal can be expressed in term of a common logarithm to a reference voltage of 1 μV **[59]** and is defined as follows:

$$\text{Peak amplitude (dB)} = 20\ Log_{10} \frac{A1}{A0} \text{-------------}(2.3)$$

Where, A0 = 1 μV and A1 = Maximum voltage of the AE signal.

AE counts: This is the number of thresholds crossing pulses in a waveform and is also called ring down counts. The number of counts from a burst type AE signal depends on the magnitude of the source event. It is defined as follows **[58]**:

$$\text{AE Counts} = \frac{\omega}{2\pi\gamma} 20\ \ln \frac{V0}{Vt} \text{-------------(2.4)}$$

Where, Vt = Fixed threshold voltage or Minimum voltage required to trigger the count or event, V0 = Initial signal voltage, ω = signal frequency and γ is the decay constant (>0).

Root Mean Square (RMS): The RMS value is defined as the square root of the mean of the squares of instantaneous values. The RMS of the AE signal can be expressed by equation 2.5 **[60]**:

$$AE_{RMS} = \sqrt{\frac{1}{N}\sum_{i=1}^{N} AE^2(i)} = \sqrt{\frac{1}{\Delta T}\int_0^{\Delta t} AE^2(t)dt} \quad \text{-----------(2.5)}$$

Where N represents the number of discrete values of AE data within ΔT, and ΔT represents the integration time constant. AE_{RMS} can be calculated by digital manner, or by analog RMS filter through the right side of the equation (2.5).

Rise Time: It is defined as the time difference between the Time of the peak signal and Time of the first threshold crossing of an AE wave **[58-59]**. This definition of rising time is used for AET applications where the signal is generated by initiation and fracture growth from materials/structures under loading **[58-59]**. Time to peak is a parameter used in AE signal analysis and is the conventional rise time. The time to peak parameter is extensively used by researchers to correlate various damage mechanism [50].

Event duration: It is defined as the time difference between the first threshold crossing to the last threshold crossing of the AE wave. It is measured in microseconds. The event duration depends upon the magnitude of the source and material properties **[58-59]**.

Only when the amplitude of a signal exceeds the threshold, it is recognized as an AE signal and recorded by the system. Fast Fourier Transform (FFT) method is used for the analysis of peak frequency characteristics present in the recorded time-domain signal. The parameter-based technique shows advantages compared to signal-based technique concerning storing speed and data acquisition. The extracted AE parameters from signals offer useful information about failure or damage behaviour of materials/structures **[11]**. The parameter-based AE system does not get crashed when processing a large amount of AE data compared to signal-based AE system. The advantage of the signal-based technique is that the post-processing of the AE signal can be performed on the saved data. Also, it is possible to apply the signal processing algorithm to eliminate undesired signals from the captured AE waveforms. The attributes of the signal-based AE technique require large storing capacity, particularly for long-term monitoring. The financial support primarily determines the preference of which approach to select and storing space of the AE system. In metallic materials, both continuous and burst type signals are generated but in concrete, only burst type signals are generated by the development of microcracks and macro cracks **[61]**. Hence, the parameter-based technique is more useful for concrete concerning low usages of system physical memory and low development cost for the long-term structural health monitoring applications. The burst type AE signals are detected from the resonant type sensor. The parameters of burst type AE signals are used for the analysis of initiation and fracture of materials/structures. Hence, this thesis only deals with the development of wireless acoustic emission sensor system (AE-SS) using resonant type sensors.

2.3 AET for damage detection of concrete

Structures fail mainly by the occurrence of damage. Early-stage damage detection received more priority from engineers/researchers towards deciding the healthiness of structural components in the last few decades. More specifically, researchers focused on monitoring the healthiness of structures using vibration technique in case of mechanical, aeronautical and civil engineering communities. Because of this, various developmental work in the field of NDT using structural vibration is seen published in recent years. It is also applied in the detection of damage, identifying the severity of damage and finding the location of the source. Moreover, the necessity for early-stage damage detection in structural components leads to an increase in the use of NDT and its further developments.

Concrete is the most abundantly construction material used in the world **[62]**. Concrete structures deteriorate with time and need to be repaired **[63-65]**. The health status of concrete structures, especially the ones under rigid circumstances is imperative to human lives and properties. AET is widely used for the assessment of concrete under various types of loadings such as impact loading, flexural loading, cyclic loading and chemical stimulus such as corrosion **[66-69]**. AET is applied to monitor internal failure of concrete, which is quasi-brittle **[70]**. AET has been successfully used to classify the types of cracking in reinforced concrete structures **[71-73]**. The real-time corrosion detection ability of AET makes it a strong candidate for serving as an efficient non-destructive test method and gives advantages compared to another method of NDT **[74-75]**. Labuz et al. [**68]** carried out compression, flexural, and indentation tests on quasi-brittle materials. They had identified six intrinsic process zones when specimens were loaded to maximum stress. The length of the zone is similar even in the samples of different sizes. Soulioti et al. **[76]** have carried out four-point bending tests on fiber reinforced concrete (FRC) slabs having different fibre content, to find the correlation between the acoustic emission characteristics and concrete properties. It is observed that the activity of AE increases with an increase in the fibre content of FRC. The transition of failure mode from tensile fracture to shear fracture has been observed in the concrete slab with higher fibre content. Chen et al. **[77]** have studied acoustic emission signal generation during three-point bend testing of concrete having various notch depths and fibre content. A time delay in the appearance of AE peak during bend testing and decrease in the amplitude of AE signal has been observed with an increase in the notch depth. Weiler et al. **[78]** studied the importance of AET in concrete with three different loading scenarios like compression, three-point bending, and axial tension.

Golaski et al. **[79]** reported the applications of AE technique for in-situ monitoring of reinforced concrete, pre-stressed concrete and concrete-steel bridges. The extent of damage in concrete structures under uniaxial compression loading was evaluated by employing rate process analysis **[80-81]**. The results show that the rate of acoustic emission count generation is capable of identifying the damage behaviour in concrete without knowing its fundamental properties like Young's Modulus. AET has been applied for studying the effect of moisture content and displacement rate on the properties of underground concrete structures **[82]**. In another investigation, crack growth behaviour of fly ash and plain concretes with different periods of curing applied during uniaxial compression test has been studied using acoustic emission **[83].** The variation in the value of cumulative count (CC) with compression loading from plain concrete is similar to that from fly ash concrete for 7 and 14 days of curing period. But the variation in the value of CC for higher curing periods (28 and 56 days) is different in the two types of concrete, as depicted in **Figure 2.2 [83]**. The result indicated three distinct stages of AE activity generation in both plain and fly ash concretes, and these are attributed to micro cracking/crack closure, steady-state crack growth and unstable growth of crack **[83]**.

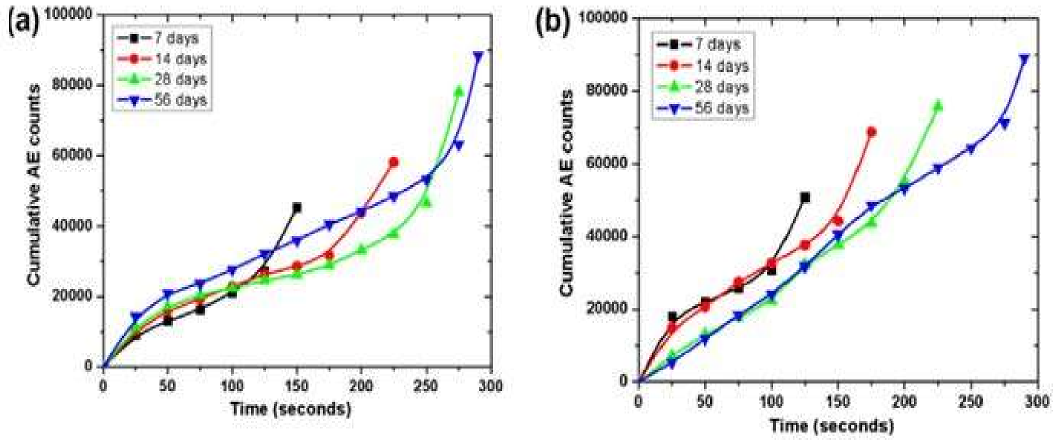

Figure 2.2 Cumulative counts (CC) by compression tests in (a) plain concrete and (b) fly ash concrete for different periods of curing **[83]**.

2.4 Acoustic emission system

A typical instrument for AET consists of sensor, preamplifier, signal conditioning unit (SCU) and computational core unit (CCU) as shown in **Figure 2.3**. The signal conditioning unit manipulates the signals received from the sensor in such a way that make them suitable for further processing without altering the characteristics of the signals. The processes involved in the CCU are data acquisition, data processing and data transmission, respectively. The data acquisition is performed by analog to digital converter (ADC). Data processing in these regards processes the signals or processes the features of the AE signals. The processed information can be transmitted through wired or wireless mode by using the communication device. Extraction of useful information from the AE signal and its interpretation through offline/online means is needed for characterizing the source. A few commercial AE systems (Mistras Physical Acoustics System, USA and Vallen System, Germany) are available, the cost of which is exceedingly high. Also, details about hardware circuit design and its software implementation towards the development of AE instrument are not furnished in the open literature because of its proprietary in nature.

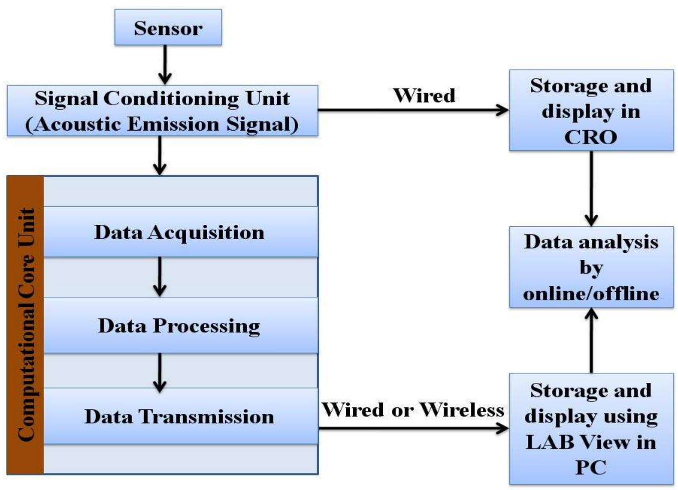

Figure 2.3 Block diagram architecture of acoustic emission sensor system.

There exist two types of systems based on data communication between the sensor unit and personal computer (PC). The one is a wired sensor system while other is a wireless sensor system. The wired system requires the use of a lengthy cable and increases workforce, wiring complexity, and maintenance cost as the number sensor nodes are increases. Also, there will be some situation where complicated in cable installation for their monitoring of a structure. With the technological improvement in wireless communication, the development of wireless sensor systems has become matured and can be applied to monitoring the healthiness of structural applications **[84-87]**.

2.4.1 Wireless structural health monitoring

Wireless structural health monitoring (SHM) systems have seen increased demand because of two reasons: low system development cost, and abilities of wireless technology for multiple distributions of sensor data for further processing **[88]**. The overall elements and working procedure in SHM involve sensor system, data gathering system, data processing and damage analysis **[89-90]**. Wireless SHM involves a much lower system and maintenance costs and saves installation time which greatly boosts the practical use of SHM. Several research papers are reported on the design development and practical use of wireless SHM. Yoon et al. **[91]** developed a wireless sensor module using AVR microcontroller and applied to the concrete beam. Yang et al. **[92]** developed a wireless SHM monitoring system with multithread sensing device using 8-bit AVR microcontroller for the measurement of vibration signals generated from the concrete structure. Hodge et al. **[93]** have carried out an extensive survey on the use of wireless sensor network for monitoring railway infrastructures. Wireless sensor-based instrumentation has been developed for natural disaster monitoring and mitigation **[94]**. A synchronized wireless sensor network for nodal analysis in SHM has been developed by using 16-bit TI microcontroller **[95]**. Sadeghioon et al. [96] have developed a smart wireless sensor network for leak detection in water pipeline using 8-bit PIC microcontroller. Chaea et al. **[97]** have developed a prototype of the wireless sensor network system using 8-bit Atmel microcontroller for health monitoring of suspension bridge using accelerometer and strain gauge sensor. Bhattacharjee et al. **[98]** have developed an intelligent wireless sensor node using 8-bit PIC microcontroller for the measurement of temperature, humidity, and light in real-time towards environment condition monitoring application. Ladgaonkar et al. **[99]** have developed a wireless sensor node using 8-bit AVR microcontroller to monitor the humidity of the high-tech poly-house environment. A prototype wireless system using FPGA and microcontroller is reported for real-time detection of active fatigue cracks in aging railway bridges using the strain gauge sensor **[100-101]**. Zhang et al. **[102]** presented the design of an acoustic emission data acquisition system using FPGA for the detection of wood damage. Grosse et al. **[103]** have developed wireless motes using 16-bit TI microcontroller for monitoring civil infrastructure in the concrete bridge by the vibration sensor. Wu et al. **[104]** presents the development of a novel wireless acoustic emission sensor platform designed using 32-bit STM microcontroller for distributed large-scale wooden structure health monitoring. Carpinteri et al. **[105]** reports a prototype acoustic emission wireless transmission system using FPGA for structural and infrastructural networks. The wireless system development and sensor networking are emerging as potential sensing models for consideration as an alternative solution to the wired monitoring system in the field of acoustic emission testing. The usefulness of AET as a potent wireless structural health monitoring system has been highlighted **[106]**.

Currently, structural health monitoring by acoustic emission technique is performed by using wired systems which have installation difficulty, noise associated with cabling, portability issues, restriction on remote monitoring capability and wiring complexity. Compared to the wired systems, the wireless systems enable remote monitoring, offer low-cost system development, and has a low maintenance cost, and thereby significantly enhancing the practical use of structural health monitoring for monitoring large-scale structures. A wireless structural health monitoring is usually a more flexible solution with the minor cost involved with the wireless system. It does not require any cable if nodes are battery-powered. Concerning a wired solution, new problems should be considered for a wireless system such as optimization of energy consumption, synchronization between the sensor unit and remote end-user, and selection of adequate low-cost sensor and sensor unit.

The development of wireless systems using different kinds of sensors based on acoustic emission, vibration, strain gauge, and accelerometer towards structural health monitoring applications is reported in open literature using FPGA and microcontroller **[92-105]**. The literature which deals with the development wireless acoustic emission sensor system is proprietary domain since the work has been carried by a limited number of organizations or agencies. Also, there is no such report available on wireless acoustic emission system using the programmable system on chip (PSoC) technology. Hence, the present work has been accomplished with minimal literature support, and cost-effective wireless sensor system has been developed by using a programmable system on chip technology. The reason for selecting PSoC is that all components of electronic circuitry (buffer, a programmable gain amplifier, successive approximation analog to digital converter (SAR ADC), comparator, counter, synchronizer, voltage digital to analog converter (VDAC), interrupt, universal asynchronous receiver and transmitter (UART), and a microcontroller to control operation and command) can be designed in single integrated circuit (IC). Because of this whole electronic circuitry can be minimized and hence reducing the board space, power consumption and system cost while improving the quality of the system development **[107-109]**. The design and development carried out in this work are the first of its kind using a programmable system on chip technology on acoustic emission technique for concrete structural health monitoring applications.

In order to develop a wireless acoustic emission sensor system (AE-SS), it is required to design, develop and validate the individual sub-systems used for designing the wireless AE-SS. These individual sub-systems are signal conditioning unit, computational core unit and a wireless communication unit. Finally, the individual sub-systems are integrated and validated for SHM of concrete. The details of individual sub-systems design with their component selection are explained subsequently.

2.4.1.1 Signal conditioning unit (SCU)

Signal conditioning unit is an integral part of the acoustic emission system, and it is required to be developed for next stage processing of AE signals. It is often necessary to acquire real-world analog signals by industrial systems for different applications. There are different physical phenomena to be measured like temperature, pressure, the intensity of light, vibration, acoustic emission, etc. by the sensor. Different applications often require the measurement of different physical entities from the real world. Different type of sensors have different electrical properties. Also, the output characteristics may vary for different analog sensors like some have voltage output and some others have current output. However, output signal amplitude of all type of analog sensors is usually weak in the range of a few hundreds of microvolts to tens of millivolts. The signal conditioning of such weak signals is required before their processing by means of amplification, filtering, isolation and range matching. The operational amplifier is most widely used in electronics design for signal conditioning of the weak signal received from a sensor. Hence, the role of the signal conditioning circuit is to modify the analog signals to make them compatible for analog to digital converter for next stage processing. The block representation of signal conditioning is shown in **Figure 2.4**.

Figure 2.4 Block diagram of signal conditioning.

A signal conditioning unit consists of buffer, amplifier, and filter corresponding to perform impedance matching, amplification, and filtering to the signal. The development of an AE-SS involves the design and development of high-performance advanced signal conditioning front-ends. The signal conditioning units are usually employed to modify the characteristics of the signals and make compatible data recording and processing by the instrument **[110]**. There are following possible set of operations to be performed like amplification, bandwidth (BW) limiting, direct current (DC) signal shifting, impedance transformation, etc. **[111]**. There are different configurations of signal conditioning units **[112].** These are used for different types of sensors like electrochemical type sensors **[113]**, MOS based type sensors **[114]**, magneto-resistive type sensors **[115]**, resistive type sensors **[116]**, inductive type sensors **[117]**, and PZT type sensors **[118]**. The switching mode type conditioning circuits are used to generate a square wave with variation in frequency **[119]** or duty cycle variation **[120]**. The growing trend for mixed-signal systems design necessitates the use of versatile signal conditioning units that require digital control for the functionality of the SCU **[121-124]**. With the integration of digitally control path to SCU, a sensor is made to operate in a smart and intelligent manner **[125]**.

It is pertinent from the above discussion that SCU is an important element in an AET system. However, sensing interface circuit design for the development of an SCU using resonant type AE sensor is not found in the open literature. Hence, the design and development of an SCU are indispensable towards obtaining correct data for interpretation for the next stage processing. It also enables to receive AE signals at a maximum dynamic range to avoid distortion using a digital gain control amplifier or by using a programmable gain amplifier.

2.4.1.2 Parameter processing of AE signal

The parameters of AE burst signals are correlated to the micromechanics of damage and fracture in materials and hence desired to be extracted in real-time. The parameters commonly used for analysis are peak amplitude, ring down count (or, AE count), root means square (RMS) value of the signal, rise time, and event duration **[57, 83]**. The burst type AE signal and its different parameters have been explained in **Section 2.2**.

For the applications related to structural health monitoring, real-time extraction of the parameters from AE signals is advantageous. The development has been reported in this direction using embedded systems **[126-129]**. But an embedded system has limitations with respect to limited computational and storage resources, transmission bandwidth, smaller data word size and relative slow clocks **[130-131]**. The challenges faced by various types of designs for embedded system approach are discussed in detail **[130-132]**. Another potential method is the combination of hardware and software co-design, which offers substantial advantages regarding cost and quality for future embedded system development **[133-135]**. The combination of hardware and software co-design enables their concurrent design and thus fulfilling the objective of the system development. This co-design concept has been implemented in the development of wireless AE sensor system for data acquisition, processing and transmission of AE signals parameters. Towards this, parameter extraction of AE signal in real-time reduces the processing load of the microcontroller, data processing and data transmission. It thus offers a solution to the constraint of an embedded system. The parameter-based technique involves comparatively low financial expense and low system physical memory usage compared to signal-based technique when implemented for long term health monitoring of concrete structures.

2.4.1.3 Data Acquisition (DAQ)

One of the essential units of AE-SS is data acquisition (DAQ). A DAQ is a system designed to acquire physical signals from the actual process **[136]**. The DAQ device is used for the acquisition and processing of acoustic emission signals without aliasing. The objective of this device is to measure, process and store the data.

A sensor can be classified in many ways, depending on how the sensor senses the incoming signal and the kind of output it delivers. In a DAQ device irrespective of the source, the signals are converted to the digital format by using an analog to digital Converter (ADC); this ADC is the crucial component of the DAQ device. The ADC must be able to track the changes in the input and should have a high resolution to reflect these changes in the output. Among various types of ADCs available most used are the Flash-type ADC, the Sigma-Delta ADC, the integrating type ADC and the Successive Approximation Register (SAR) ADC. The key difference among various types of ADCs is the way the incoming signal is sampled. Due to different methods of quantization, different ADCs provide outputs with varying sampling rate. In an ADC, the incoming signals are sampled, and once they are quantized, each signal level is assigned a binary value which is the representation of the analog signal in digital format. The DAQ main clock triggers sampling of the input signal at a periodic rate. Hence, the performance of the DAQ device will depend on the performance of ADC parameters which include resolution, dynamic range and sampling rate.

2.4.1.4 PSoC based DAQ device and computational core unit (CCU)

In an acoustic emission system, DAQ is used to acquire AE signals from SCU and transmit the signal data to a personal computer (PC)/Laptop. Whereas the role of computational core unit is to perform acquisition of signals, process the parameters of the signals and transmit the processed data to the PC/Laptop. The selection of a DAQ device or CCU is important to meet the application-specific criteria for concrete. Several embedded devices for the DAQ application are available in the market. The technological progress in the field of embedded system design has achieved the trade-off in the field of application-specific areas like automobiles, telecommunications, smart cards, missiles, satellites, computer networking, and digital consumer electronics. It is also used for real-time monitoring of the healthiness of structures as an intelligent sensor. The programmable system on chip based technology has been selected for the data acquisition and processing of AE signals. By this technology, the analog, as well as digital components, can be designed and interfaced in a single IC **[137]**. The PSoC is a family of microcontroller integrated circuits developed by the manufacturer Cypress Semiconductor. There is some other technology available such as FPGA, ASIC and microcontroller, which was established a decade ago. After comparing these technologies, it is found that FPGA is less expensive than ASIC. In a situation where both of them are required, FPGA is designed in the Lab, but ASIC is designed outside the Lab. Because of this, FPGA is less costly than that of ASIC. But, ASIC is technologically superior and most versatile compared to FPGA. Whereas both PSoC and FPGA are quite handy, PSoC is less expensive and consumes less power than FPGA. The embedded system is programmed on the software side only. Whereas, PSoC possesses the advantage that the user can program on both software and hardware sides. Kansal **[138]** explained the benefit of PSoC selection compared to ASIC, FPGA and microcontroller.

The difference between PSoC and micro-controller unit (MCU) is that the PSoC includes both analog and digital modules, and can have hundreds of built-in functions. Consequently, there is a drastic reduction in design time using PSoC **[139]**. **Figure 2.5** shows the block diagram of a typical MCU that contains Central Processing Unit (CPU) and a set of peripheral functions such as ADC, DAC, UART, Serial Peripheral Interface (SPI), and general input/output (I/O), all linked to the CPU's register interface **[140]**. CPU is the heart of MCU and manages everything from setup to data movement to timing. **Figure 2.6** shows the block diagram of PSoC 5, which is quite different from MCU. The Central Processing

Unit, analog, digital, and I/O units are equally important in the PSoC system. In a PSoC, the analog and digital peripherals are interconnected with a highly configurable routing matrix, which allows users to create custom design program to meet the desired application requirements. The PSoC can be programmed to emulate an MCU, but the MCU cannot be programmed to emulate a PSoC.

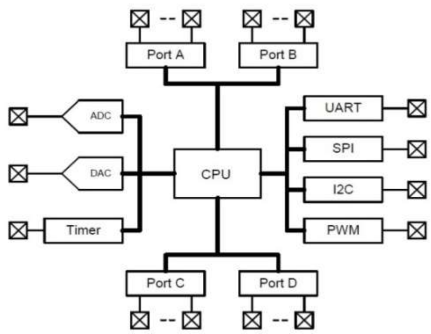

Figure 2.5 Block diagram of typical MCU **[139]**.

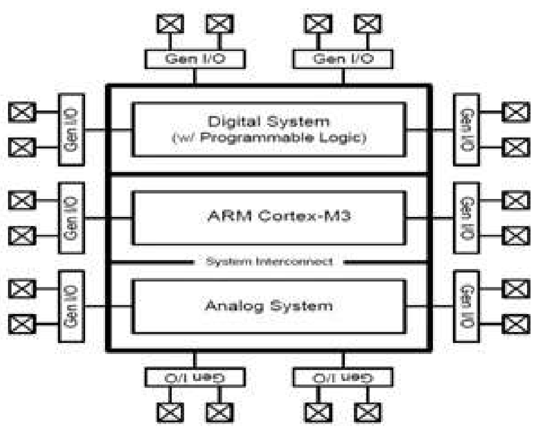

Figure 2.6 Block diagram of PSoC 5LP **[139]**.

2.4.1.5 PSoC family

There are three families of a programmable system on chip (PSoC), namely, PSoC 1, PSoC 3 and PSoC 5. The PSoC 1 uses 8-bit microcontroller core which works at a speed of 4 MIPS (million instruction per second). The PSoC 3 also uses an 8-bit microcontroller which operates at a speed of 33 MIPS. The production of PSoC 3 stared in December 2010.

PSoC is a mixed-signal array which consists of programmable digital block and analog block, and processor core giving programming routine and their interconnection. The available microcontrollers from different manufactures such as ST microelectronics, Texas instrument, Analog devices, Microchip, Intel etc. only have 8-bit, 16-bit or 32-bit processor core. PSoC enables the integration of complete analog and digital circuit design along with microcontroller single integrated circuit (IC). Because of this, the overall bill of material (BOM) costs for system design gets reduced. Also, PSoC has exceptional flexibility for programmable analog and digital circuit design that uses a PSoC creator integrated development environment (IDE). This IDE provides the combined hardware and software design to the programmable system on chip for version 1, 3 and 5 based system development. The processor used in PSoC 1, PSoC 3, and PSoC 5 is M8C, 8051 and ARM Cortex M3 processor core respectively. PSoC has three separate memory such as memory registers, flash memory for instructions and fixed data, and SRAM for data, accessing and command control to the configurable logic block and their intended functions. Application peripheral Interfaces (APIs) initialize the user selected components in Visual Studio (VS) or LabView for the graphical user interface (GUI). PSoC 5 is the latest disruptive technology because of its powerful ARM-based processor. The IDE design tools and architecture of PSoC 3 and PSoC 5 are compatible with each other. PSoC 5 has 32-bit ARM Cortex M3 processor core which performs at a speed of 100 MIPS. **Figure 2.7** shows a comparison of PSoC 1, PSoC 3, and PSoC 5.

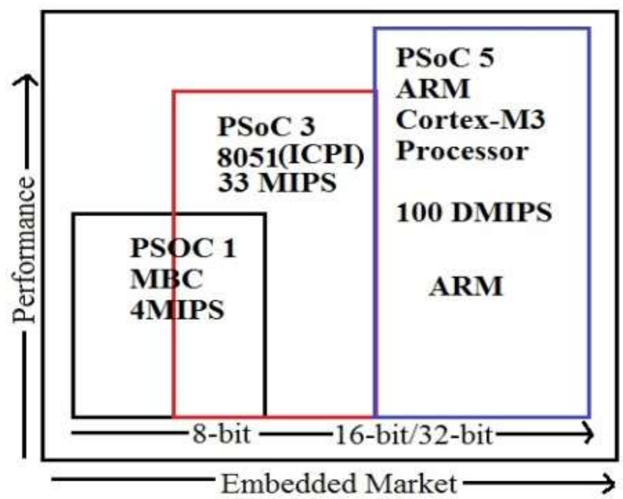

Figure 2.7 Comparison of PSoC family.

PSoC architecture is widely used for numerous applications. Fernando et al. **[141]** have used the PSoC architecture to design a data acquisition system for the educational purpose. In another study, J. Guevara et al. **[142]** have designed data acquisition, control and wired remote display system using PSoC. Similarly, in **[143]**, PSoC-5 based system has been used by Hyejung Kim et al. to demonstrate a technique to design low-cost and highly accurate ECG data acquisition system. In a separate study **[144],** the analog system of PSoC-1 has been used by Cabrera Lopez et al. to realize a reconfigurable filter stage. This system can adapt itself as per the incoming signal. Usage of PSoC in the wireless sensor node is proposed **[145],** where, Fatecha et al. have used the configurable capabilities of the hardware to minimize the power consumption.

The programmable system on chip kits has a right balance among different components, i.e., analog blocks, digital blocks and processor. This offers a single chip solution to different design applications. The production of PSoC 5 started in the second quarter of 2011. PSoC 5 architecture has programmable and configurable analog and digital blocks of sub-systems. There are different blocks of programmable analog sub-systems with a good precision used in PSoC 5. These are 12-bit SAR ADC, 20-bit Delta-Sigma ADC, DAC, Mixers, PGA (programmable gain amplifier) with 25 mA driving capacity, Op-Amps etc. which can be configured to satisfy the design requirements. There are different blocks of digital sub-systems used in PSoC 5 which include digital logic blocks, counter, timer (8, 16, 24 and 32-bit timers), and pulse width modulation (PWM) that can be configured and programed. There are some digital peripheral components available with PSoC 5 like pseudo-random sequence (PRS) generators, quadrature decoders, and cyclic redundancy check (CRC). It also supports wide ranges of communication interfaces including UART, SPI, I2C, CAN and USB, for data communication. The current consumption for PSoC 5 in sleep mode is 2.0 μA, whereas it is 2.0 mA in active mode **[137]**. The new and disruptive architecture of PSoC 5 consumes extremely low power and can be operated in a 0.5 to 5.5

voltage range. It offers programmable routing for any analog signal or digital signal to any general-purpose input/output device for easy circuit board layout. By considering the characteristics of different PSoCs, it is found that PSoC 5 is a new disruptive technology which can work with both analog and digital circuit blocks along with the microcontroller on a single system on chip IC.

2.5 Motivation and objective

A wireless AE system offers several advantages over the existing wired based AE systems for online monitoring of structures. Some of the benefits of wireless AE systems are compactness, ease of installation, low wiring complexity, low power consumption capability, economical (associated with low cabling cost) and remote operational capability. Thus, the development of a wireless AE system seems attractive.

A few commercial AE systems are available, the cost of which is very high and the details of instrumentation are also not furnished. A few papers have reported the design and development of wireless systems for vibration, strain gauge, and accelerometer towards SHM applications based on FPGA and microcontrollers. However, for continuous monitoring of structures, typical AE sensing systems demand compact, portable and less power consuming (preferably battery operated) devices. Distributed AE sensing also demands less wiring complexity for ease of deployment and maintenance. Thus, the development of a programmable system on chip based wireless system is expected to be efficient for AE applications. However, information related to wireless AE systems lies in the proprietary domain and scarce in the open literature. Hence, there is a strong requirement for dedicated efforts to develop wireless acoustic emission sensor system for structural health monitoring applications. In order to design and develop the wireless AE sensor system, several novel design steps, challenges and issues were addressed in the thesis, as mentioned below:

1) Design of signal conditioning circuit for acoustic emission signals which enables maximum dynamic range and rail to rail input-output swings for next stage processing of AE signals.
2) Development of methodologies and its hardware implementation to extract the AE features and transmission of data in a wireless environment.
3) Design of compact system on chip-based hardware and software for acquisition and processing of AE signals for structural health monitoring applications.
4) Selecting the appropriate protocol towards establishing communication between the sensor unit and the control unit for wireless data transmission.
5) Finally, implementation and test validation of the designed and developed wireless AE system for typical SHM applications.

Following objectives have been set to meet the above challenges and to address the issues.

1) Design development and validation of a signal conditioning unit for the acoustic emission signals.
2) Design of hardware-based parameters extraction for the burst type AE signals using Multisim software.
3) Design development and validation of embedded hardware and software for acquisition and processing of an event of AE signals using a programmable system on chip.
4) Acquiring AE signals from sensors through embedded hardware and software using the programmable system on chip. Extraction of AE parameters from the received signal and wireless transmission of AE parameters.
5) Validating the performance of the wireless AE system with a commercially available wired AE system in the laboratory for SHM of concrete.

2.6 Organization of the thesis

The rest of the thesis is organized into four major working chapters addressing the identified objectives, towards developing a wireless acoustic emission sensor system for structural health monitoring applications, followed by conclusions and future works.

Chapter 3 presents the design and development of signal conditioning unit for the acquisition of acoustic emission signals towards application to concrete as well as to metallic materials. The performance of the in-house developed SCU has been compared with a commercially available one, and the results are presented in this chapter.

Chapter 4 proposes a simulation study for the extraction of parameters from AE signal such as peak amplitude, ring down count or AE count, RMS, rise time and event duration. Multisim software is used for simulation of the hardware design, and the results are presented in this chapter.

Chapter 5 explains the data acquisition of acoustic emission signals using the programmable system on a chip. Fast Fourier Transform (FFT) has been performed for the signal analysis and validation of the acquisition unit.

Chapter 6 discusses the prototype design aspects and development of wireless AE-SS for structural health monitoring of concrete. The integrated prototype system has been fabricated, assembled and validated in the laboratory by signal validation tests, and by conducting compression tests and corrosion test on concrete specimens for dynamic detection of defects.

Chapter 7 summarizes the major conclusions drawn from the research work and provides the scope for future research.

3 Design development and validation of the signal conditioning unit

3.1 Preamble

This chapter presents the details of in-house design and development of a signal conditioning unit (SCU) for the acquisition of acoustic emission signals from metallic and concrete materials. The performance of the developed SCU has been compared with a commercially available one, and the results are presented in this chapter.

3.2 Introduction

A piezoelectric type sensor is used to detect acoustic emission signals generated from the surface of an object under test. For most of the metallic and concrete structural health monitoring applications, the AE sensor frequency lies in the range of 100 kHz to 400 kHz and 20 kHz to 100 kHz, respectively **[146]**. The raw AE signal acquired by a piezoelectric sensor is of very low level, usually in the range of microvolts (μV), and needs to be amplified for further processing. Hence, there is a strong requirement to develop SCU to maximize the dynamic range of AE signals and to make it suitable for analog to digital conversion for correct AE data representation. A schematic representation of a typical acoustic emission system consists of (a) sensor with an integral pre-amplifier, (b) signal conditioning unit and (c) data acquisition (DAQ) as shown in **Figure 3.1**. The detailed descriptions of each block are explained in the subsequent sections.

Figure 3.1 Block diagram of the acoustic emission system.

3.3 Sensor with integral pre-amplifier

3.3.1 Sensor

Selection of the proper frequency range of an AE sensor is important for any particular application, and different factors to be considered for sensor selection are the nature of material or object under test, type of environment, and test condition. Acoustic emission sensors are mostly specified for normal environmental condition as one would practice during field testing or testing in the laboratory. **Table 3.1** provides the specifications of two different piezoelectric resonant sensors used for the validation studies of the developed SCU for application to metallic materials. Both sensors have integral pre-amplifier and are manufactured by M/s. Physical Acoustics Corporation (PAC), USA. The sensors (PK15I and R15I) resonate at 150 kHz and operate in the frequency range from 100 to 450 kHz and 50 to 400 kHz, respectively. The sensor PK15I, selected for the validation test requires 5.0

mA current in an active mode which needs an excitation of 5.0 volts and is used with the developed SCU in the laboratory. The sensor R15I needs DC excitation of 28 volts to the pre-amplifier and is used with the commercially available SCU (PAC, USA) system. Both sensors are directly mounted on the metallic plate by using vacuum grease as couplant.

Table 3.1 Specifications of the sensors used for metallic material

Specifications	Sensor (PK15I)*	Sensor (R15I)**
Type	Integral	Integral
Operating Frequency Range	100-450 kHz	50-400 kHz
Resonant Frequency	~150 kHz	~150 kHz
Input Voltage	5 Volt	28 Volt
Pre-amplifier Gain	26 dB	40 dB

* Sensor (PK15I) is used with the developed SCU in the laboratory
** Sensor (R15I) is used with the PAC, USA system

Table 3.2 provides the specifications of the sensor used for the concrete specimen. The sensor PK6I has been used for the validation of SCU. The AE signal generated from concrete is burst type. Hence, the resonant type AE sensor has been selected for this work. The sensor (PK6I) manufactured by M/s. PAC, USA is used in the system which requires 4 to 7 Volts DC power supply and has a resonant frequency at 55 kHz. The sensor gives a good response in the frequency band of 35 to 65 kHz and has an integral pre-amplifier of 26 dB gain. The sensor is directly placed on the concrete beam using vacuum grease as couplant so that AE event can be easily sensed with less noise.

The sensor has an integrral pre-amplifier. The weak signal acquired by the sensor is amplified by the integral pre-amplifier and the amplified signal becomes sufficiently strong to tolerate any noise, towards post-amplification or further processing. The pre-amplifier matches high impedance of sensors to low impedance of signal cable in order to avoid signal degradation (typically 20 kΩ to 50 Ω). High input impedance requires only a minimal amount of current to sense the input signals. The pre-amplifier is kept very close to the sensor. The sensor with integral pre-amplifier has been selected for the detection of AE signals in this work. The integral pre-amplifier is a charge-coupled amplifier having moderate gain, high bandwidth, high common-mode rejection ratio (CMRR) and excellent signal-to-noise ratio (SNR).

Table 3.2 Specifications of the sensor used for concrete specimen.

Specifications	Sensor (PK6I)*
Type	Integral
Operating Frequency Range	35-65 kHz
Resonant Frequency	~55 kHz
Input Voltage	5 Volt@5mA
Pre-amplifier Gain	26 dB

* Sensor (PK6I) is used with the developed SCU in the laboratory.

A low power sensor with integral pre-amplifier of 26 dB fixed gain is used to increase the signal level form microvolt (μV) to millivolt (mV) range of the output of pre-amplified signal interfaces with the SCU. The design details of sensing SCU is explained below.

3.4 Signal conditioning unit

The signal conditioning unit is an integral part of the acoustic emission system, and it is a basic component of all measurement devices. A wide range of sensor signals can be fed as input to the SCU towards giving their optimal level for next stage processing and analysis. **Figure 3.2** shows the schematic functionality of the proposed SCU.

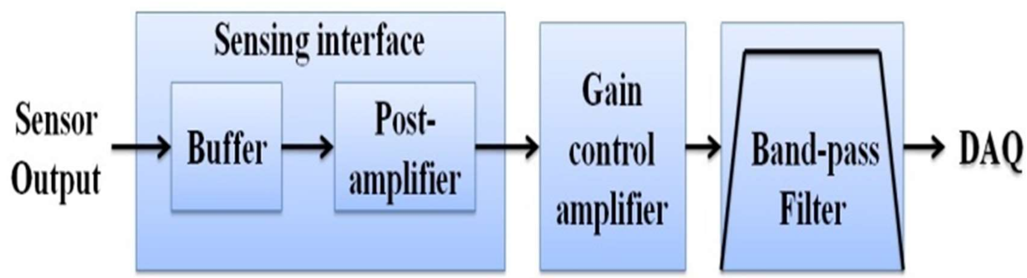

Figure 3.2 Block diagram of the signal conditioning unit.

As shown in **Figure 3.2**, the SCU consists of a buffer, post-amplifier, gain control amplifier and bandpass filter. The SCU is directly connected to the sensor output, and the output of the SCU is connected to the data acquisition (DAQ) which essentially consists of an analog to digital converter (ADC). The commercially available Agilent DAQ is used for a preliminary study of the AE signal received from the conditioning unit. Development of a dedicated DAQ for wireless AE system is presented in **Chapter 5**. The design details of signal conditioning blocks are discussed in subsequent sections.

3.4.1 Sensing interface circuit

The primary function of the conditioning unit is to acquire a signal from an AE sensor without degrading the signal to noise ratio. The sensing interface circuit senses the pre-amplified signal from the sensor. The amplified signal is fed to the buffer and subsequently to the post-amplifier, as shown in **Figure 3.2**. There are diffrent important parameters are to be consider while designing the sensing interface circuit which include:

1. Impedance matching
2. Amplification gain
3. Frequency bandwidth

The buffer provides impedance matching to the load. Impedance matching is in practice used for maximizing the power transfer or minimizing signal reflection from the load. The voltage buffer is a unity gain amplifier which is also called a voltage follower because the output voltage follows or tracks the input **[147]**.

The signal amplitude received from the sensor may vary significantly depending on the strength of the source generating AE. Therefore, gain adjustment is required to amplify the output voltage levels appropriately for optimal use of the analog to digital conversion by using post-amplifier.

The decibel (dB) is the most common way of quantifying the gain of an amplifier. The gain is expressed by the following equations **[147]**.

$$\text{(Gain)dB} = 20 * log\frac{Vout}{Vin}\text{----------------------------}\textbf{(3.1)}$$

where, Vout = output voltage of the amplifier, Vin = input voltage of the amplifier

The dual operational amplifier based small outline integrated circuit (SOIC) AD8629 (manufactured by M/s. Analog Devices) has been selected for this buffer and post-amplifier design in a single integrated circuit. The integrated chip AD8629 has features of wide bandwidth, rail-to-rail input and output swing, and low noise **[148]**. The circuit interconnection and the components used in the design of the sensing interface circuit are shown in **Figure 3.3**.

The post amplifiers have the gain of 12 dB to the pre-amplified signals. Thus, a total gain of 38 dB has been provided to the raw AE signals to bring the voltage level from mV to Volts range. In this design, the signal is shifted to a DC level of $V_{cc}/2$ to see the full swing of the AE signal in the range of zero DC level to V_{cc}. Where V_{cc} is the supply voltage of 5 volts. A supply voltage of 5 volts is required for the excitation of integrated circuit (IC). The DC shifted signal is corrected in the software while processing the AE data.

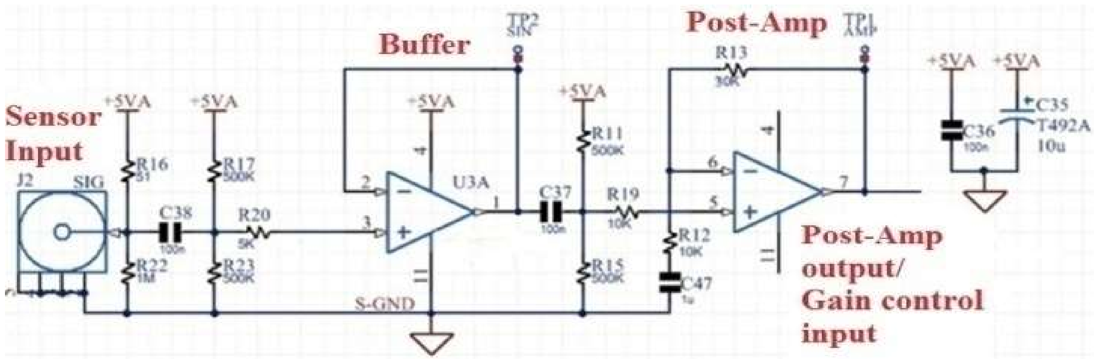

Figure 3.3 Sensing interface circuit design.

3.4.2 Gain control amplifier

A digital gain control amplifier is used in this design to provide a wide amplitude input signal range. The gain-bandwidth product (GBP) is an important parameter for the performance and its selection of the operational amplifier **[147]**. The GBP for a given amplifier is constant. It means that if gain increases then BW reduces **[147]**.

Several gain control stages provide the best coverage of the input signals, which can be varied in steps of 3 dB and maximum up to 45 dB **[149]**. The IC AD8369 (M/s. Analog Devices) has been selected for the high performance digitally controlled gain control amplifier having a wide bandwidth of 600 MHz **[149]**. Hence, the selected IC is suitable for the application of both concrete as well as metallic materials without distortion of signals. The post-amplifier output is routed through the digital gain control amplifier. The biasing circuit of the gain control amplifier is shown in **Figure 3.4**.

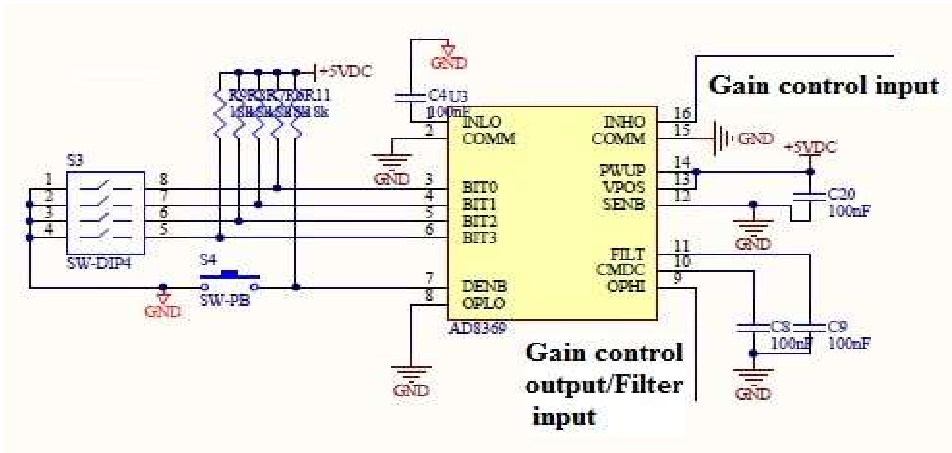

Figure 3.4 Circuit design for the digital gain control amplifier.

3.4.3 Filter design

Noise is a common and pervasive problem in electronics design and debug. It originates from numerous external and internal sources to disturb the signals of interest **[150]**. A major concern in noise-related signal is the measurement of true voltage of the signal. Noise makes the measurement of timing difficult by increasing jitter. It is required to have the signal noise-free and clean for the intended design of signal conditioning **[150]**. The pickup sensor output signals are affected by external noise; hence a filter circuit is to be included to reduce noise. The frequency of application of acoustic emission signals for metallic and concrete lies in a certain frequency band. Hence there is a strong need to design bandpass filters that can be used to isolate or filter out certain frequencies of AE signals that are lying within a particular band or range of frequencies. There are two cascading stages involved in the design of bandpass filter, one stage is high pass filter, and another is low pass filter. The bandpass filter is designed by cascading the high pass filter and the low pass filter. The bandpass filter passes signals within a certain band or spread of frequencies without distorting the input signal. The equation for the upper and lower cut-off is given below **[151]**.

$$\text{High pass cut} - \text{off frequency} = \text{fL} = \frac{1}{2\pi \text{R1C1}} - - - - - - - - - (\mathbf{3.2})$$

$$\text{Low pass cut} - \text{off frequency} = \text{fH} = \frac{1}{2\pi \text{R2C2}} - - - - - - - - - - (\mathbf{3.3})$$

A passive linear bandpass filter circuit has been designed and simulated with an artificial signal of 150 kHz in Multisim, as shown in **Figure 3.5**. The simulated result is used for the design of the filter. It is clearly seen that the passband width of the filter can be controlled by the positioning of the two cut-off frequency points of the two filters. The upper and lower cut-off frequencies of the bandpass filter are approximately 402 kHz and 100 kHz respectively for metallic material.

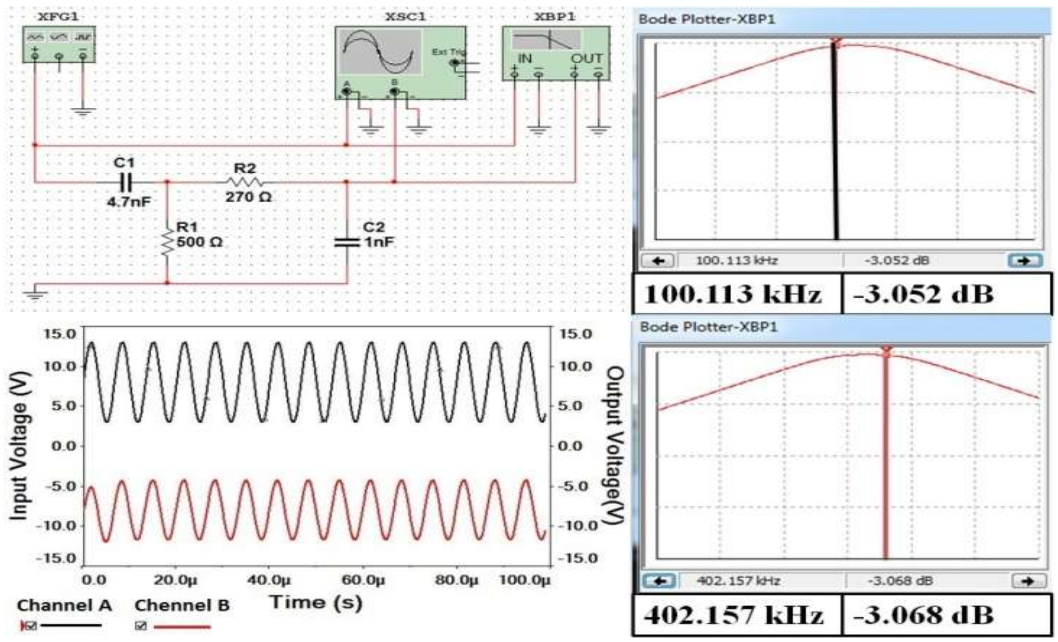

Figure 3.5 Schematic design and simulation results of the bandpass filter.

As per the design, sensing interface circuit, gain control amplifier, and bandpass filter has been fabricated and assembled in a two-layer PCB. The photograph of the assembled prototype signal conditioning unit is shown in **Figure 3.6**. The integrated prototype SCU has been validated by conducting pencil lead break (PLB) tests on both metallic materials (AISI type 310 stainless steel) and concrete in the laboratory. The experimental descriptions and their results are presented in the subsequent section.

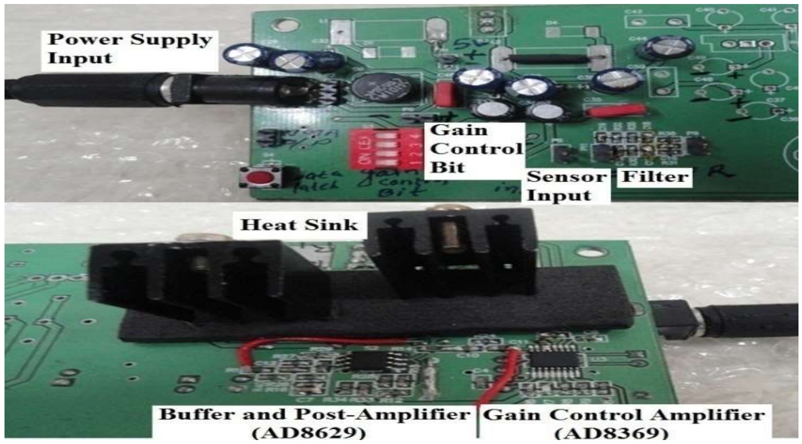

Figure 3.6 Photograph of prototype signal conditioning unit.

3.5 Design validation of the SCU

3.5.1 Metallic material

Experiments have been performed for the validation of signal conditioning unit by capturing artificial AE events generated on a 310 stainless steel (SS) plate by using a commercially available wired AE system. The experimental setup has been made in the laboratory for the acquisition and analysis of AE signals using the in-house developed SCU as well as a commercially available one from M/s. Physical Acoustics Corporation (PAC), USA. The photograph of the experimental setup is shown in **Figures 3.7 (a)** and **(b)**. The pencil lead is made to break against the surface of the material/structure under test. The surface of the structure gets deformed by breakage of the pencil lead and this results in the sudden release of acoustic energy which propagates throughout the structure **[152]**.

The AE signals generated from the PLB tests at different locations of the SS plate are stored in ASCII form by using the data acquisition unit for post-analysis. Two similar sensors of the model (PK15I) were connected to channels 1 and 2 of the data acquisition unit of the developed SCU (**Figure 3.7a)**. Two other similar sensors of the model (R15I) were connected to channels 1 and 2 of the PAC system (**Figure 3.7b**). In **Figure 3.7**, Sensor 1 and Sensor 2 represent Channel 1 and Channel 2 of the two systems. The event of AE signals was captured by both the developed SCU coupled with Agilent DAQ system (**Figure 3.7a**) and the PAC, USA system (**Figure 3.7b**) simultaneously when it crosses the particular threshold voltage. The value of the threshold voltage varies depending on the background noise generated from the physical environmental condition. The PLB tests were conducted at different distances of 20 cm, 40 cm, and 60 cm from sensor 1 to capture the single event of AE signal using both sensors 1 and 2. The event of the AE signal generated by the PLB tests at different locations was stored in the data acquisition unit as well as in the PAC system for plotting and further analysis using Origin software.

Figure 3.8 and **Figure 3.9** show the time domain AE signals from pencil lead break test acquired by the developed SCU and by the PAC system, respectively. **Figure 3.8** and **Figure 3.9** show the measured time differences between the signals captured by two sensors from PLB tests. The PLB tests are performed at locations of 20 cm, 40 cm and 60 cm from sensor 1 and 100 cm, 80 cm, 60 cm from sensor two respectively. The pattern of AE signals and the measured time differences of the signals from the developed SCU (**Figure 3.8**) matches well with the results obtained from the commercially available PAC system (**Figure 3.8**).

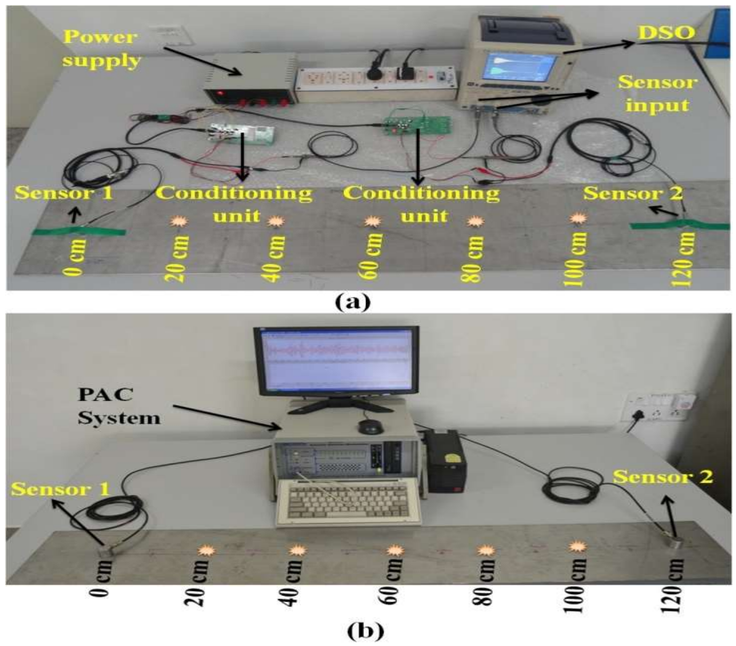

Figure 3.7 Photograph of experimental setup used for acoustic emission testing on a metallic plate using **(a)** developed signal conditioning unit and **(b)** commercially available PAC system.

The measured time differences are 259 μs, 129.5 μs, and 0 μs. In this 0 μs delay indicates that the source of AE lies at the midpoint of the two sensors. The longitudinal velocity of the stress waves computed with this time delay was found to be 3088 m/s which also matches well with the longitudinal velocity of the sound wave in AISI type 310 stainless steel **[153]**.

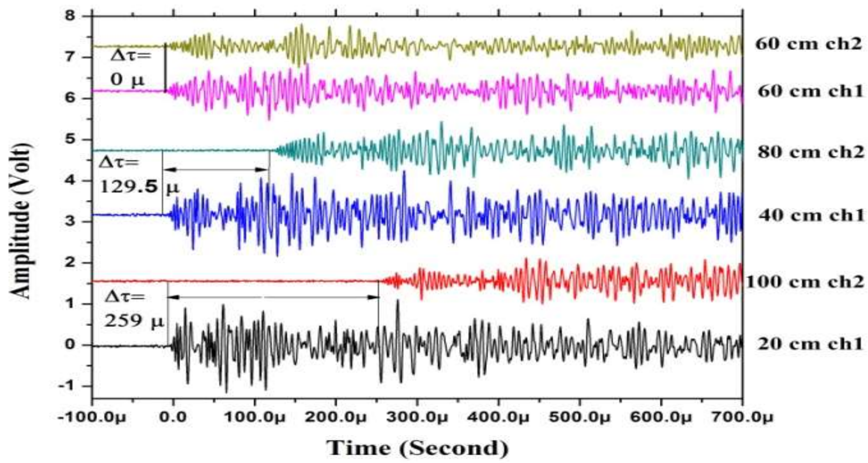

Figure 3.8 Result of pencil lead break test of AE signals for the plate received from sensor one and sensor two respectively by the developed conditioning unit.

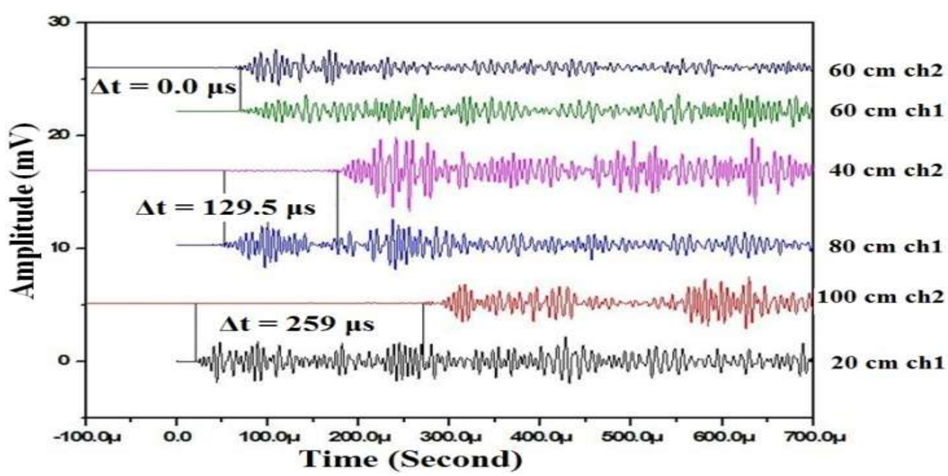

Figure 3.9 Result of pencil lead break test of AE signals for the plate received from sensor one and sensor two respectively by the PAC system.

The frequency spectra of the captured AE events were also compared by computing Fast Fourier Transform (FFT) of the time domain signals captured at different locations. **Figure 3.10** shows the power spectral density of the signals received by the PLB tests of the SS plate at distances of 20 cm, 40 cm and 60 cm from sensor one which is connected to channel 1 (ch1) of the in-house developed SCU. **Figure 3.11.** shows the similar results obtained using the commercial PAC system. It can be seen that the peak frequency of the signals acquired by both the systems is approximately the same. Also, it can be seen that the peak frequency of the event occurring at different locations for both the systems is approximately the same, i.e., peak frequency is 125.34 kHz for tests at distances of 20, 40, and 60 cm from channel 1 using the developed SCU; and frequency is 122 kHz for tests at 20, 40, and 60 cm from channel 1 using the PAC system. In both the systems, the peak frequency varies within the operating frequency range (100 kHz to 400 kHz) of the sensor. However, there is statistical fluctuation in frequency caused by any minute difference in excitation by an external force applied during the pencil lead break test. Since the characteristics of the source influence the frequency content of the propagating AE signal [152].

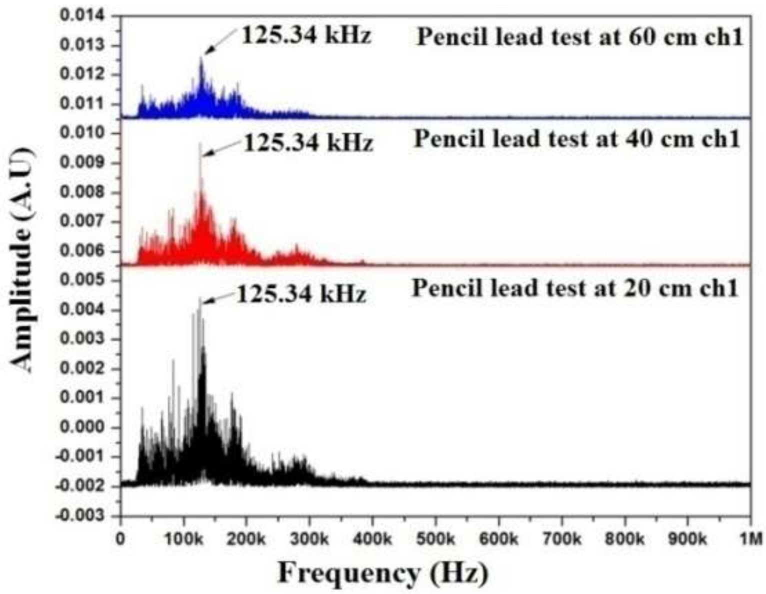

Figure 3.10 FFT of PLB test signals acquired using the developed SCU.

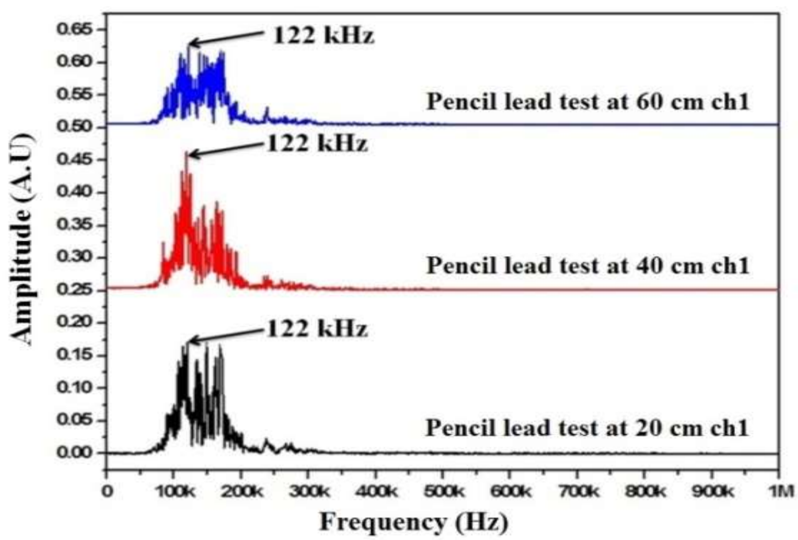

Figure 3.11 FFT of PLB test signals acquired using the PAC system.

3.5.2 Concrete

An experiment has been performed for the validation of the developed signal conditioning unit for concrete material. The frequency of operation of AE for concrete is different from metallic materials. Hence, the bandpass filter has been designed with their upper and lower cut-off frequencies of 27 kHz and 90 kHz respectively for concrete material.

An experimental setup was made for the acquisition and analysis of AE signals using the in-house developed signal conditioning unit. A concrete beam of dimension (length = 400 mm, breadth = 100 mm, thickness = 100 mm) was used for the experiments. The experimental photograph of the test setup is shown in **Figure 3.12**.

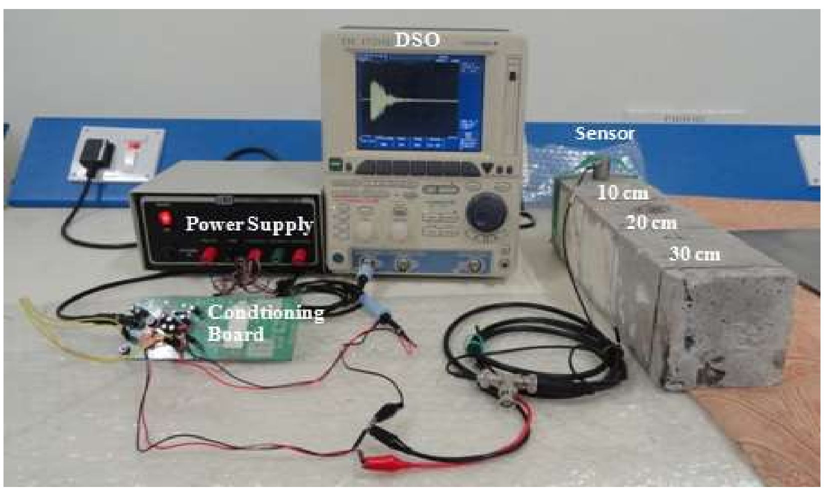

Figure 3.12 Photograph of the experimental setup used for acoustic emission testing in concrete.

The commercially available Agilent digital storage oscilloscope (DSO) was used for data recording and display. The measured voltage level in the DSO is 20 mV without pencil lead break test, and the trigger was set in the channel to capture the signal event on DSO. The pencil lead break test was done at different locations on the concrete beam, i.e. at 10 cm, 20 cm and 30 cm from the PZT sensor to capture the single event of the AE signal. The sensor PK6I was used with the developed SCU, as shown in **Table 3.2**. When the signal level crosses the particular threshold voltage, one event is recorded. The event of the AE signal generated by pencil lead break tests at different locations is stored in the DSO for further analysis. The captured AE signals were analyzed by processing, computing the event statistics and peak analysis.

The signals acquired by the PLB tests at different locations on the concrete beam were used for finding the resonant frequency and peak amplitude of the AE signal. Figure 3.13(a), Figure 3.13(b) and Figure 3.13(c) show the PLB signals and the corresponding FFT for the distances of 10 cm, 20 cm and 30 cm from the sensor respectively.

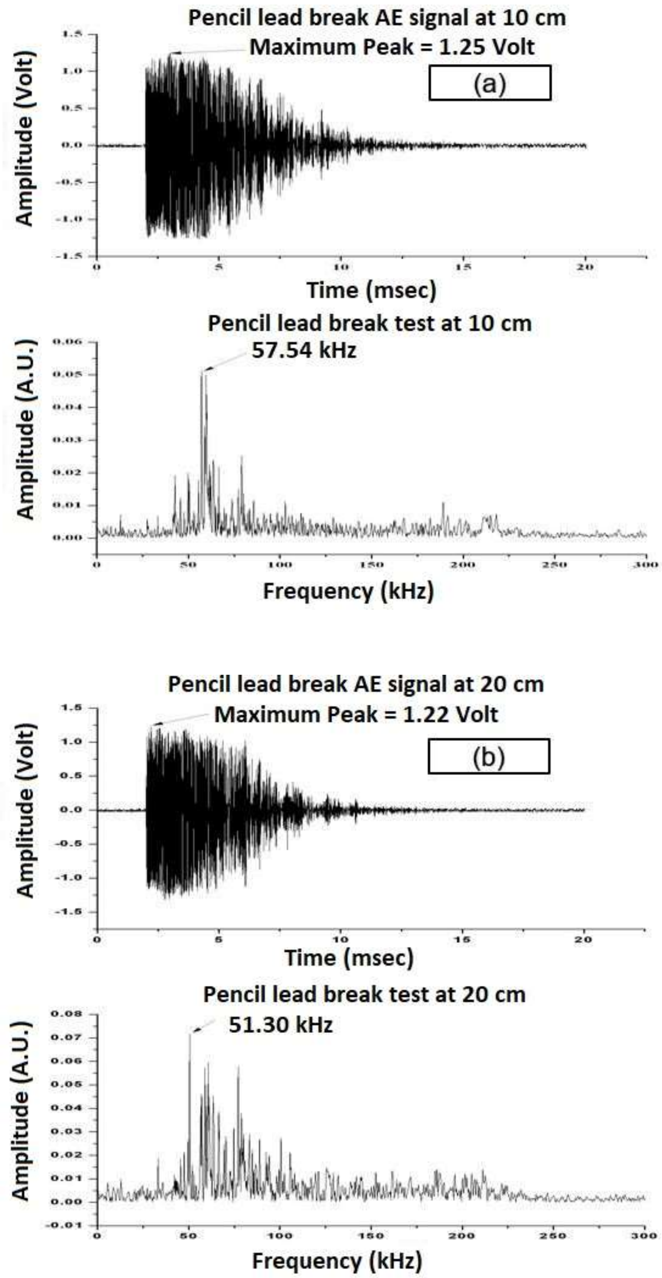
Pencil lead break AE signal at 10 cm
Maximum Peak = 1.25 Volt
(a)
Amplitude (Volt)
Time (msec)
Pencil lead break test at 10 cm
57.54 kHz
Amplitude (A.U.)
Frequency (kHz)
Pencil lead break AE signal at 20 cm
Maximum Peak = 1.22 Volt
(b)
Amplitude (Volt)
Time (msec)
Pencil lead break test at 20 cm
51.30 kHz
Amplitude (A.U.)
Frequency (kHz)

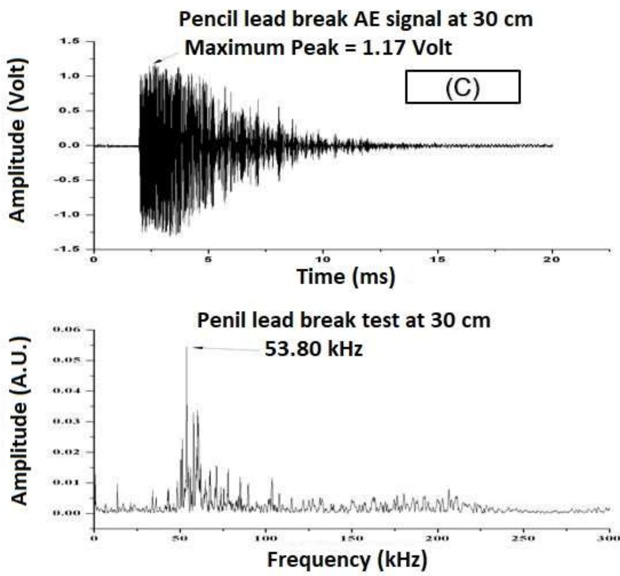

Figure 3.13 PLB signals and corresponding FFT for distances of 10 cm (a), 20 cm (b) and 30 cm (c) from the sensor.

It can be absorved that the resonant frequency of the event occurring at different locations is approximately the same (51 kHz to 57 kHz), which varies around the resonating sensor frequency (55 kHz). As the distance of the AE source increases from the sensor, the amplitude of the signal decreases. This is due to the attenuation of the AE signal as given in **Figure 3.14**. The result of decreasing amplitude with the increasing distance shown in **Figure 3.14** is in line with that reported in the literature **[154]**.

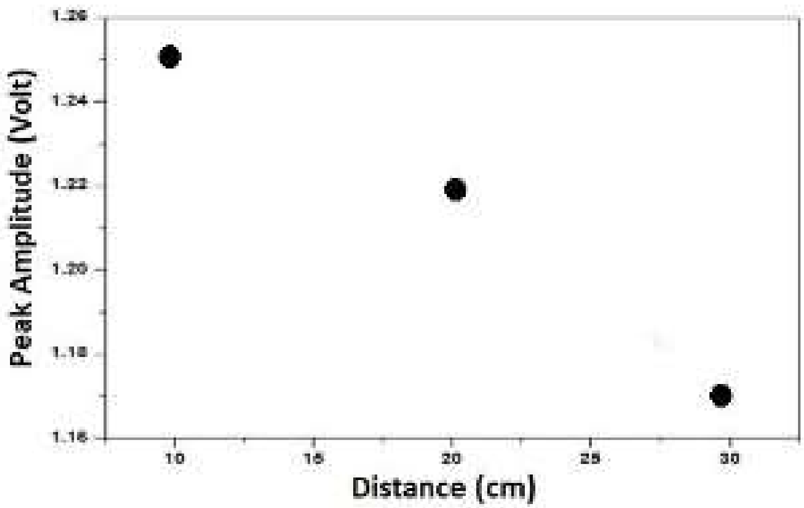

Figure 3.14 Peak amplitude of the AE signal versus distance from the sensor.

3.6 Summary

A signal conditioning unit has been designed and developed for amplification and filtering noise in the acoustic emission signals for the resonant sensor. The buffer, post-amplifier, gain control amplifier, and filter has been designed and integrated for the development of SCU. The developed SCU provides a wide range of sensor signals, rail-to-rail input and output swings, and reduces the complexity of biasing and provides an optimal level for further processing of AE signals. An appropriate bandpass filter has been designed and simulated for application to metallic materials as well as to concrete structures to avoid external noise interruption with AE signals. A combination of high pass and low pass filter has been designed with their 3 dB cut-off frequency of 100 kHz- 400 kHz for metallic material and 27 kHz - 90 kHz for concrete respectively. The performance of the in-house developed SCU has been compared with a commercially available system through the pencil lead break test. The time-domain and power spectral density of the AE events reproduced by the in-house developed SCU and a commercially available system has been found to agree with each other. The resonant frequency at different locations is found to be the same and lies within the operating frequency range from 100 to 400 kHz for metallic material and 35 to 65 kHz for concrete respectively.

4 Simulation study for parameters extraction of burst type AE signals

4.1 Preamble

This chapter proposes a new approach for transmitting the parameters of burst type AE signals as against the entire signals over a wireless network, which would require huge computational and hardware resources. It presents the hardware design using Multisim simulation software and experimental validation of the hardware for extracting the AE signal parameters.

4.2 Hardware design for parameter extraction

Subsequent to the amplification and filtering of AE signals from the source using the SCU, processing of the signals needs to be carried out to extract features for meaningful interpretation of the results. But, wireless transmission and processing of the complete AE signals require huge bandwidth and computational resources, respectively. In this context, the new and novel hardware-based design has been proposed for extracting the parameters of AE signals. Hence, this chapter is dedicated to the development of hardware for feature extraction from AE signals and its validation. A combination of analog and digital circuit design is presented in this chapter for the extraction of AE parameters using Multisim simulation software. There are different parameters of acoustic emission signals such as peak amplitude, root mean square (RMS), counts, rise time, and event duration. Parameter-based analysis technique is routinely applied for the burst type AE signals. The derived parameters in turn are correlated to the deformation and fracture behaviour of materials. In this technique, parameters from received burst type signals are extracted without saving the waveforms at the controller. Parameter-based AE technique is advantageous over the signal-based technique with reference to storing speed and data acquisition. The parameter-based AE system will not have any shortage of computational resources and requirement of bandwidth compared to waveform-based or signal-based AE system when dealing with a large amount of data to be acquired and transmitted. The attributes of signal-based technique require huge computational resources and large transmission bandwidth. The parameter-based technique seems beneficial and advantageous in view of low cost, low physical system memory, and low transmission bandwidth towards long term monitoring of structures.

The schematic design of a hardware system for extraction of the parameters from the AE signal is shown in **Figure 4.1**. It consists of a signal processing board (AE Board) and microcontroller blocks in addition to the sensor and the SCU. The details of the SCU have been discussed in the previous chapter. The output signal from the SCU is fed into the AE Board, as shown in **Figure 4.1**. A combination of analog and digital circuit design is embedded in the AE board for extracting the AE parameters. The AE Board uses two crystal clocks (frequencies 100 kHz and 50 kHz) which will be used for measuring timing-related AE parameters. The microcontroller block is used for parameter processing and real-time control.

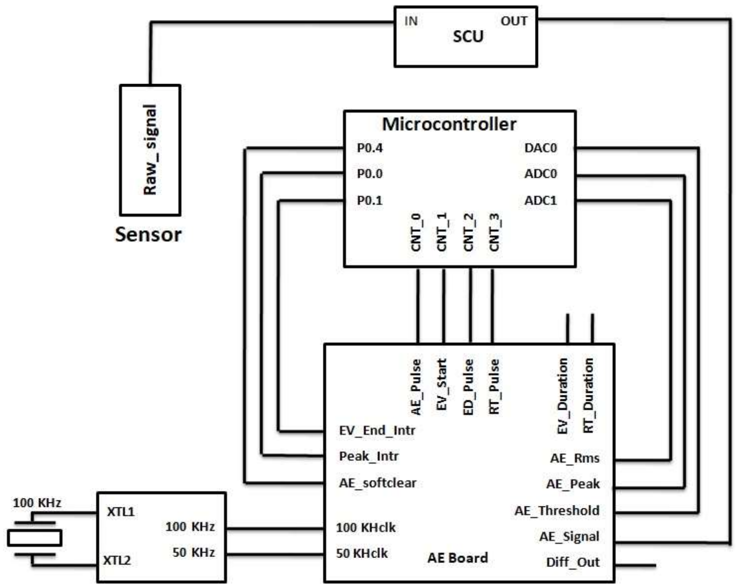

Figure 4.1 Schematic design of a hardware system for parameter extraction of the AE signal.

A flow chart representing the working function of the hardware system design is shown in **Figure 4.2**. An AE signal event occurs randomly, and it could be attributed to the redistribution of localized strain energy that is generated by microscopic changes in a material/structure under load. When the system starts, it continuously monitors the activity of AE signals during loading condition. The event of the AE signal is detected when the signal level crosses the threshold set by the digital to analog converter (DAC0) of the controller block. Typically, an AE signal consists of a train of bursts of diminishing energy, and there is no activity between the consecutive bursts. The controller block starts extracting the parameters when the burst signal reaches the peak amplitude and completes at the end of the signal. Therefore, at the end of each AE burst, the circuit has to extract all the parameters. The controller block triggers the software command signal (AE_Softclear) to reset the AE board so that the system becomes ready for the parameter extraction from the next burst. The design description of the AE board is explained in the subsequent section.

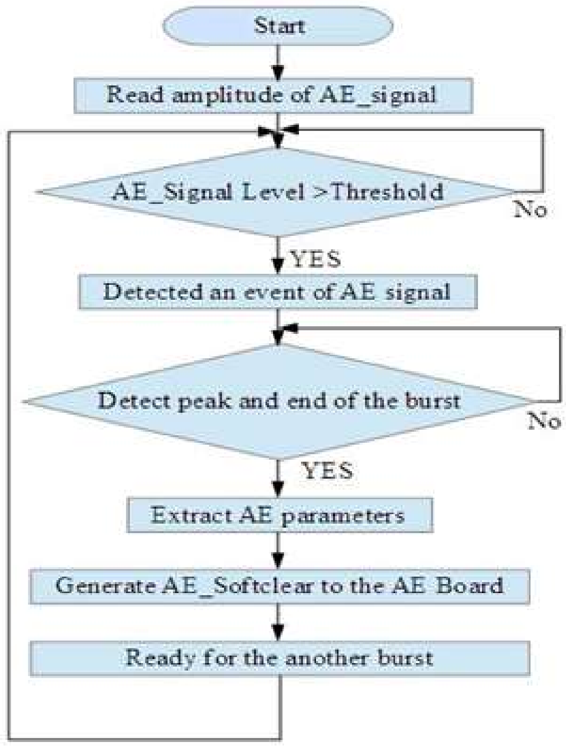

Figure 4.2 Flow diagram representation of the hardware system functionality.

4.2.1 Processing board (AE Board)

AE Board is an electronic circuit and is the heart of the hardware system extracting the signal parameters. The block diagram of the AE Board with the components used in the design is shown in **Figure 4.3**. It consists of two major building blocks, namely analog and digital circuit blocks. The components such as comparator, peak detect circuit, RMS circuit, differentiator circuit and rise time clock circuit are used for the design of the AnalogCircuit block. While, the components such as pulse circuit, monoshot circuit, retriggable monoshot circuit, AND gate, OR gate, NOT gate and T-FF (Toggle Flip Flop) are used for the design of digital circuit block.

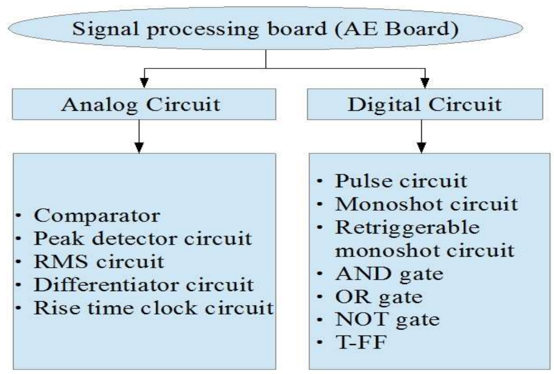

Figure 4.3 Block diagram of AE Board with the components used in the design.

The interconnection of input and output signals from the two blocks for the AE Board design in Multisim software is shown in F**igure 4.4**. As for as the design is concerned, there are two types of parameters associated with the burst type AE signals, namely analog and digital. The AE signal parameters such as peak amplitude and RMS are analog parameters while counts, rise time and event duration are digital parameters. The analog parameters are extracted from the analog circuit block, and the digital parameters are extracted from the analog as well as digital circuit block. The design description of the two blocks is explained in the subsequent sections.

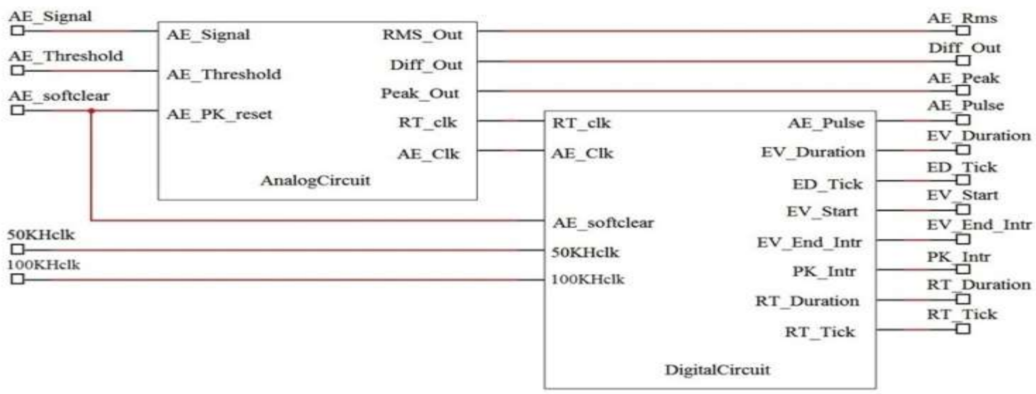

Figure 4.4 AE Board design.

4.2.1.1 Analog circuit block

The analog circuits block measures the peak amplitude and RMS values of AE burst signal and also generates prerequisite signals for the timing measurement by the digital circuit. A Multisim design of the analog circuit block with the interconnection of different circuit blocks such as comparator, PeakDetect, RMScircuit, Differentiator and RTclkGen is shown in **Figure 4.5**.

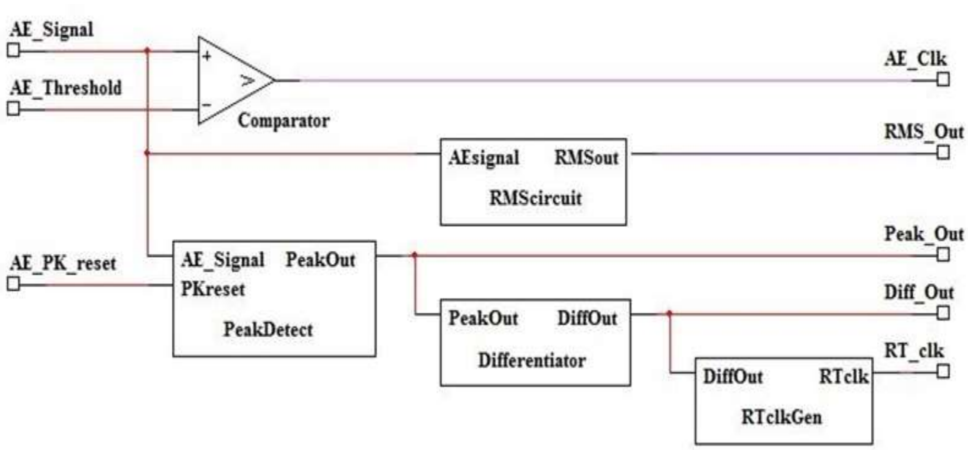

Figure 4.5 AnalogCircuit (Analog circuit) block design.

In the burst signal, a threshold voltage is used to distinguish the signal form background noise **[155]**. AE activities are counted only when the signal level crosses the set threshold. As shown in **Figure 4.5**, a comparator compares the AE_Signal received from the signal conditioning unit with the threshold voltage (usually set in the DAC0 of the micro-controller) to generate a TTL (Transistor-Transistor Logic) compatible clock denoted as AE_Clk (Acoustic Emission Clock). Cumulative count (sum of the AE clocks), event count, event duration and rise time parameters of the AE burst are embedded within this AE_Clk and hence extensively used for the timing measurement by the digital circuit block.

a) Comparator

The comparator compares the input signal (AE_Signal) level with a reference voltage (AE_Threshold) to produces an output signal.

$$if AE\_Signal > AE\_Threshold = +Vcc = AE\_Clk$$

$$if AE\_Signal < AE\_Threshold = 0\ Volt\ = AE\_Clk$$

where Vcc is the comparator supply voltage.

b) Peak amplitude measurement

The peak detect circuit is an important building block of the AE Board and used to measure the peak amplitude parameter of the signal. The peak detect circuit design is shown in **Figure 4.6**. The Peak detect circuit holds the last detected peak value until it gets the next higher amplitude in an AE burst signal (as shown in the inset of **Figure 4.6**). This process continues until the AE signal reaches an absolute maximum of the burst. The circuit also produces a peak reset signal, as shown in **Figure 4.6**. The peak circuit design is embedded in the peak detector block with their input and outputs as AE_Signal, Peak_Out and PKreset. This peak amplitude value is read by ADC1 of the controller block.

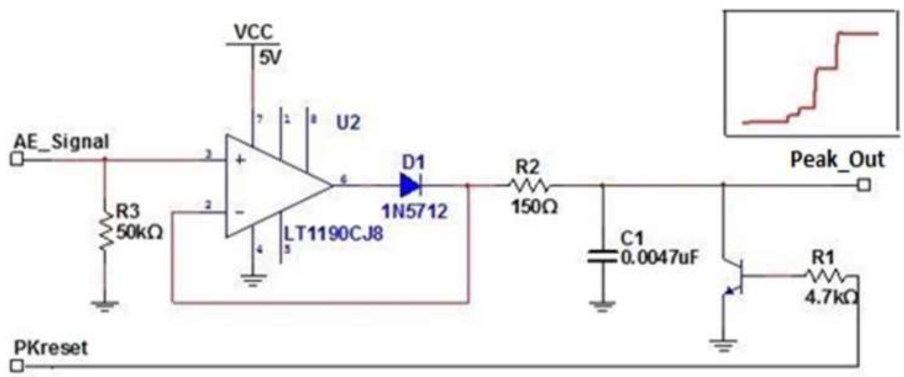

Figure 4.6 Peak detect circuit along with peak reset.

c) RMS measurements

Root Mean Square (RMS) is the most useful measurement of the amplitude of the time-variant signals. RMS is only unifying metric of all time-varying signals. It is implied to an AC quantity of current or voltage in terms of functionality equivalent to their DC values **[156]**. Measurement of the RMS value requires an RMS-to-DC converter, which provides a DC output equal to the RMS value of any input AE signal. The AD536AJD IC (manufactured by M/s. Analog devices) is used in the Multisim design as an RMS-to-DC converter. The RMS circuit design is shown in **Figure 4.7.** The RMS circuit design is embedded in the RMScircuit block with their input and output pin as AEsignal and RMSout respectively. The output of the RMS circuit is read through the ADC0 of the microcontroller block.

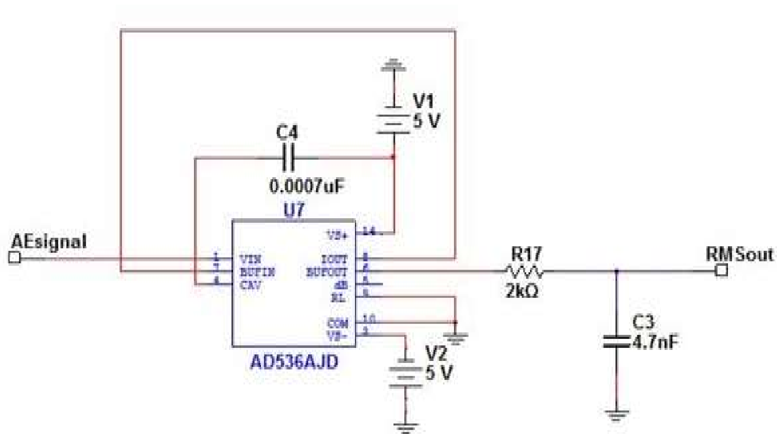

Figure 4.7 RMS circuit design.

d) Differentiator circuit and rise time clock circuit

In addition to the peak amplitude and RMS parameters of the burst type AE signal, the analog circuit block generates a differentiated signal of the peak detect circuit called differentiated output (Diff_Out) signal. The differentiator produces an output voltage which is proportional to the rate of change of input voltage. The output voltage depends on the circuit RC time constant and input frequency. The differentiator circuit is embedded in the differentiator block with input and output pin as PeakOut and DiffOut respectively. The differentiator circuit design is shown in **Figure 4.8**.

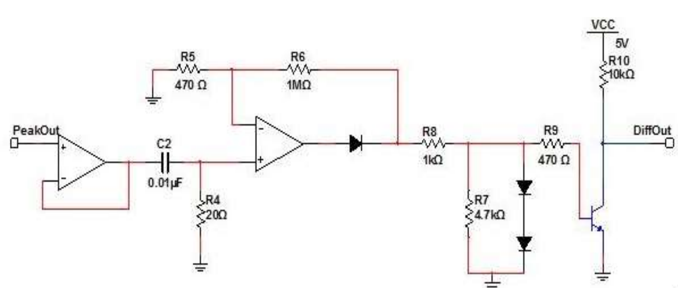

Figure 4.8 Differentiator circuit design.

The derived clock signal from the differentiator output is called rise time clock (RT_Clk) signal. The rise time circuit design is embedded in the RTclkGen block with their input and output pin as DiffOut and RTclk respectively. The rise time clock circuit design is shown in **Figure 4.9**. The Diff_Out and RT_Clk are the output signals from the differentiator block and RTclkGen block respectively, which are used during timing measurement of AE signal using digital circuit block. The design description of the digital circuit block is explained in the subsequent sections.

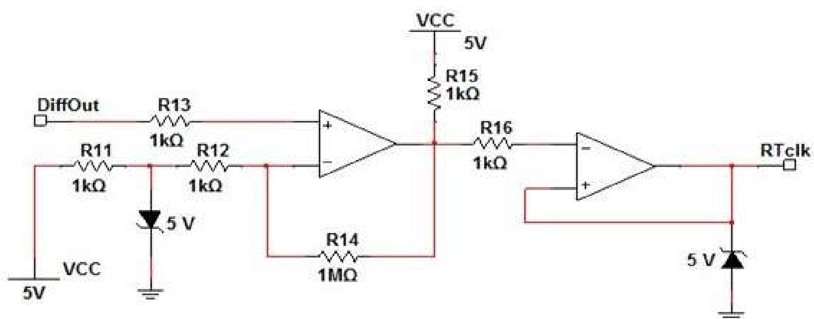

Figure 4.9 Rise time clock circuit design.

4.2.1.2 *Digital circuit block*

Digital circuit block measures all the timing and count related parameters such as AE count, event duration and rise time. The digital circuit block consists of a monoshot, retriggerable monoshot and short pulse circuits, to generate pulses required for the timing measurements. A Multisim design of the digital circuit block with their interconnection of circuit blocks such as RTmonoshot and Pulse with the AND gate, OR gate, NOT gate and T-FF is shown in **Figure 4.10**.

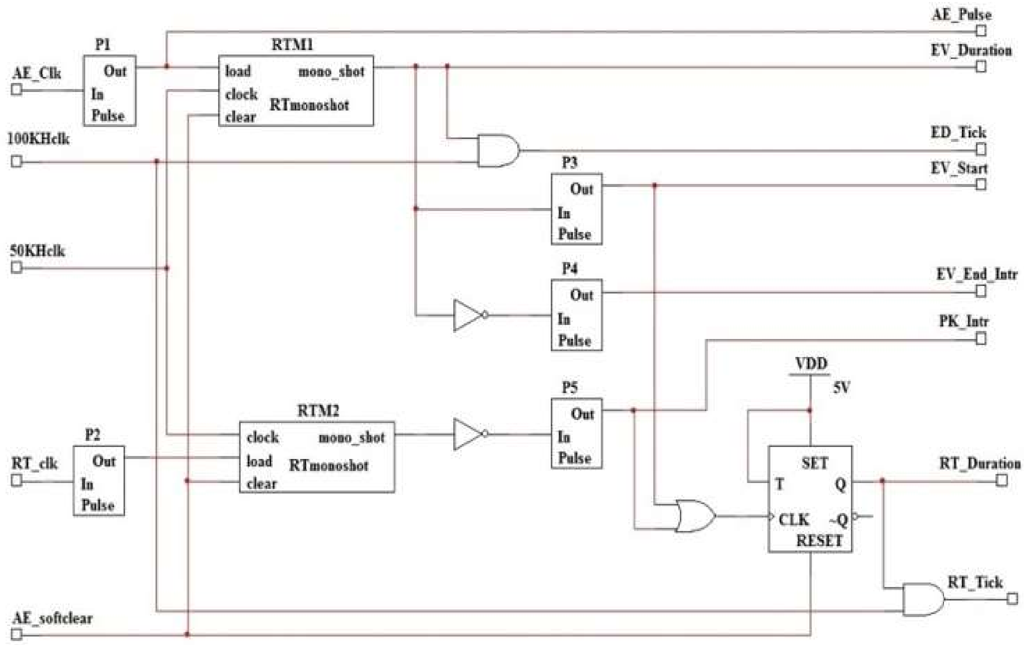

Figure 4.10 Digital circuits (DigitalCircuit) block design.

The monoshot circuit has only one stable state and produces a single output pulse when it is triggered externally. The design circuit for the monoshot using the logic gate and JK Flip Flop is shown in **Figure 4.11**. In a retriggerable monoshot the output will be extended by the additional input pulses by keeping the circuit in an unstable mode. The monoshot circuit design is embedded in the RTmonoshot block. The design circuit for the retriggerable monoshot is shown in **Figure 4.12.** The Short pulse circuit generates a very narrow single shot for every rising edge in its input of AE clock. The pulse circuit design is embedded in the Pulse block and is shown in **Figure 4.13**.

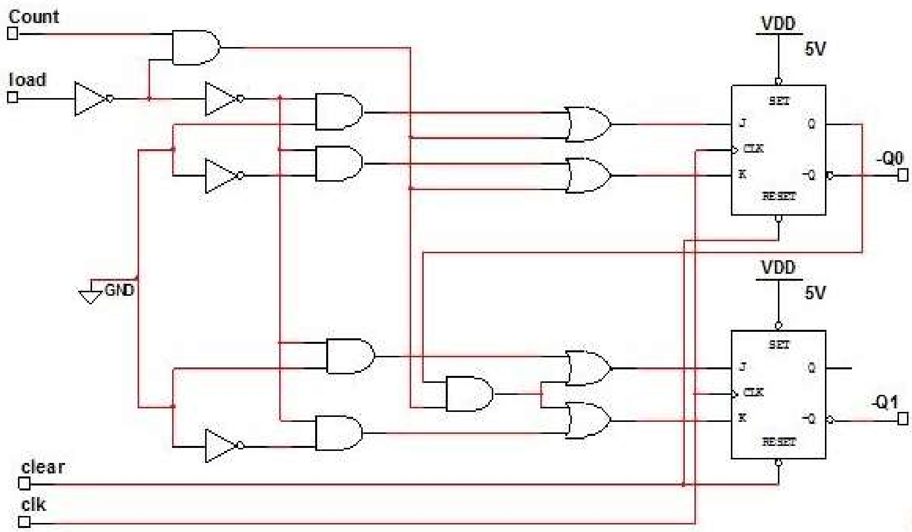

Figure 4.11 Monoshot circuit design.

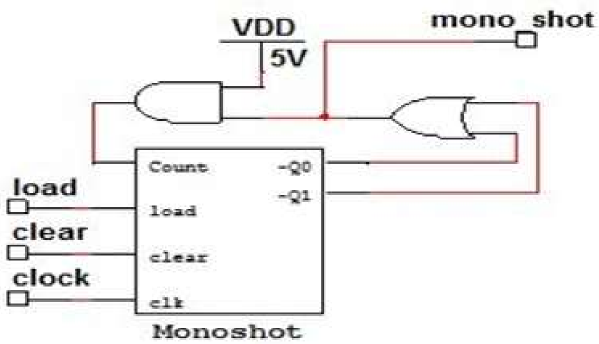

Figure 4.12 Retriggerable monoshot circuit design.

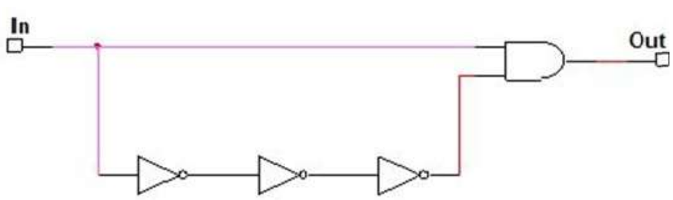

Figure 4.13 Short pulse circuit design.

a) Count measurements

The AE_Clk output from the AnalogCircuit block (**Figure 4.4**) is interfaced with the pulse sub-block of the DigitalCircuit block (**Figure 4.10**) for the measurement of counts. The pulse sub-block generates a very narrow single shot for every rising edge in its input of AE_clk. This single narrow shot is required for noise immunity, and the counters count these narrow shots. The AE_Pulse output from the DigitalCircuit block is counted by the counter zero (CNT0) to get counts and cumulative counts (sum of counts in each event) from the controller block (**Figure 4.1**).

b) Event duration and event counts measurement

AE_clk is also fed to two retriggerable monoshot circuits to generate RTM1, and RTM2 signals and are used for event duration and event count measurements respectively. In order to measure the event duration, the RTM1 signal is clocked by 50 kHz clock. The internal delay of RTM1 is set to be 3T where T is the pulse width of 50 kHz clock, i.e., 20 µs (microsecond). This 3T should be wider than the largest possible width of AE_Clk. So, for every AE_Pulse, the output of the RTM1 extends to 60 µs, which results in a constant offset in event duration. Hence, the actual event duration is determined by subtracting 60 µs from the measured time difference between the start and end of the events. The event duration pulse is ANDed with a 100 kHz clock (10 µs tick width) to generate ED_Tick (Event Duration Ticks). CNT_2 counts the ED_Ticks. The count value (the number of ED_Tick) multiplied by the ANDed clock period of 10 µs minus 60 µs (3T) is the value of measured event duration. EV_Start (Event Start) and EV_End_Intr (Event End Interrupt) are generated from the rising and falling edges of an Event Duration signal. EV_start pulse is used to count the event count by CNT_1 counter.

c) Rise time measurement

In order to measure the rise time of the burst, one has to know the time elapsed from the first occurrence of AE count until it reaches the peak. The first occurrence of the AE counts starts from when the AE signal crosses the threshold. The rise time clock (RT_clk) generated from AnalogCircuit block and interfaced to the DigitalCircuit block is shown in **Figure 4.4**. The RT_clk generated by using interfacing of peak detect circuit (PeakDetect), differentiator circuit (Differentiator) and rise time clock generator circuit (RTclkGen) is shown in **Figure 4.5**. The output of the peak detect circuit has a rising edge followed by a steady-state, and it continues until it reaches the maximum amplitude of the AE_Signal (inset of **Figure 4.6**). So, the rising edge ceases to exist after the arrival of the peak. If the peak output is differentiated by the differentiator circuit (**Figure 4.8**), there will be pulses at every rising edge of the PK_out (Peak out) signal. The Diff_out signal from the differentiator circuit of the analog circuit block is used for this purpose of generating the pulse at every rising edge of the PK_out signal. The pulses (Diff_out) are then amplified and made TTL level by RTclkGen block (**Figure 4.9**). Finally, we get RT_clk (Rise Time clock) pulses. The last pulse of RT_clk indicates the end of rise time. Therefore, the time duration between event start pulse and the last pulse of RT_clk will be the rise time. RT_Clk is used to measure the rise time duration. RTM2 also has an extra 3T delay as explained previously in the event duration measurement. Although RTM2 is used for the generation RT_Duration (Rise Time Duration) but there will be an error in RT_Clk. The RT_Clk is generated from an analog differentiator block where sufficient growth in peak value is required to get RT_Clk. So, the initial RT_Clk may arise stochastically before or after EV_Start. To avoid this ambiguity, the rise time is evaluated between the EV_Start and PK_Intr (Peak Interrupt). 100 kHz clock ANDed with RT_Duration is used to get RT_Tick (Rise time Tick). The number of RT_Ticks are counted by CNT_3 counter for rise time measurement in μsec. Thus all the parameters are extracted in the hardware.

4.2.2 Results and discussion

Multisim is an advanced SPICE simulation environment. The simulation is done on real AE data collected by the pencil lead break tests on a concrete block, as discussed in the previous chapter. The AE data is stored in ASCII format using the developed signal conditioning board. The pencil lead test AE signal is amplified and stored for 2 ms (millisecond) and the signal contains four AE bursts (AE_Signal). Approximate duration of each AE burst varies from 150 to 200 μs. The AE_Signal is applied to the AE Board and simulated in the Multisim simulator. The simulated result of analog circuit (AnalogCircuit) blocks such as AE_clk, AE_RMS, AE_Peak, Diff_Out and RT_clk are shown in the **Figure 4.14a**.

Similarly, the simulated result of digital circuit (DigitalCircuit) blocks such as AE_Clk, AE_Pulse, EV_Duration, EV_Start_Pulse, EV_End_Intr, EV_Tick, RT_Clk, PK_Intr, RT_Duration, RT_Tick, 100 kHz and 50 kHz are shown in the **Figure 4.14b**. The simulated result from AnalogCircuit blocks are used for the measurement of analog parameters such as peak and RMS of the AE signals. The simulated result of DigitalCircuit blocks are used for the measurement of digital parameters such as counts, event duration and rise time of the AE signals.

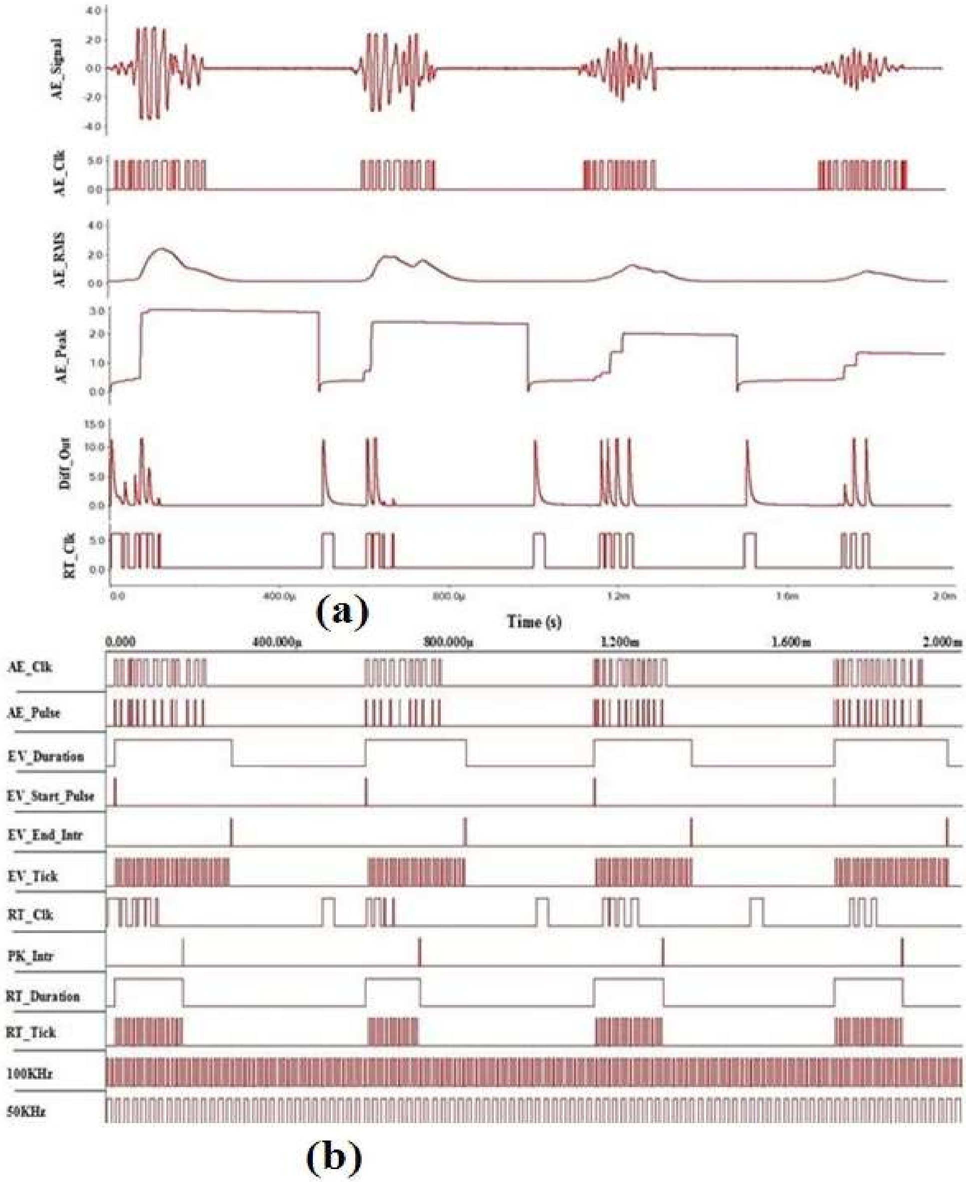

Figure 4.14 Simulation results of (a) AnalogCircuit block and (b) DigitalCircuit block.

As observed from **Figure 4.14a**, the comparator output of the analog circuit block is a TTL compatible AE_Clk. The RMS of the AE signal is a DC signal with nominal fluctuations **[139]**. The peak detector output as expected rises steps by step (for every event) till it reaches the maximum peak. Differentiator circuit generates pulses at the rising edge of AE_Peak signal. The RT_Clk generation depends on the RC time constant of the differentiator. Differentiator output should be amplified largely so that small changes in the peak amplitude are detected. This large gain after differentiation sometimes gives pulses even before the AE signal crosses the threshold. Because of this, the start and end are considered as event start (EV_Start) and end of rise time respectively (PK_Intr). Once all the parameters are read, the controller sends AE_softreset (acoustic emission software reset) to reset capacitor of the peak detect circuit, CNT_1 and CNT_3 counter simultaneously. Diff_Out signal is made TTL compatible pulse, called RT_Clk (**Figure 4.14a**). The simulated results of AE parameter values such as peak amplitude, RMS, AE counts, cumulative count and event count are given in **Table 4.1**. This timing diagram clearly demonstrates that the extracted parameters are reliable.

Table 4.1 AE parameters measurement values (**Figure 4.14a** and **Figure 4.14b**)

Burst No.	RMS (Volt)	Peak (Volt)	AE Count	Cumulative Count	Event Count
1	2.42	2.85	13	13	1
2	1.88	2.44	10	23	2
3	1.27	2.06	12	35	3
4	0.86	1.38	15	50	4

The simulated result of event duration calculation along with the results of percentage error is given in **Table 4.2** The event duration pulse (EV) width is calculated by the time difference between event end (EV_End) and event start (EV_Start) pulse of the signal. However, a minor error has been observed in event duration values. The error in the event duration values is calculated by the difference between the designed event duration (EV1) and measured event duration (EV2) divided by the designed event duration (EV1) as given in **Table 4.2**. The value of EV1 is determined by subtracting 60 μs from the time difference between the event end (EV_End) and event start (EV_Start) pulse of the signal, i.e. EV as given in **Table 4.2**. The measured event duration (EV2) is determined by counting the number of EV_Tick multiplied by the ANDed clock period of 10 μs and subtracted with extra 3T (60 μs). The EV_Tick is generated by using an input of AND gate clock frequency (100 kHz) with the event duration pulse width (EV).

Similarly, the simulated result of rise time calculation along with the results of percentage error are given in **Table 4.3.** The rise time duration pulse (RT) width is calculated by the time difference between peak interrupt (PK_Intr) and event start (EV_Start) pulse of the signal. However, a minor error has also been observed in the rise time values.

The error in the rise time duration is calculated by the difference between the designed rise time duration (RT1) and measured rise time duration (RT2) divided by the designed rise time duration (RT1) as given in **Table 4.3**. The measured rise time duration (RT2) is determined by counting the number of RT_Tick multiplied by the ANDed clock period of 10 μs and subtracted with extra 3T (60 μs). The RT_Tick is generated by using an input of AND gate clock frequency (100 kHz) with the rise time pulse width (RT).

The maximum error in the event duration (<2%) is less than that in rise time (<12%). This is due to less number of clocks are associated with the rise time measurements. However, error associated with the event duration and rise time can be further reduced by increasing the clock frequency since the number of EV_Tick and RT_Tick increases by increasing the input of AND gate clock frequency.

Table 4.2 Event duration measurement values taken from the simulation data (**Figure 4.14b**)

Burst No.	Ev_Start (S) in µs	Ev_End (E) in µs	EV_Duartion (EV) (E-S) in µs	Designed Ev_duration (EV1) (EV-60) in µs	No of Ev_Tick (T)	Measured Ev_duration (EV2) $(T * \frac{1}{100\,kHz} - 60\ \mu s)$	Ev_Duration Error % $(\frac{EV1 - EV2}{EV1} * 100)$
1	18.5	291	272.5	212.5	27	210	1.17
2	605	838	233	173	23	170	1.73
3	1136	1364	228	168	23	170	-1.19
4	1696	1963	267	207	27	210	-1.44

Table 4.3 Rise time measurement values taken from the simulation data (**Figure 4.14 b**)

Burst No.	Ev_Start (S) in µs	PK_Intr (P) in µs	RT_Duartion (RT) (P-S) in µs	Designed RT_duration (RT1) (RT-60) in µs	No of RT_Tick (T)	Measured RT_duration (RT2) $(T * \frac{1}{100\,kHz} - 60\ \mu s)$	RT_Duration Error % $(\frac{RT1 - RT2}{RT1} * 100)$
1	18.5	176.05	157.55	97.55	16	100	-2.51
2	605	728.47	123.47	63.47	12	60	5.46
3	1136	1286	150	90	16	100	-11.11
4	1696	1846	150	90	16	100	-11.11

4.3 Summary

In this chapter, the design of new hardware for extraction of acoustic emission signal parameters were presented, and these are peak amplitude, RMS, AE counts, event count, cumulative count, event duration, and rise time. Combinations of analog and digital circuits were employed in this design, and the simulation results were presented. Implementation of the hardware had resulted in reliable extraction of the parameters and has been found to be promising for wireless transmission for SHM applications. The hardware extracted AE signal parameters showed good agreement with the offline measurements. This design concept can be effectively utilized for the development of a wireless acoustic emission sensor system for monitoring concrete structures.

5 Design development and validation of data acquisition device

5.1 Preamble

This chapter deals with the deployment of a programmable system on chip (PSoC) based data acquisition device for efficiently acquiring the AE signals and parameters in a wireless environment. It presents the hardware and software developments using PSoC. Generating and acquiring burst type AE signals has been demonstrated in this chapter.

5.2 Introduction

Digital storage oscilloscopes (DSOs) are well suited for acquiring data using sensors in a laboratory environment, as has been reported in the previous chapter. However, for field applications, surged and dedicated systems capable of acquiring AE signal parameters are essential. Moreover, a DSO is a general-purpose equipment designed to acquire, display and record the signal from any transducer and hence has many additional features which are not essential for integrating with AE equipment. Thus, a portable and modular data acquisition (DAQ) system needs to be developed for wireless AE applications. Such a DAQ system should meet the following requirements.

1. The throughput of the DAQ system should be reasonably high so that the system can acquire all possible changes in the physical processes.
2. The DAQ should be rugged for structural health monitoring applications.

3. The DAQ should have the capability for interactive human-machine interface.
4. It should be possible to control the data export rate to an external computer for further processing.
5. It should have the simplest of design and control features so that the same can be operated by another user.
6. The DAQ should be cost-effective and extremely portable.

Considering these aspects, work has been carried out to design and develop a data acquisition system based on PSoC for structural health monitoring. The configuration software has been designed using the PSoC creator 4.0 platform. Subsequently, a Human Machine Interface (HMI) has been developed for an interactive layout and to process the event of AE signals acquired using the PSoC. The development of the PSoC based DAQ has been validated by acquiring artificial AE signals in the laboratory. It is shown that the results are comparable with those obtained using DSO. This device can be used as an alternative to DSO for dynamic defect detection by AE signals. A detailed description of how the design evolution of the PSoC based system was made and how the design concept was used for wireless AE sensor system development, are described in this chapter.

5.3 Description of PSoC family and its selection

The PSoC is a highly configurable system-on-chip architecture for embedded control and design, manufactured by Cypress Semiconductor. It integrates the configurable digital and analog circuits controlled by an on-chip microcontroller. System on chip (SoC) is a technique where all the components of electronic circuitry can be designed in single IC, and because of this, whole electronic circuitry can be minimized and hence reducing the board space, power consumption, and system cost while improving the quality of the system development. Even noise immunity can be improved, which is one of the most important aspects when dealing with acoustic emission. The PSoC has several blocks like Read-Only Memory (ROM), Random Access Memory (RAM), Flash Memory, etc. It also encompasses Ethernet Port, UART (Universal Asynchronous Receiver/Transmitter), SPI (Serial Programming Interface), and USB (Universal Serial Bus). Hence, PSoC provides a perfect platform to design an instrument based on the specific embedded design for acoustic emission testing that needs to be in a single board. There are various members of the PSoC family. A brief description of their types and specifications are given in **Table 5.1**.

Table 5.1 PSoC types and specifications

PSoC 1	**PSoC 3**	**PSoC 5**
8-bit Microcontroller and optimized performance	8-bit 8051 core and optimized performance	32-bit ARM Cortex-M3 processor core and high performance
Flash memory of 4 kB to 32 kB, The clock frequency of 24 MHz and 4 MIPS, Static RAM of 256 bytes to 2kB and Operating voltage 1.7 to 2.5V	Flash memory 8 kB to 64 kB, The clock frequency of 67 MHz and 33 MIPS, Static RAM of 3 kB to 8 kB and Operating voltage 0.5 to 5.5V	Flash memory 32 kB to 256 kB, The clock frequency of 67 MHz and 84 MIPS, Static RAM of 16 kB to 64 kB and Operating voltage 2.7 to 5.5V
6-14-bit one Delta-Sigma ADC, 131 kSPS @ 8-bit, 6-8-bit up to two DACs	8-20-bit one Delta-Sigma ADC, 192 kSPS @ 12-bit, 8-bit up to four DACs	8-20-bit, one Delta-Sigma ADC, 192 kSPS @ 12-bit,

		12-bit two SAR ADCs @1 MSPS, 8-bit up to four DACs
2 mA active current and 3 μA sleep current Communication protocol: UART, I^2C, FS USB 2.0, and SPI	2 mA active current 1 μA sleep current and 200 nA hibernate Communication protocol: UART, I^2C, FS USB 2.0, SPI, LIN and CAN	2 mA active current 2 μA sleep current and 300 nA hibernate Communication protocol: UART, I^2C, FS USB 2.0, SPI, LIN and CAN
Requires ICE Cube and Flex Pods	Programming interface: SWV, SWD, On-chip JTAG and Debug and Trace	Programming interface: SWV, SWD, On-chip JTAG and Debug and Trace
64 input/output port	72 input/output port	72 input/output port

The number of bits and sampling frequency of the PSoC member (**Table 5.1**) are essential features to be considered while selecting PSoC for the AE application. The dynamic range can be improved by increasing the number of bit conversion of an ADC **[157]**. The useful frequency ranges for acoustic emission generated from concrete based materials/structures is 20 kHz to 100 kHz. In the case of Analog to digital conversion (ADC), in order to satisfy the Nyquist criteria, the minimum sampling rate should be twice of the maximum frequency present in the signals **[147]**. However, for true representation of the signals ten times sampling frequency is widely used **[158]**. Based on these, a PSoC-5 based CY8CKIT-059 PSoC 5LP Prototyping kit has been selected for the development of DAQ. It has successive approximation (SAR) ADC with a maximum sampling rate at a speed 1 MSPS with 12-bit resolution, which makes it suitable for further correct representation of AE data. In addition, the performance of PSoC 5LP architecture is enhanced through the following features **[108]**:

1. 32-bit ARM Cortex-M3 high-end processor, Direct Memory Accesses (DMA), and clock frequency up to 80 MHz.
2. It has ultra-low power consumption.
3. Programmable analog and digital peripherals.
4. Provide the flexible routing of digital and analog peripheral function to any input/output pin.

The block diagram representation of CY8CKIT-059 PSoC 5LP development kit is shown in **Figure 5.1**. The PSoC 5LP kit has the following key features:

1. Programmable Kit (KitProg): It has onboard debugger/programmer for debugging and programming to the target Kit. The PSoC 5LP device can also be programmed through the SWD (Serial Wire Debug) interface in standalone mode. It acts as a bridge between USB and UART or UART and I2C.
2. Expansion Headers: It brings all input/output in two expansion header, which allows the maximum accessibility to the device.
3. Micro-USB Connector: The onboard micro-USB connector provides access to the USB block of the device to develop the USB applications.
4. User LED: This user LED on the board can be used for display and brightness control to indicate different states of the PSoC 5LP device.
5. Push Button: It can be used to provide input to the device.
6. Reset Button: It is used for resetting the device.
7. Kit Programming (KitProg) Boatload: It is used to provide KitProg into the boot loader mode when the key is pressed while connecting trough USB port of the Laptop/PC.

The application-specific system on chip can be designed in the PSoC creator, which is provided by the manufacturer Cypress Semiconductor. PSoC Creator is a tool for providing integrated design environment (IDE) towards concurrent hardware configuration and software editing, debugging, and compiling of PSoC **[108]**. The digital and analog components are represented by a symbol which an user can drag and drop into his design, interconnect, and configure for PSoC applications.

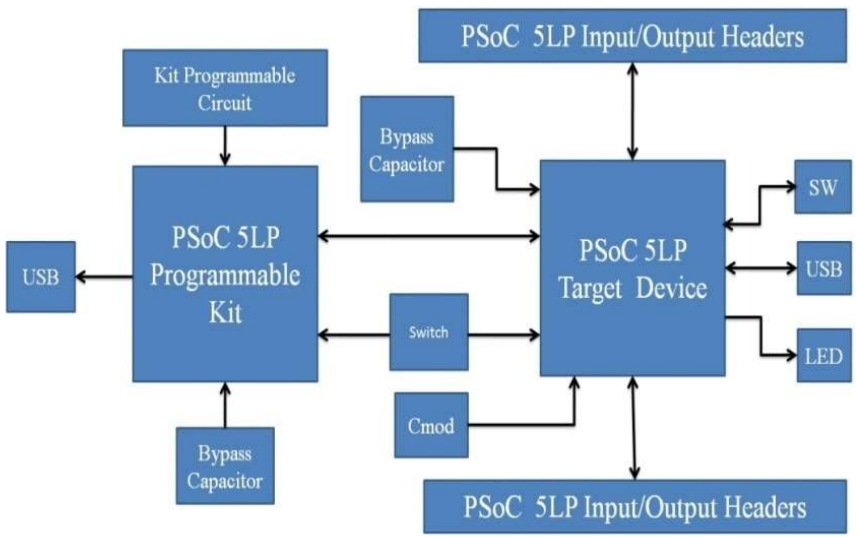

Figure 5.1 Block diagram representation of PSoC 5LP kit **[108]**.

The components used in mixed-signal Cypress catalogue is configured and dynamically generate API (Peripheral Application Interface) libraries. Different components and their peripherals used in the design are configured. Routing, firmware executing and debugging can be performed in the PSoC Creator IDE. The PSoC creator code can be exported to third-party IDEs like IAR Embedded Workbench, Eclipse, and ARM microcontroller based kit. PSoC Creator is available freely in the window-based integrated development environment (IDE) with no code size limitation. The PSoC creator includes the following features:

1. Easy hardware design schematic capture and its wiring.
2. Readily available pre-verified components
    - It includes different communications library such as Bluetooth, I2C, SPI, USB, CAN, UART, and LIN.
    - It provides graphical configuration to digital peripherals.
    - It supports different analog components like ADC, Filter, DAC, CMP, and amplifier (AMP)
    - It generates dynamically API libraries
3. The compiler has no limitation in coding size.
4. The Integrated source editor performs inline diagnostics, code snippets and auto-complete.
5. It has a built-in debugger

5.4 Data acquisition system

The architecture block diagram of the data acquisition system (DAS) for the acquisition of AE signals is shown in **Figure 5.2**. The system consists of a signal generator device, DAQ, and a personal computer (PC). The output signal from the signal generator device is interfaced with the DAQ. The signal generator device is used in this investigation for validating the design concept for DAQ. The PSoC based DAQ is designed to acquire the AE data, and this has the capability to transmit the acquired signal through RS232 interface of the board to an external computer for post-processing.

Figure 5.2 Data acquisition system block diagram.

Hence, to do all these activities, the PSoC has the main code to integrate hardware and software design processes along with the external user interactions. All these processes are designed in a PSoC Creator integrated development environment. The functions behind different processes are stated below. Firstly, communication between the user and system is established through serial communication (RS232) on the board. The serial communication is achieved by using UART module in PSoC. This UART module is responsible for receiving command from the user and transmitting the information.

ADCs are one of the most important aspects required to design an effective data acquisition. This part is composed of several types and configurations of ADC in order to compare the results and study about the signal acquiring. The different types of ADC are Delta-sigma, Successive Approximation Register (SAR), integrating type, etc. Depending on ADC type, resolution and sampling rate can be selected. The selection of ADC for the AE signal is explained above. The main code makes it possible to switch among various functions such as accessing UART, memory, etc. The communication is made through RS232 when a command is received by PSoC from the user end. The instruction goes to the functional called and the desired parameters are set. The detail description of hardware and software designs of DAQ is given subsequently.

5.4.1 Design of data acquisition hardware

The basic building blocks of a DAQ are operational amplifiers, successive approximation analog to digital converter (SAR ADC), voltage digital to analog converter (VDAC), Comparator (Comp), Interrupt, universal asynchronous receiver and transmitter (UART), and a microcontroller to control operation and command as shown in **Figure 5.3**.

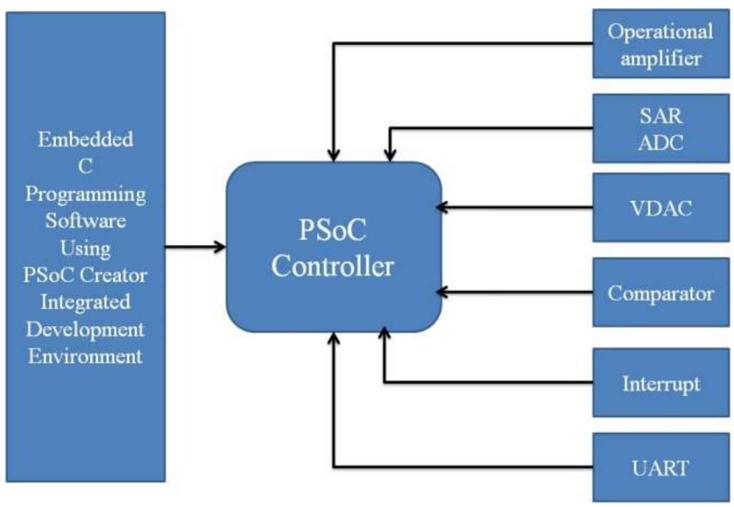

Figure 5.3 Block diagram representation of components used for the DAQ.

The software for the DAQ and its interconnections, as programmed in the PSoC Creator 4.0, is shown in **Figure 5.4**. The Analog_Input pin is used for interfacing with a signal generator. The Analog_Input pin is connected to a unity gain Opamp component and to the non-inverting terminal of a comparator component. The Opamp component is a follower and provides impedance matching to the signal generator device. The output of the Opamp is connected to the SAR ADC, which has been configured for 1 MSPS sampling speed and 12-bit resolution. The VDAC8 component is an 8 bit DAC that is used for generating the threshold reference at the inverting terminal of the Comparator component. The threshold voltage is set from 0 to 4.08 V in a step of 16 mV per bit.

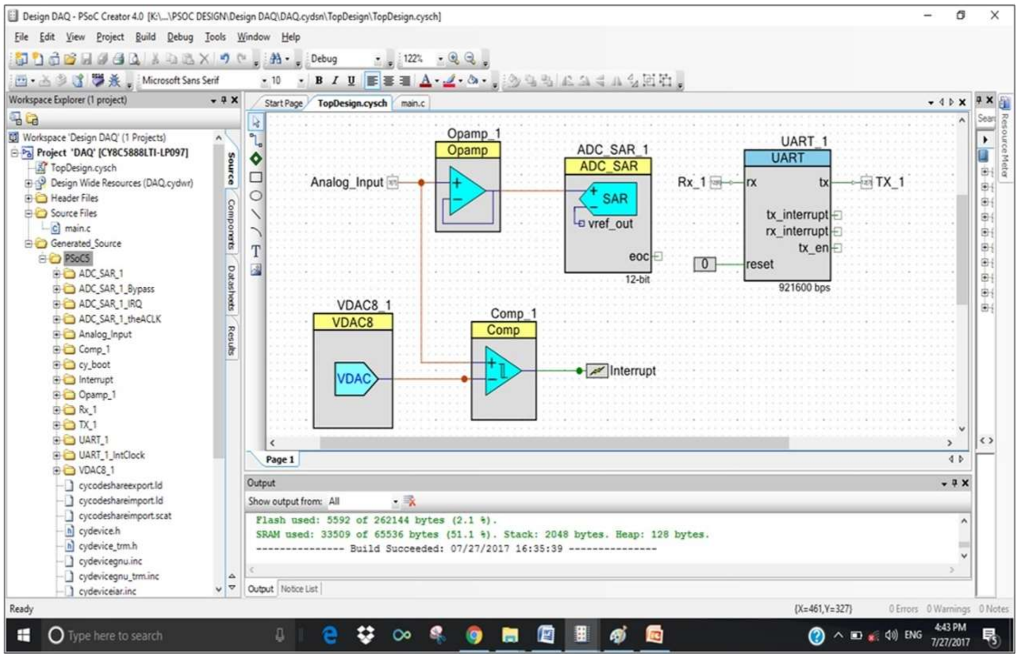

Figure 5.4 Schematic design of the DAQ in PSoC creator 4.0 IDE.

It can be controlled either by hardware or software or a combination of both. The Comparator component generates an output signal based on the comparison between the AE signal levels and the threshold reference set at the comparator. The Interrupt component is connected to the output of the comparator and is configured in the rising edge of the signal. The USB UART interface is used to establish communication between DAQ and personal computer for display, storage and analysis. The configuration of the UART for data transfer rate is 921600 bits per second with the following features such as full-duplex communication, 8-bit of data length, parity type as none, stop bit like one and flow control as none. The development of the embedded software code for enabling the hardware component and signal processing algorithm for acquisition, processing, and transmission of the AE signal is explained in the subsequent sections.

5.4.2 Data acquisition software design

The PSoC Creator 4.0 has been used as an integrated development environment enabling concurrent firmware and hardware editing, compiling and debugging of PSoC 5 development kit. The interrupt component is used in this design for identifying the event of an AE signal. The Interrupt component generates an interrupt on the rising edge of the comparator output. Data acquisition is performed by the SAR ADC only when the interrupt is generated. The triggering of interrupt enables to perform an interrupt service routine (ISR) whenever the voltage level of AE signal (Analog_Input) exceeds the threshold voltage. The signal acquisition, processing, and transmission are made within the ISR. After servicing an ISR, control reaches the main program, and the same process is continued. The software flowchart for the acquisition of AE signals is shown in **Figure 5.5**.

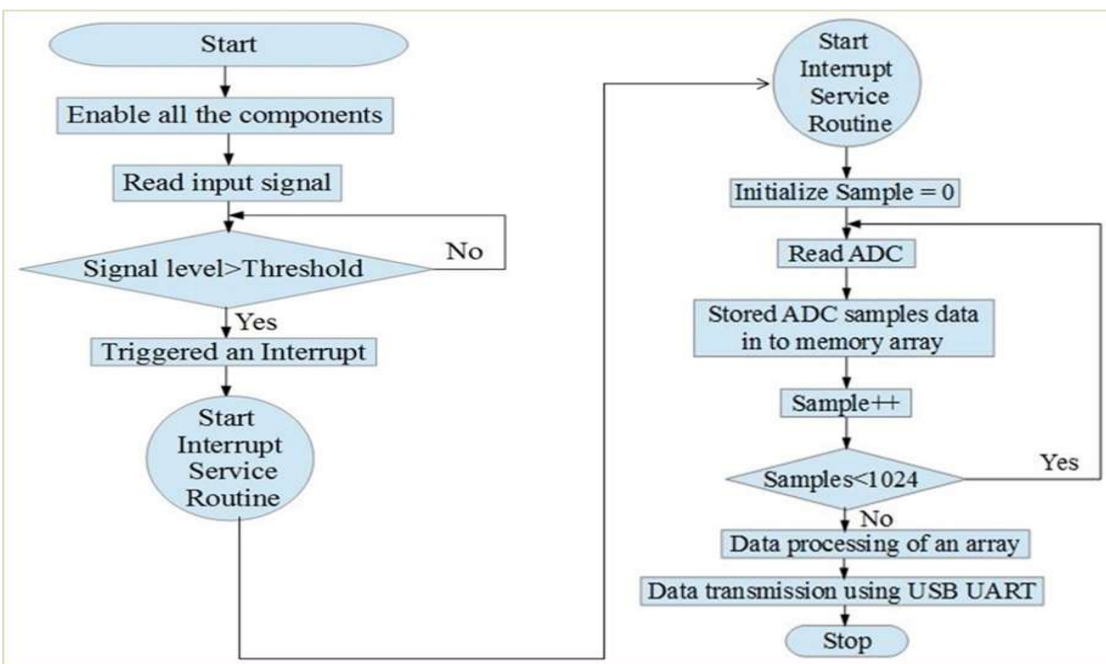

Figure 5.5 Software design flow chart for the acquisition of AE signals.

One thousand twenty-four samples of AE signal length with a duration of 1.03 milliseconds is recorded with a sampling rate of 1 MSPS. These one thousand twenty-four samples are processed and transmitted through USB UART. The embedded software has been developed in C programming language for this purpose and is given in **Appendix A**. An artificial burst type AE signal has been generated by a signal generator device in the laboratory and acquired using the designed PSoC hardware to validate the design of the DAQ.

5.5 Signal generator device

Similar to the analog-to-digital converter, a digital to analog converter (DAC) has also been designed and developed using the PSoC hardware for testing and validating the DAQ. A burst type AE signal with a frequency of 50 kHz has been generated using the DAC. One thousand twenty-four samples are covered in a 1.023 millisecond decaying signal of frequency 50 kHz. The signal is normalized with respect to 2.5-volt reference DC level. Where the decay constant is 10000, and the duration between the samples is one microsecond. The generated samples of signals are made compatible to read 8-bit digital to analog converter and can be found in the software programming code in Appendix B. The schematic hardware design of the DAC for the generation of AE burst using a PSoC Creator 4.0 is shown in **Figure 5.6**.

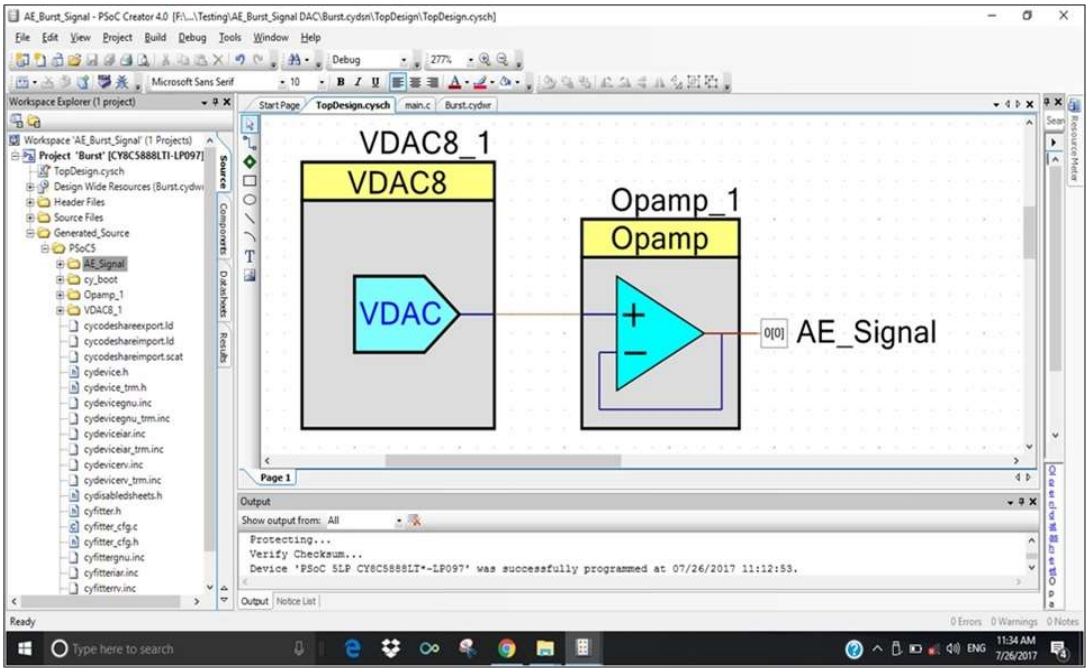

Figure 5.6 Schematic design of the signal generator device in PSoC creator 4.0 IDE.

The components used in this design are VDAC8 (voltage digital to analog converter of 8 bit) and Opamp (operational amplifier). The Opamp component works as a voltage follower which provides the same voltage to a load irrespective of the input to the Opamp. The output signal from VDAC8 is connected to the non-inverting terminal of the Opamp. The Opamp output is routed to one of the analog pins (0.0) of the development kit. The embedded software for the signal generator has been written in C programming language and is given in **Appendix B**. The combined hardware and software development has been imported into the development kit. The block diagram of the signal validation test for the signal generator device is shown in **Figure 5.7**. The validation has been carried out to confirm the frequency of the artificial signal using a digital storage oscilloscope.

Figure 5.7 Block diagram of signal validation test.

The photograph of the experimental test setup for the validation of the signal generator device is shown in **Figure 5.8.** The signal output from the analog pin is connected to the input channel of the digital storage oscilloscope (DSO) for display.

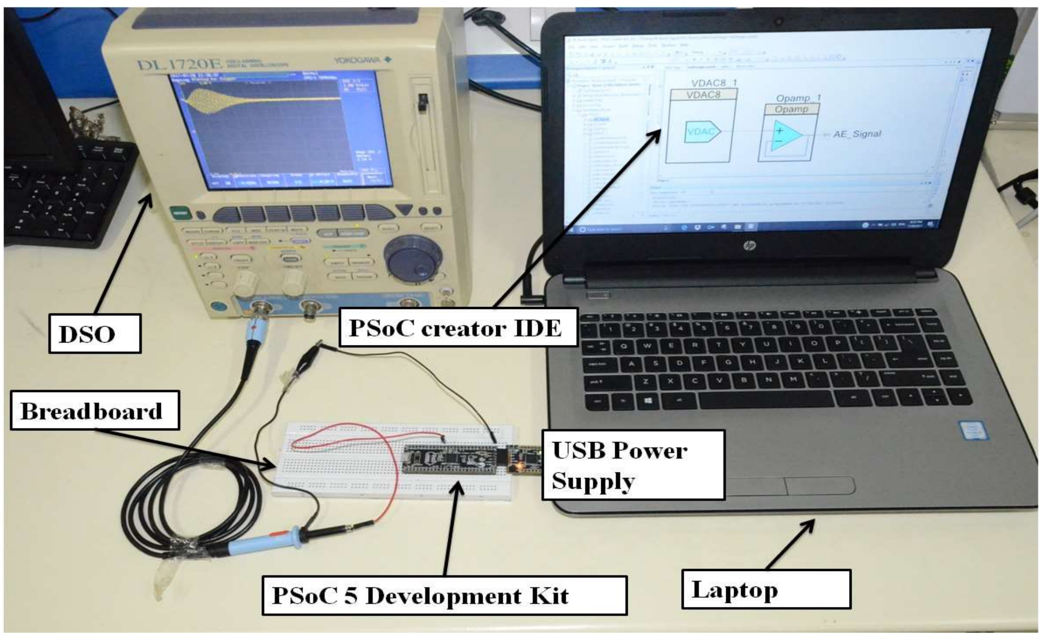

Figure 5.8 Photograph of the experimental setup for validation of the AE signal generator.

The artificial burst signal generated in the PSoC hardware and acquired by the DSO has been saved in ASCII format. Fast Fourier Transform (FFT) has been performed on the stored signal to verify the frequency components present in the signal. **Figures 5.9 (a) and Figure 5.9 (b)** show the AE burst signal and its Fourier transform respectively. It can be observed from **Figure 5.9 (b)** that only 50 kHz frequency component is present in the signal as expected. This experiment validates the functioning of the signal generator. Further experimental work to validate the DAQ for the acquisition of burst type AE signals is explained in the subsequent section.

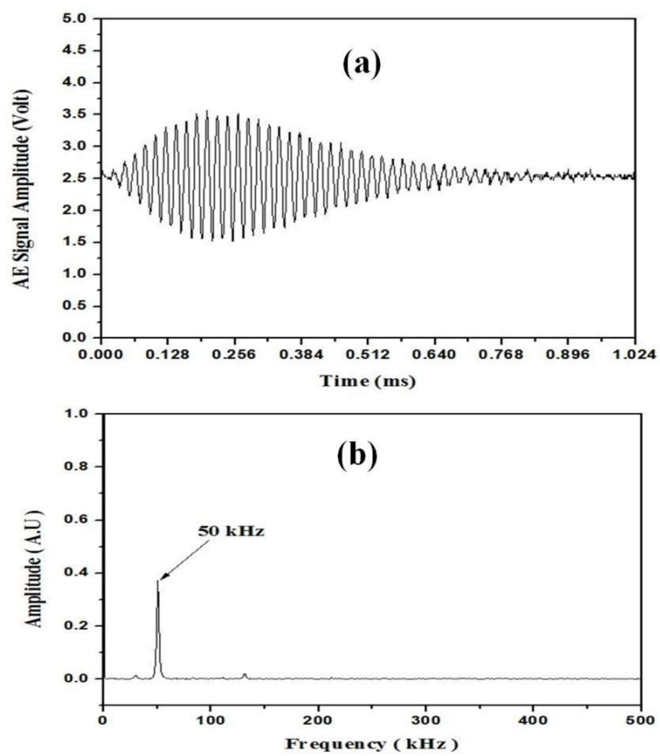

Figure 5.9 (a) Burst type AE signal generated and it's (b) FFT received from signal generator device.

5.6 Communication interface

LabVIEW tool has been used with a laptop for the data display and saving the AE signals. NI Visa serial communication interface has been established with USB UART COM port. NI Visa is a software tool which is used for serial communication in the LabVIEW. USB

UART is used to transfer and receive the serial data between two devices. The USB UART follows an asynchronous serial protocol to ensure reliable data transfer. There are different UART parameters that are used to communicate the DAQ with PC such as mode, bits per second (Baud rate), data bits, type of parity, stop bit and flow control. The detail description of the parameters is given below.

Mode of communication: There are different mode of communications in UART such as half-duplex mode, transmit mode (TX), receiver mode, and full-duplex mode.

Bits per second (BPS): It is used for the data to Tx/Rx at a rate of bits per second called baud-rate. There are different baud rate that can be configured with varying internal clock frequency such as 1200, 2400, 4800, 19200, 38400, 57600, 115200, 230400, 460800 and 921600 bits per seconds.

Data bits: It is used for the number of data (5, 6, 7, or 8-bit) to be transmitted between the start and stop of single UART transfer.

- 8-bit data is the default configuration for the data transfer.

Parity Type: The parity bit location (Even, Odd or None) is used with the data transfer.

Stop bit: This defines the number of stop bits (1 or 2 bits) and are used with the data transfer.

Flow Control: It allows to choose between hardware or None.

The UART configuration of DAQ and laptop should be the same to communicate between them. The required setting for UART communication for both the devices is given in **Table 5.2**.

Table 5.2 The UART parameters configuration for DAQ and the PC.

Parameters	DAQ/PC
Mode	Full Duplex UART (TX + RX)
Baud rate	921600 bit per second
Data Bits	8 bits
Parity Type	None
Stop bits	1 bit
Flow Control	None

5.7 Experimental, results and discussion

The photograph of the PSoC based DAQ set up in the laboratory for acquiring AE data is shown in **Figure 5.10**. As seen, two PSoC 5LP development kits of similar types are used in this design. One is used as the signal generator device and the other as the data acquisition device, as explained earlier. The AE signal output from the signal generator is interfaced with the data acquisition device, as shown in **Figure 5.2**. The burst type AE signal generated from pin number (0.0) of the signal generator is fed to pin number (3.6) of the DAQ and also to the DSO. The USB UART communication is established between the data acquisition device and the PC.

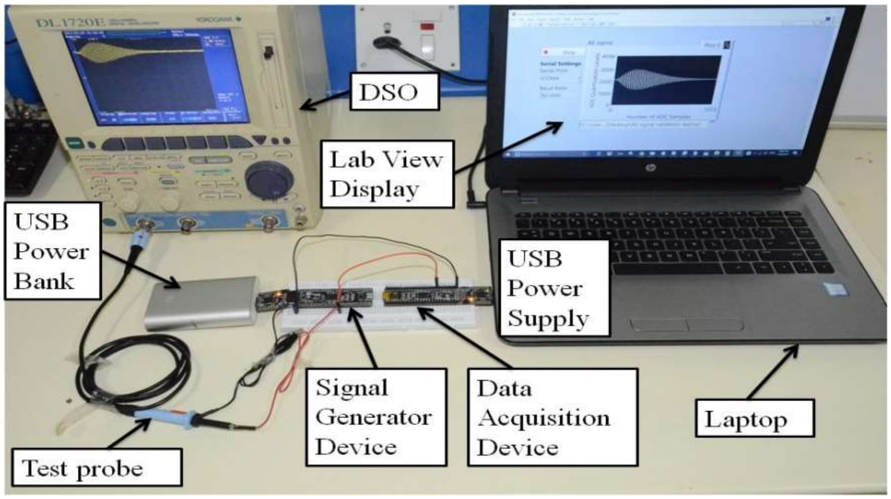

Figure 5.10 Photograph of the experimental setup for the data acquisition system.

Once the signal voltage level crosses the threshold, the event of the AE signal is detected, and one thousand twenty-four samples of the signal are acquired and transmitted using USB UART communication. The duration between the samples is set to one microsecond. The recorded AE signal length of 1.023 microseconds is displayed in the LabVIEW graphical user interface, as shown in **Figure 5.11**.

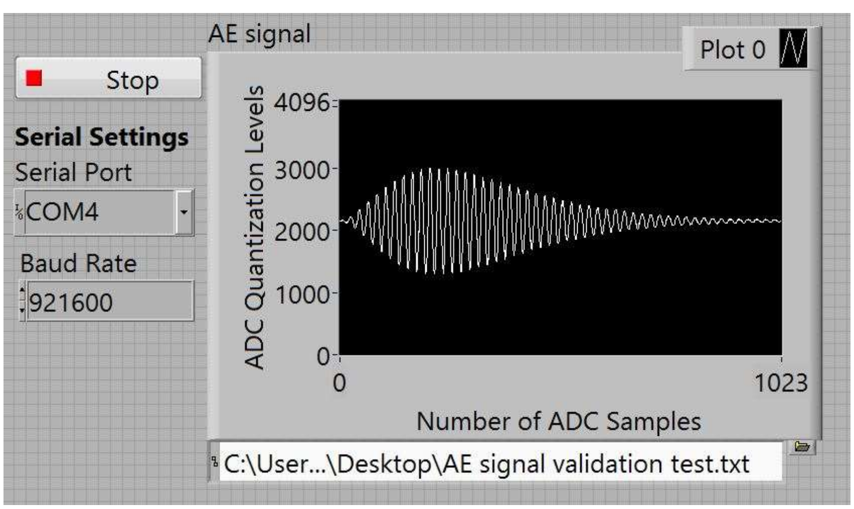

Figure 5.11 Burst type AE signal received from DAQ displayed using LabVIEW.

The transmitted data is saved in ASCII format in the PC. The data is transmitted in the 12-bit ADC quantization levels. The maximum dynamic range of 5 volts corresponds to 4096 quantization level of the ADC. The signal of ADC quantization levels is plotted against the number of ADC samples and is shown in **Figure 5.12 (a)**. The time difference between two consecutive samples corresponds to a one-microsecond time duration. Fast Fourier Transform (FFT) has been performed on the received signal from DAQ to examine the frequency component present in the signal, and the same has been shown in **Figure 5.12 (b)**. It can be observed that the only single frequency component is present in the received signal from the DAQ with a frequency of 50 kHz. The frequency components present in the received signal from the developed DAQ exactly match the artificial AE signal of the signal generator device, as shown in **Figure 5.9 (b).** These experiments validate the performance of the developed DAQ. This design concept for the acquisition of burst type AE signal will be explored for the development of the wireless acoustic emission sensor system for parameter extraction and is explained in the next chapter.

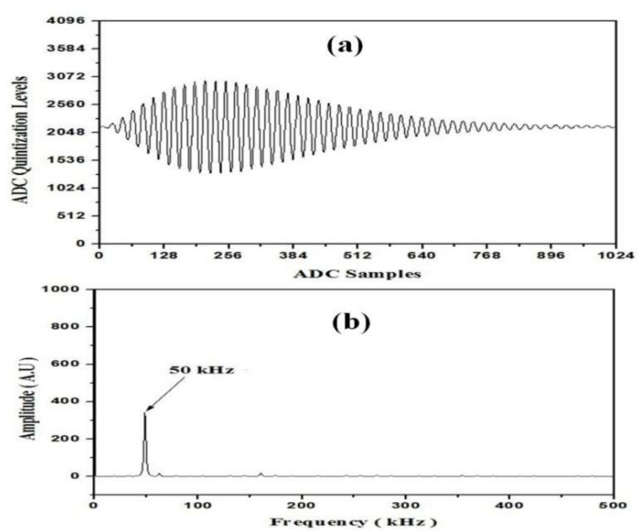

Figure 5.12 AE signal received from the (a) DAQ and its (b) FFT.

5.8 Summary

A programmable system on chip based data acquisition device for dynamic detection of an event of AE signal has been designed and developed. The performance of the developed DAQ has been successfully demonstrated with the in-house developed signal generator device for detecting dynamic AE events. The developed data acquisition is capable of acquiring, storing and processing AE data up to a speed of 1 MSPS and provides 12-bit resolution to the signal which is sufficient for the correct data interpretation of AE signals in the frequency range 20 to 100 kHz. Validation of the DAQ has been carried out by the signal generator device and DSO using FFT. The frequency components (50 kHz) present in the received signal has been found to be in good agreement with the frequency components (50 kHz) present in the signal generator device.

6 Design development and validation of wireless AE sensor system

6.1 Preamble

This chapter provides the overall design concept and architecture of the wireless AE sensor system. It deals with the deployment of a programmable system on chip (PSoC) based wireless sensor system for efficiently extracting and wireless transmission of the parameters of AE signals. It also presents the validation of the developed wireless sensor system by applying the signal validation test along with two different applications, namely compression test and corrosion detection test of concrete specimens in the laboratory.

6.2 Wireless sensing hardware design and architecture

Existing wired based AE systems have several drawbacks such as high installation time, high power requirement, noise associated with cabling, and portability issue due to the large size of the instrument, and restriction on remote monitoring. The wireless AE system overcomes the constraint of the wired AE system. By considering all these aspects, the PSoC based wireless AE sensor system has been designed and developed. Typical wireless AE unit consists of a sensor, signal conditioning unit, computational core unit, base station and wireless communication unit for transmission and reception of signals and commands, as illustrated in the functional block diagram given in **Figure 6.1**. Commands are instructions given by the base station to the sensor unit for control and handshaking. The important design aspects of the wireless sensor unit for SHM applications are onboard processing capability of the computational core unit and battery power of the system. Accordingly, the wireless sensor unit has been designed in such a way that it consumes minimum power to extend its lifetime and uses minimum hardware, which makes the sensor unit compact and cheap.

The wireless AE system includes a single wireless sensor unit communicating with a base station. In this prototype implementation, the base station is a computer either desktop or laptop, connected through a compatible wireless transceiver through a USB UART communication port. The wireless AE sensor unit is responsible for the acquisition of AE signal, processing various parameters associated with the signal, and finally transmitting the processed information wirelessly to the base station for permanent storage and further data analysis.

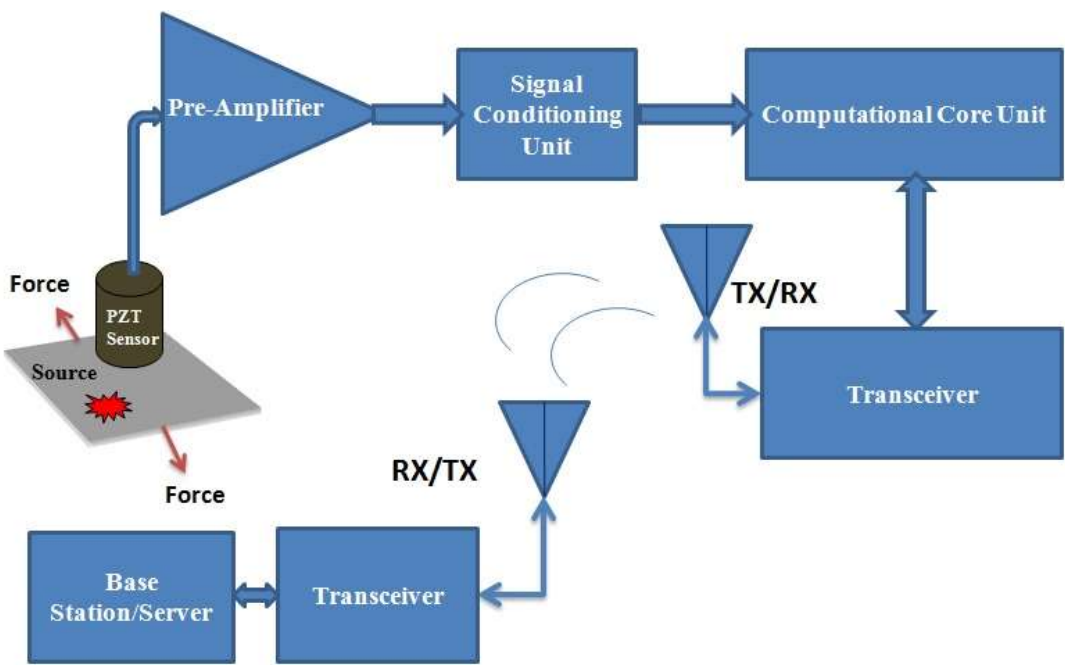

Figure 6.1 System architecture block diagram for the wireless AE sensor system.

6.2.1 Redesign of the signal conditioning unit

The development of the wireless sensor unit involves the design of three functional units viz., signal conditioning unit, computational core unit, and a wireless communication unit. The design and developmental aspects of SCU have been discussed in Chapter 2. In order to reduce the size and the power consumption, the SCU has been redesigned to accommodate it in a single chip of AD8630ARUZ manufactured by M/s. Analog Devices. This single chip SCU has a buffer, post-amplifier and filter. The integrated circuit chosen for the SCU has four operational amplifiers, out of which the first one has been used as a buffer, second one as a post-amplifier and the remaining two for active bandpass filter circuit. The Sallen-Key configuration, one of the most widely used filter, has been adopted for the design of bandpass filter. The Multisim design of the bandpass filter with 3 dB lower, and upper cut-off frequencies of approximately 27 kHz and 90 kHz respectively, is shown in **Figure 6.2**. The simulation results are used for the design of the bandpass filter. The optimized circuit diagram of the SCU in a single IC based on the simulations is shown in **Figure 6.3**.

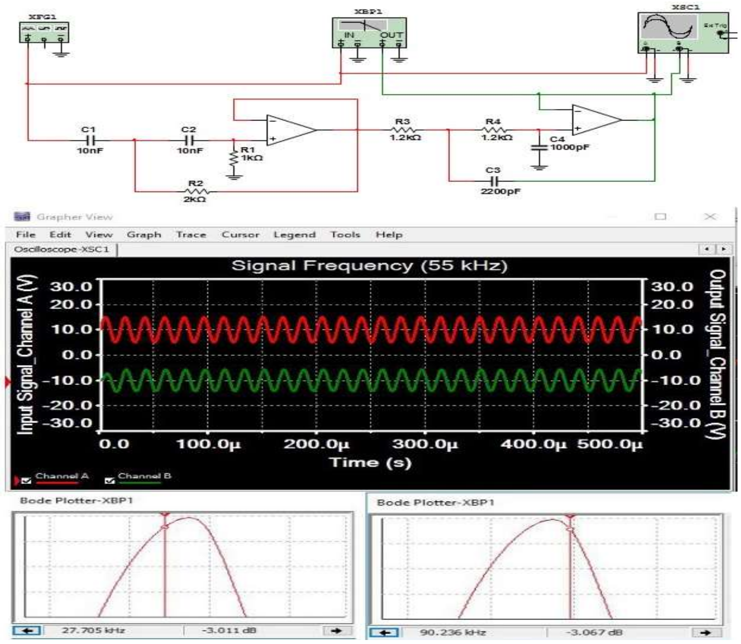

Figure 6.2 Multisim simulation result for the bandpass filter.

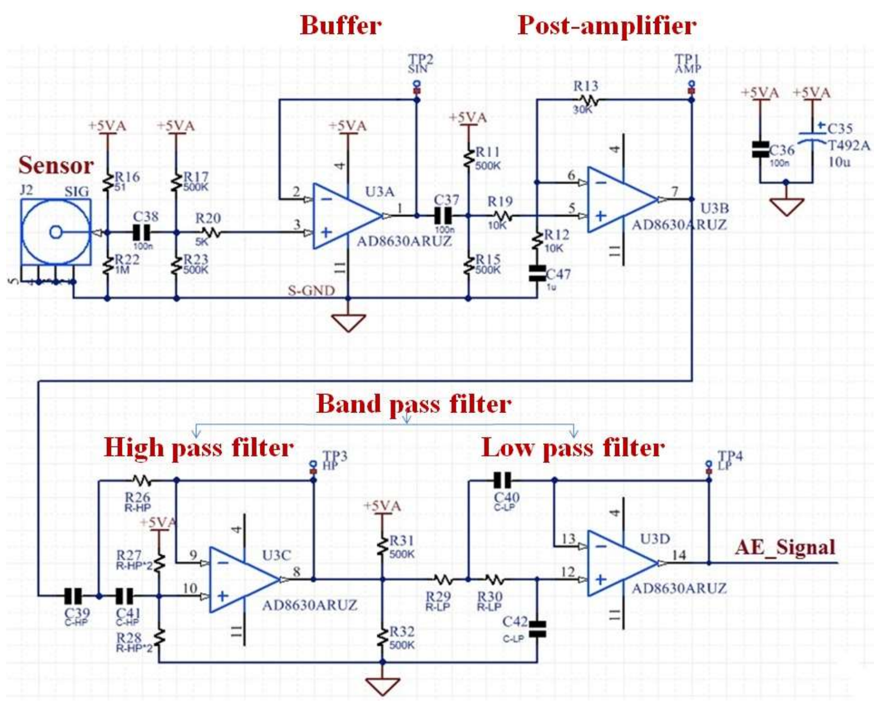

Figure 6.3 Optimized circuit diagram of SCU in a single IC.

6.2.2 Design of the computational core unit

The functional blocks of the computational core unit are DAQ, real-time clock and hardware for the parameter extraction from AE signals. The development of the DAQ on the PSoC platform has already been presented in **Chapter 5**. PSoC platform has been chosen for the development of the computational core unit also. The PSoC components used for the real-time measurement of AE events are sync (Synchronizer) and counter. The design of CCU in PSoC Creator 4.0 IDE is shown in **Figure 6.4**.

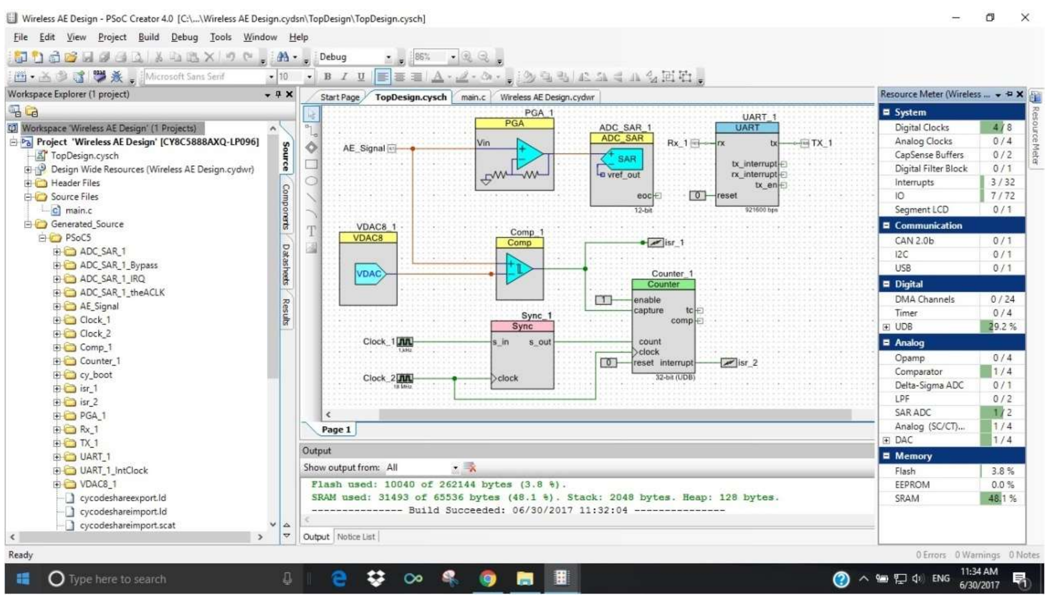

Figure 6.4 Design of computational core unit in a PSoC creator 4.0 IDE.

The reason for selecting the PSoC is due to the components of electronic circuitry (buffer, a programmable gain amplifier, comparator, counter, synchronizer, successive approximation, voltage digital to analog converter (VDAC), analog to digital converter (ADC), universal asynchronous receiver and transmitter (UART), interrupt, and a microcontroller to control operation and command can be designed in single IC. Because of this, whole electronic circuitry can be minimized and hence reducing the board space, power consumption, and system cost while improving the quality of the system development.

The AE_Signal output from the signal conditioning unit is internally connected to the programmable gain amplifier (PGA) input pin of the CCU. The PGA output is connected to the input pin of the SAR ADC. The detail configurations of the PGA, SAR ADC, VDAC8 and isr_1 component with their inter-connection have been explained for the design of DAQ in the previous chapter. The comparator compares the AE_signal voltage level with the preset threshold voltage reference (VREF) and yields the output signal based on this voltage level comparison. The comparator output is connected to isr_1. The isr_1 component is used for generating an interrupt on the rising edge of the comparator output. The 32-bit counter component is implemented along with the sync component to synchronize the input clock (Clock_1) with the source clock (Clock_2) to capture the real-time occurrence of an event of the AE signal. The sync component resynchronizes the input signal to the rising edge of the source clock. The CCU then extracts the parameters of AE signals such as ring down count or AE count, rise time, event duration, peak amplitude and root mean square (RMS). The hardware implementation of the feature extraction module has been presented in **Chapter 4**. A wireless communication unit has been interfaced with the CCU for transmission of AE parameters, the detail of which is dealt with in the subsequent sections.

The system includes one base station and one wireless AE sensor unit. The base station is responsible for:

1) Commanding the wireless AE sensor unit to perform data collection,
2) Controlling the process,
3) Receiving data from the wireless AE sensor unit, and

4) Storing the received data in a file.

A personal computer with a ZigBee wireless transceiver connection is used as the base station. The software for the wireless AE sensor system is divided into two parts, i.e., embedded software for the wireless AE sensor unit and software for the base station. The base station always initiates communication. The base station repeatedly sends commands until an expected response is received from the sensor unit.

The basic requirement for software design is to configure the sensor unit for achieving the required gain, threshold level and enable or disable data acquisition remotely. These requirements are set at the base station. The second requirement is to acquire processed data from the sensor unit and transmits the data to the base station. LabVIEW environment is used for the data analysis, display and data storage at the base station. The implemented embedded software can execute two tasks in parallel. The sensor unit can collect data from the sensor whenever the signal voltage level crosses the threshold reference of the comparator and can perform another operation simultaneously, i.e., wireless data transceiver or execute a computational algorithm to interrogate the sensor data. Multitask implementation is made a success by interrupt service routine (ISR) offered by the microcontroller. The interrupt function is a powerful feature that allows the software to momentarily pause and execute a certain task. This includes the processing of data and transmitting wirelessly when it is scheduled time to sample data from the sensor unit. The paused task resumes immediately after servicing. The above description of software development is implemented in the PSoC Creator integrated development environment (IDE). The software is written in the embedded C programming language. The details of embedded C programming code are included in **Appendix C**.

6.2.3 Wireless communication unit

A significant achievement is made when the raw data is processed locally, and only the results are transmitted. The transmission of only processed results leads to a decrease in data size to be communicated. Hence, a reduction in the decrease in data size after processing is relatively more power-efficient compared to the transfer of raw data to the base station.

Currently, many types of wireless technologies are available for transmitting data. The most predominant wireless technologies are Bluetooth, Zigbee, mobile communication and Wi-Fi. The data transfer rate of Wi-Fi communication is high, but it requires high power for long term SHM. The data transfer rate of Bluetooth communication is relatively high, but the range of data transmission is less (approx. 10 meters). Mobile data communication covers long-distance communication, but the service fees increase the cost for large scale monitoring of structural applications.

Zigbee shows many advantages compared to other wireless communications with respect to high network capacity, self-organization capability, low cost, and low power consumption. Due to this, ZigBee is the most predominantly used communication mode in a sensor network for monitoring of large-scale structural applications.

Robust data communication between the wireless AE sensor unit and the base station is essential for monitoring any structure. The estimated communication range for the civil structure may perhaps be several hundred meters. Generally, high power is associated with the long-range communication of wireless transceiver. Hence, it is required to keep a balance between low power consumption and long-range communication for monitoring of structures. However, the communication range can be extended by the use of a repeater.

The features of the ZigBee wireless transceiver are shown in **Table 6.1**. The communication range of 100 m outdoor (LOS) and 30 m indoor for ZigBee wireless transceiver is sufficient for most of the small civil structures and for laboratory works. ZigBee wireless transceiver consumes much less power in sleep mode. The maximum transfer rate of the ZigBee wireless transceiver is 921600 bps. The ZigBee wireless transceiver is an interface to the base station for continuous data communication in real-time. ZigBee wireless transceiver has different modes of communication between AE sensor unit and base station like point-to-point, point to multipoint and peer to peer, for local data analysis.

Table 6.1 Key characteristics of the ZigBee wireless transceiver.

Parameters	Specifications
Indoor/Urban Range	up to 30 m (100 ft)
Outdoor RF line-of-sight Range	up to 100 m (300 ft)
Serial Interface Data Rate (software selectable)	1200 - 921600 bps
Supply Voltage	2.8 – 3.4 Volt
Transmit Current (typical)	45mA @ 3.3 Volt
Operating Frequency	ISM 2.4 GHz
Network Topologies	Point-to-Point, Point-to-Multipoint & Peer-to-Peer

6.3 Assembled prototype wireless sensor unit

Based on the hardware design architecture, the wireless AE-SS has been developed in the laboratory. The components used for the wireless sensor unit are fabricated on a single two-layer printed circuit board (PCB). The photograph of the complete PCB with all the essential integrated circuits (ICs) is shown in **Figure 6.5**. The dimension of the two-layer PCB is 85 x 56 mm and can be further reduced by using multilayer PCB manufacturing techniques. To protect the wireless AE sensor unit and batteries from harsh weather condition, it is stored within a weather-proof polypropylene enclosure with an IP65 (ingress protection) rating of dimension 110x80x60 mm.

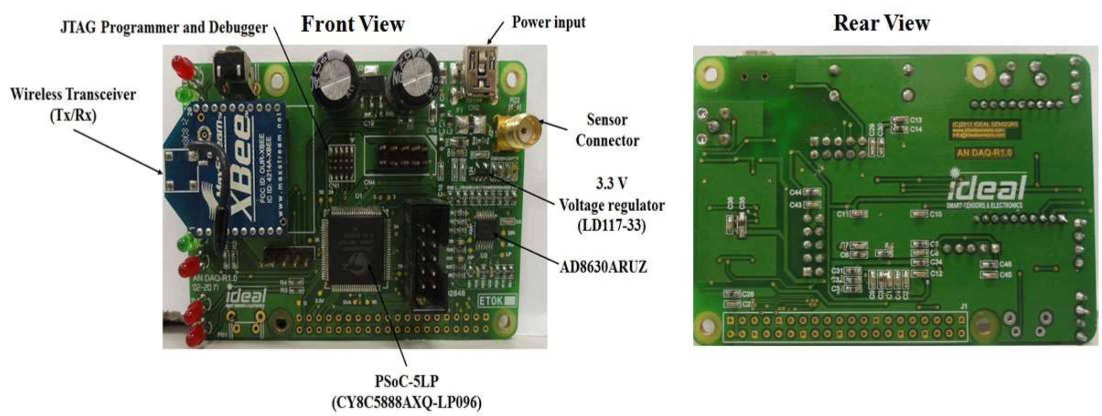

Figure 6.5 Front and rare views of integrated prototype wireless AE sensor unit.

In order to calculate the power consumption of the wireless AE sensor unit, the power rating specifications have been studied. All the design hardware components are internally referenced at 5V except the wireless transceiver, which needs 3.3V. The wireless sensor unit can collect, process, and transmit the AE data when it is active. In contrast, the wireless sensor unit can be kept in a sleep mode from which it can be easily awakened. In the sleep mode, the wireless unit consumes very low electrical current. The current consumption in slip mode is called standby current. The maximum and standby currents consumed by the elements are given in **Table 6.2**.

Table 6.2 Approximate current consumption of different components.

Components	Maximum Active current	Standby current
AD8630ARUZ (IC)	1.0 mA	100 pA
PSOC-5LP (CY8C5888AXQ-LP096)	2.0 mA	2.0 µA
ZigBee transceiver	45.0 mA	20.0 µA
Total	48.0 mA	22.0 µA

In the current prototype, 10000 mAh Lithium-ion rechargeable power bank has been used. The total active current consumption of the developed wireless AE sensor unit with the wireless transceiver in operation is measured by USB type voltage and current meter in the laboratory, are found to be 5.09 Volt and 50 mA respectively, as shown in **Figure 6.6**.

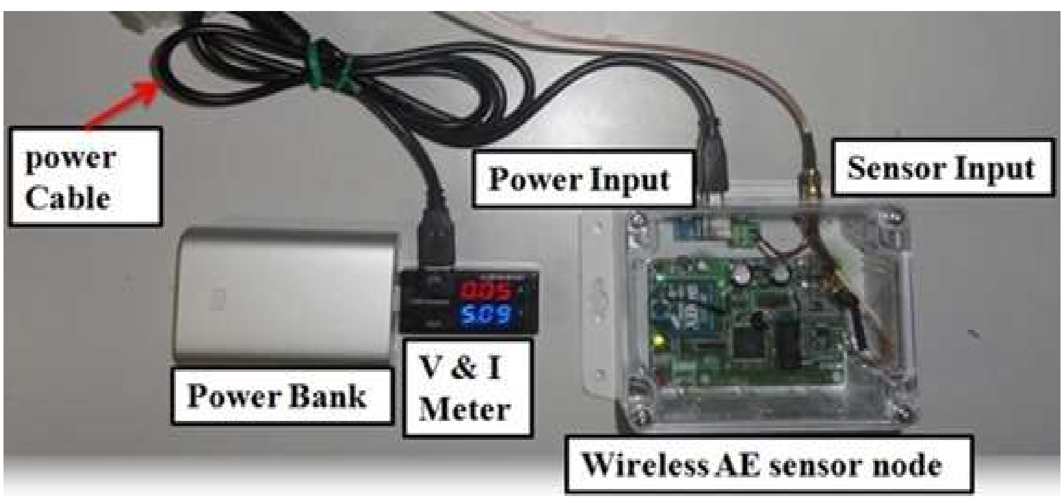

Figure 6.6 Voltage and current are measured by USB meter.

The estimated lifetime of the wireless sensor unit for continuous monitoring is expected to be:

$$Active\ time = \frac{Energy\ capacity}{current\ consumption} = \frac{10000\ mAh}{50\ mA}$$

$$= 200\ h \quad = 8.33\ days$$

This expected active life is conservative because it assumes continuous operation of the unit at all times.

6.4 Performance validation of the wireless sensor unit

Three different types of tests have been performed for validation of the developed prototype wireless AE-SS. These are the signal validation test, concrete compression test and concrete corrosion test. The experimental results of the tests are presented in subsequent sections.

6.4.1 Signal validation using artificial AE signal

An artificial burst type AE signal of 50 kHz has been generated using a signal generator device, as explained in **Chapter 5**. This signal generator device has been used for validating the developed prototype wireless system. The block diagram representation of the experimental setup for signal validation test using artificial AE events is shown in **Figure 6.7**. The actual photograph of the experimental setup is shown in **Figure 6.8**. AE_Signal is the output of the signal generator device interfaced with the developed wireless sensor unit and also to digital storage oscilloscope (DSO). The DSO has been used for recording the event of an AE signal crossing the defined threshold and for saving as ASCII format. The event of the AE signal is also acquired and transmitted by the wireless sensor unit to the base station. The transmitted event of AE data is stored and displayed at the base station, as shown in **Figure 6.8**.

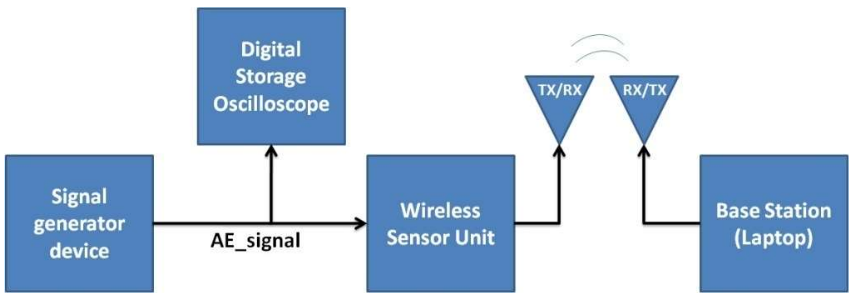

Figure 6.7 Block diagram representation of test setup for signal validation test.

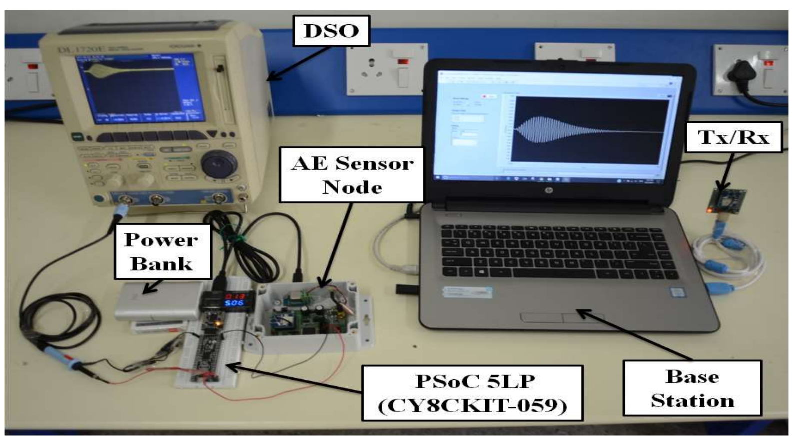

Figure 6.8 Photograph of the test setup made in the laboratory for validation of wireless AE sensor system.

The recorded AE signals at the transmitted and received sides were subjected to FFT to check for any loss of information. **Figure 6.9** shows the frequency spectra of the AE signals at the received sides. As can be seen, only 50 kHz frequency component is present in the received signal, which matches the frequency of artificial burst type AE signals **(Figure 5.9b**). Moreover, the frequency spectra of both the signals exactly match with each other, indicating that there is no loss of information during the wireless transmission.

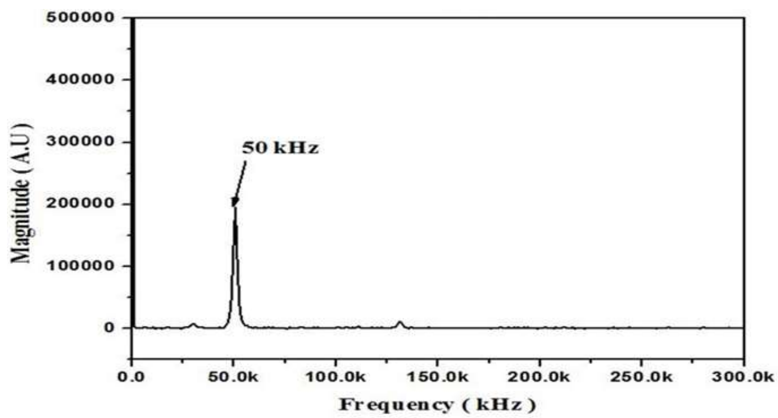

Figure 6.9 FFT of the signal received from the wireless sensor system.

6.4.2 Signal validation using pencil lead break

A setup has been made in the laboratory to validate the AE signal acquired by the wireless AE sensor unit and is shown in **Figure 6.10**. The validation has been done by comparing the signals acquired by the developed wireless AE sensor system with that obtained by a commercially available AE system (PAC). The entire setup is divided into two parts: (a) Test setup for the developed wireless AE system which consists of AE sensor unit, PK6I PZT sensor, power bank, V & I meter and Base station; and (b) Test setup for commercially available Physical Acoustic Corporation (PAC) system. This consists of DISP AE workstation, R6α PZT sensor, pre-amplifier and power supply.

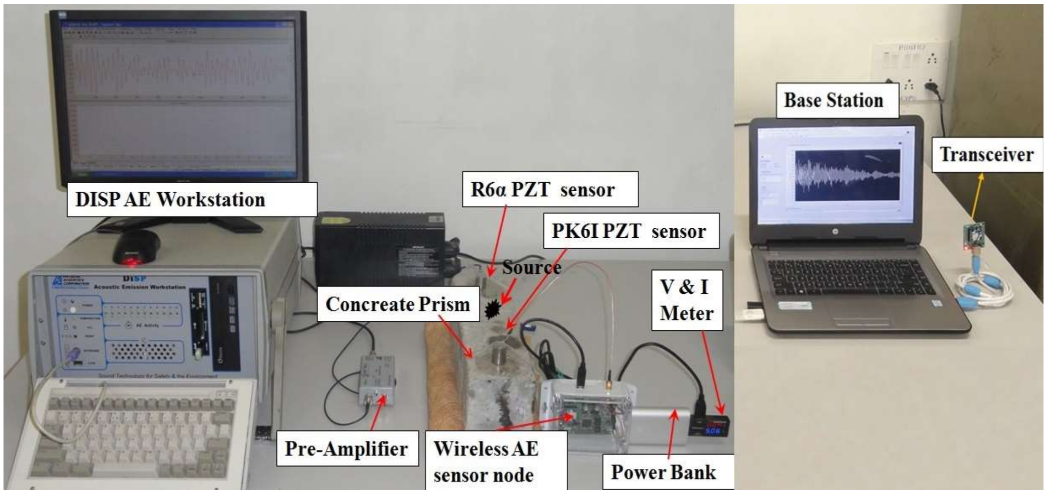

Figure 6.10 Photograph of the experimental setup of the wired based PAC system along with the wireless AE sensor system in the Lab.

The signal validation has been carried out by the pencil lead break (PLB) test. The PLB signal is considered to generate an AE event akin to that generated by the growth of a crack. The sensors for both the systems are mounted on the top surface of a concrete block separated by 40 cm. The pencil lead break tests were carried out at a location midway between the two sensors. The event of an AE signal is detected when the signal level crosses the defined threshold reference. In an AE signal, the threshold voltage is set and used for discrimination of the signal from the background noise. When an event is detected a thousand samples of AE data is recorded with a sampling rate of 1 MSPS (one-microsecond duration between samples) which means the duration of one millisecond data are recorded by both the systems. The frequency spectrum has been performed to the pencil lead break test signals. FFT is used to characterize the frequency content present in the time domain signal. One typical signal acquired by both the sensors and its FFT is shown in **Figure 6.11**. The signals received by both the sensors are almost similar in nature. The resonant frequency from the wireless AE system and PAC system is found to be 55.68 kHz and 46 kHz respectively, which varies within the operating range of frequency and around the sensor resonant frequency. The developed wireless AE system has been further validated by conducting a compression test and corrosion test on the concrete specimen.

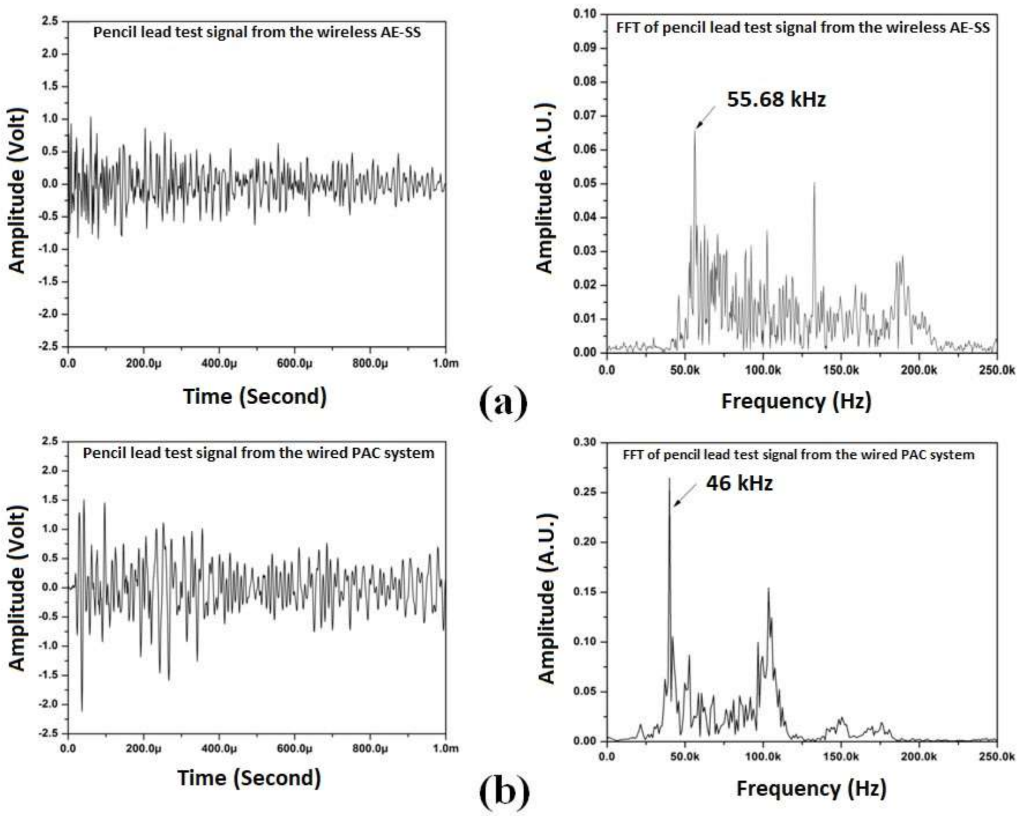

Figure 6.11 Pencil lead break test signal and it's FFT from (a) wireless AE system and (b) wired PAC system.

6.4.3 Application of the wireless AE sensor system to concrete compression test

The compression test is widely used to estimate the compressive strength of concrete. The compressive strength provides many characteristics of concrete, such as cement strength, water-cement ratio, quality control, and quality of concrete material during the production. **Table 6.3** gives detail descriptions of concrete specimens used for the compression tests. Two different grades of concrete (M30 & M45) and two different geometries of the specimen (cube & cylinder) were used. All the concrete specimens were cured for 28 days and then subjected to compression tests. AE signals generated during the compression test provide a wide range of information concerning the quality of the concrete. The tests were conducted according to the standard procedure in IS: 516-1959 with a constant loading rate of 5.2 kN/s.

Table 6.3 Details of specimens used for compression tests

Serial No.	Concrete grade	Specimen shape	Specimen dimension
1	M30	Cube	100x100x100 mm^3
2	M30	Cylinder	200 mm Height and 60 mm in Diameter
3	M30	Cylinder	300 mm Height and 60 mm in Diameter
4	M45	Cube	100x100x100 mm^3
5	M45	Cube	150x150x150 mm^3
6	M45	Cylinder	200 mm Height and 60 mm in Diameter

The photograph of the experimental setup for concrete compression and AE testing is shown in **Figure 6.12**. The entire setup is divided into two parts: (a) Test setup for the developed wireless AE system which consists of AE sensor unit, PK6I PZT sensor, power bank, V & I meter and Base station; and (b) Test setup for the commercially available Physical Acoustics Corporation (PAC, USA) system.

The test set up for the commercially available AE system consists of DISP AE workstation, R6α PZT sensor, pre-amplifier and power supply. DiSP-16 is a 16 channel wired system with dynamic range >82 dB and has a variable sampling rate from 1 MSPS to 10 MSPS. The system has an ADC resolution of 16 bit. The developed wireless system has a sampling rate of 1 MSPS and ADC resolution of 12 bit. Two PZT AE sensors (PK6I and R6α) both having a resonant frequency at 55 kHz were fixed firmly at the opposite faces of the concrete specimens. Silicon grease was used as couplant. The specification of the sensor PK6I has already been given in **Table 3.2**. The specifications of the sensor R6α used with the commercial wired PAC, USA system is given in **Table 6.4.**

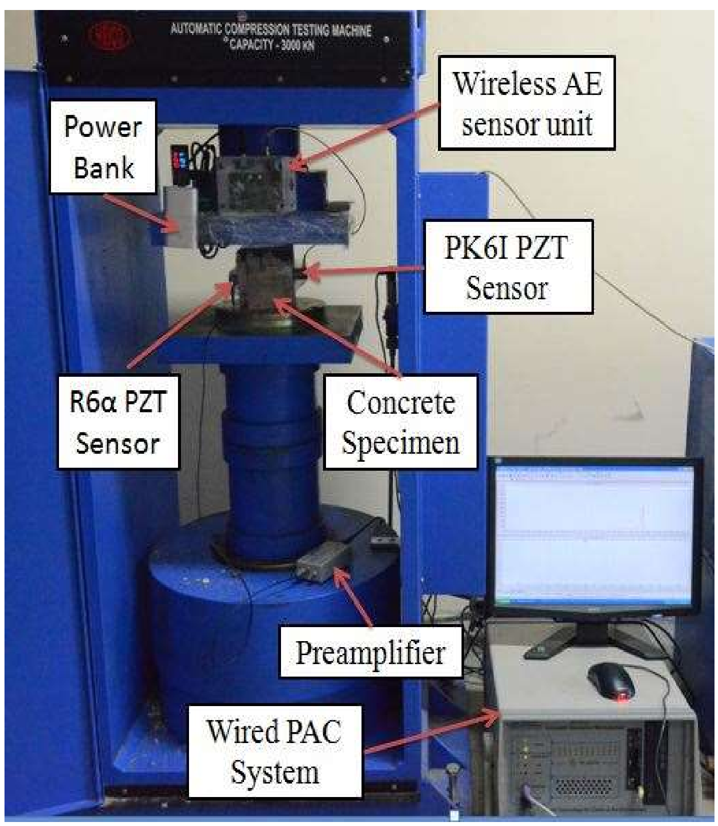

Figure 6.12 Photograph of an experimental setup for the compression test of concrete specimen.

Table 6.4 Specifications of the sensor used with the wired PAC, USA system

Specifications	Sensor (R6α) *
Type	External
Operating Frequency Range	35-100 kHz
Resonant Frequency	~55 kHz
Input Voltage	28 Volt@ 30mA
Pre-amplifier Gain	40 dB

*Sensor (R6α) is used with the wired PAC, USA system

The overall gain of the PAC system and the developed system were 40 dB and 38 dB, respectively. Prior to the compression test, the PLB test has been carried out to simulate AE events for calibration purpose. After calibration, the threshold of 55 dB and 50 dB has been fixed for the wireless and wired system, respectively. During the compression test, the applied load as a function of time has been recorded. The parameters of the AE signals generated during the compression tests after crossing the threshold were recorded by the developed wireless AE sensor system as well as by the commercially available wired PAC system. The signals were recorded at the speed of 1MSPS by both the systems. The computed AE signal parameters have been continuously transmitted through the wireless system and captured and plotted using the LabVIEW program. Similarly, AE parameters from different tests are also obtained using the commercial system. The results from one of the tests (M30 grade concrete cube of dimension 100x100x100 mm^3) are shown here. **Figure 6.13** shows the variations of counts and applied load as a function of time from (a) developed wireless AE system and (b) wired PAC system. Similar plots for other AE parameters such as cumulative counts, RMS, peak amplitude, rise time and event durations along with the load as a function of time from the wireless and wired PAC systems, are shown in **Figure 6.14 - 6.18**.

The variations of the parameters of AE signals with time, obtained from the developed wireless system are found to be a good agreement with the parameters obtained from the commercially available system. The result of cumulative counts shows a strong representation of the AE activity during the test. Three different AE activity regions can be observed from the plots, as highlighted in **Figure 6.14**. In region I, many AE signals or activity are generated due to the closure of pre-existing cracks and formation of microcracks through weak boundaries of particles within the concrete specimen. In the second region, there is a continuous increase in AE counts because of the steady growth of the cracks. AE counts generated in this region are related to multiple crack branching, fracture of large pores, and aggregate to cement interface cracking. In region III, a drastic increase in AE counts is observed when the load increases to the ultimate strength of the concrete specimen where unstable cracking occurs. These three regions of activity are also seen in other AE parameters. The difference in AE activity in the two systems is due to different characteristics of the instrument, and different gain and threshold of the sensor systems. The results of AE activity observed in different regions are in agreement with the results reported in the literature **[83]**.

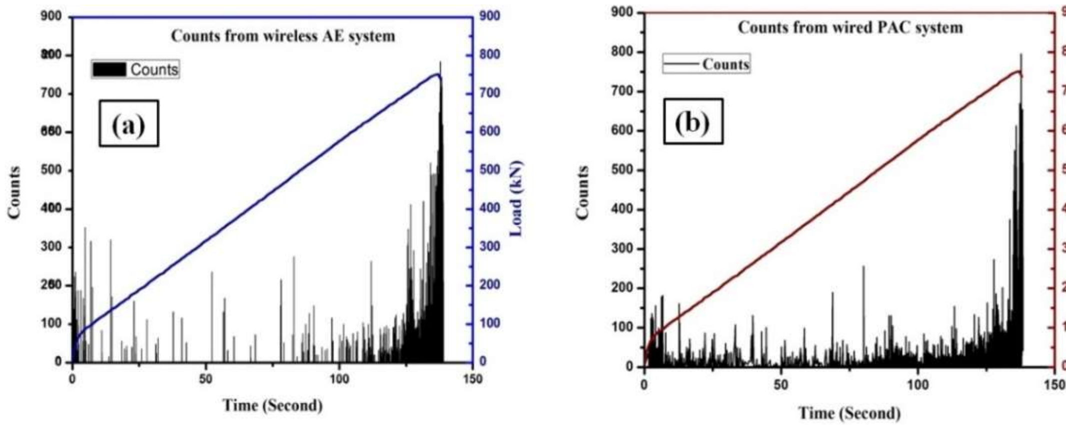

Figure 6.13 Counts and applied load as a function of time from (a) developed wireless AE system and (b) wired PAC system.

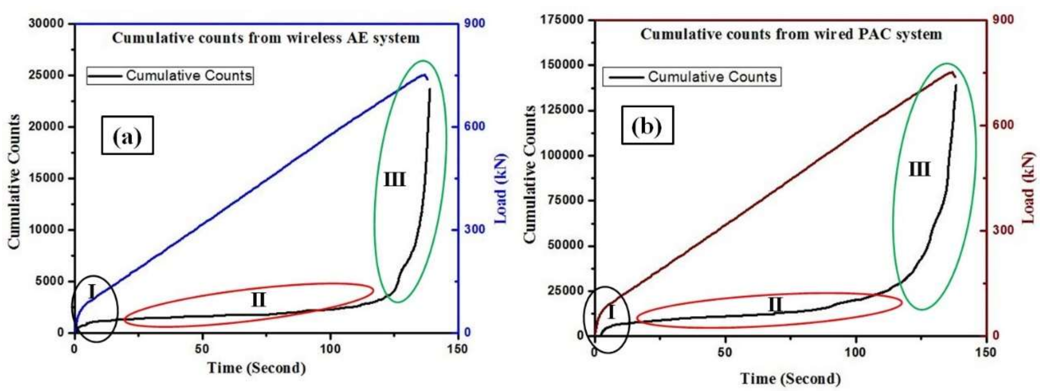

Figure 6.14 Cumulative counts and applied load as a function of time from (a) developed wireless AE system and (b) wired PAC system.

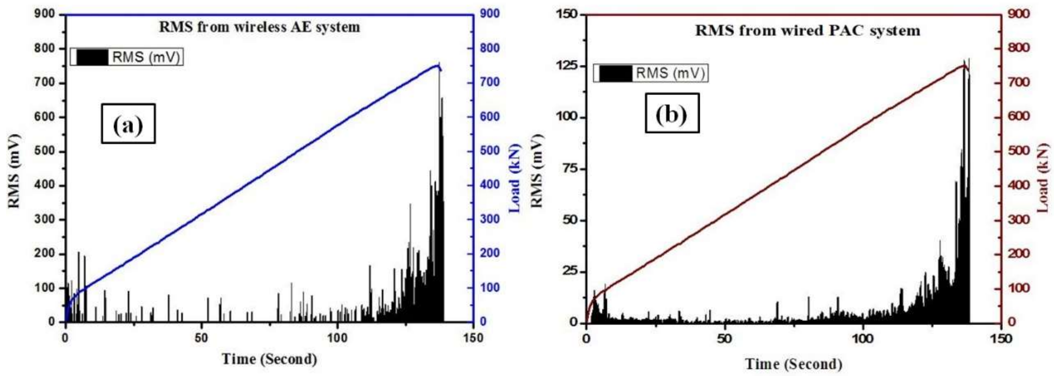

Figure 6.15 RMS and applied load as a function of time from (a) developed wireless AE system and (b) wired PAC system.

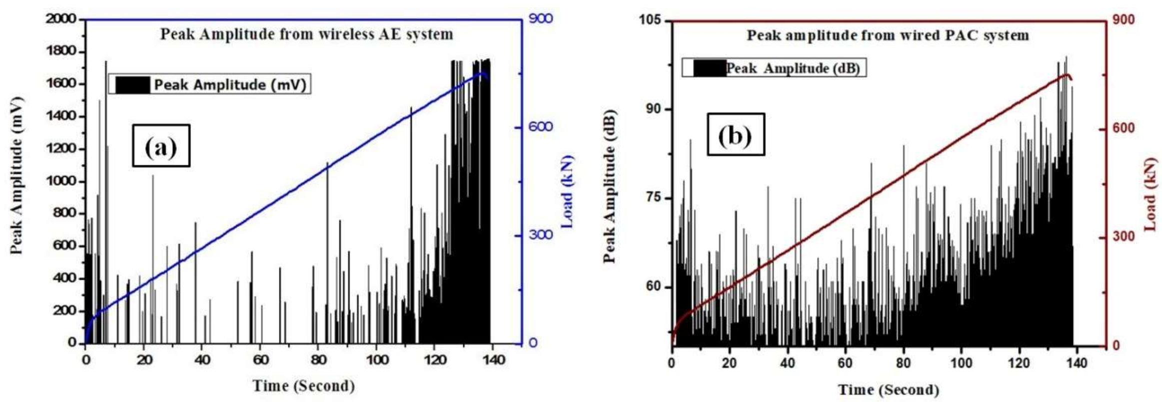

Figure 6.16 Peak amplitude and applied load as a function of time from (a) developed wireless AE system and (b) wired PAC system.

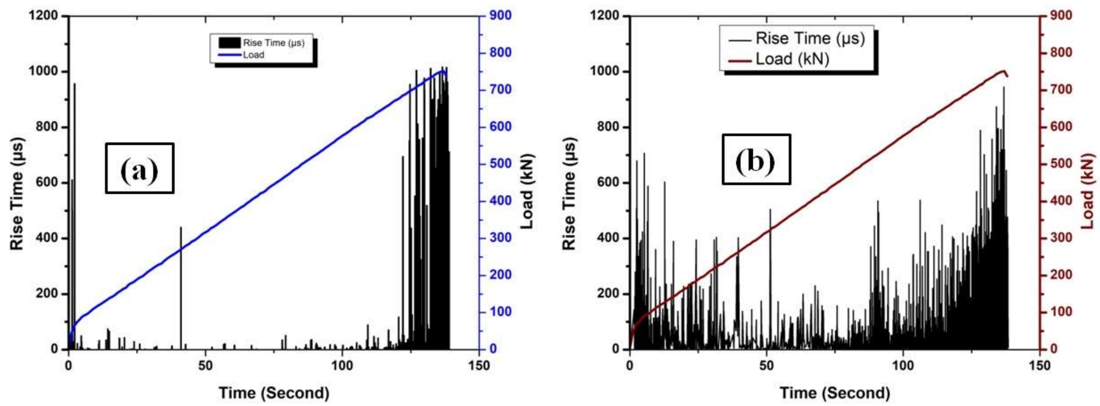

Figure 6.17 Rise time and applied load as a function of time from (a) developed wireless AE system and (b) wired PAC system.

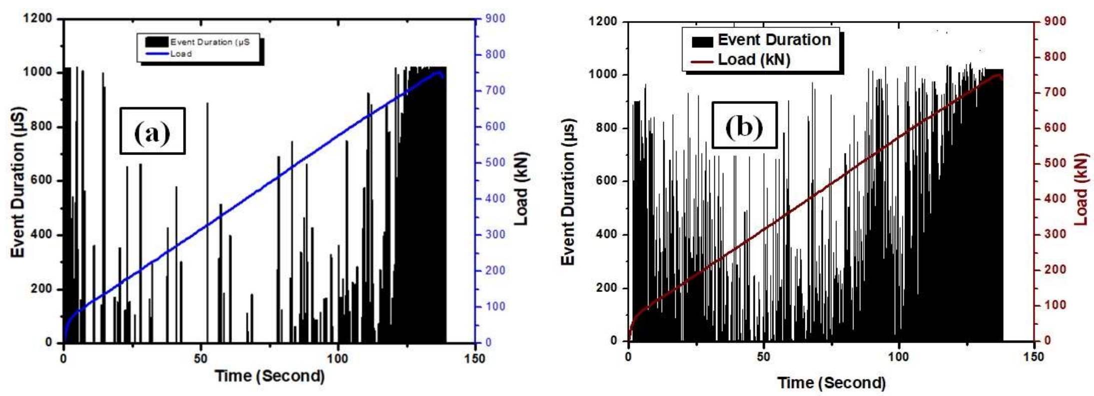

Figure 6.18 Event duration and applied load as a function of time from (a) developed wireless AE system and (b) wired PAC system.

The cracking behaviour in the concrete specimen due to the compression load has been confirmed by using a Camscan scanning electron microscope (SEM) investigation. **Figures 6.19 (a-b)** show SEM micrographs of fracture surface (different locations) of concrete after compression test. The SEM micrograph shows multiple pores at different locations and localized failure regions. These multiple cracks originated from pores and other weak boundaries and propagated into many directions after the compression test, as shown by the arrows in **Figure 6. 19**.

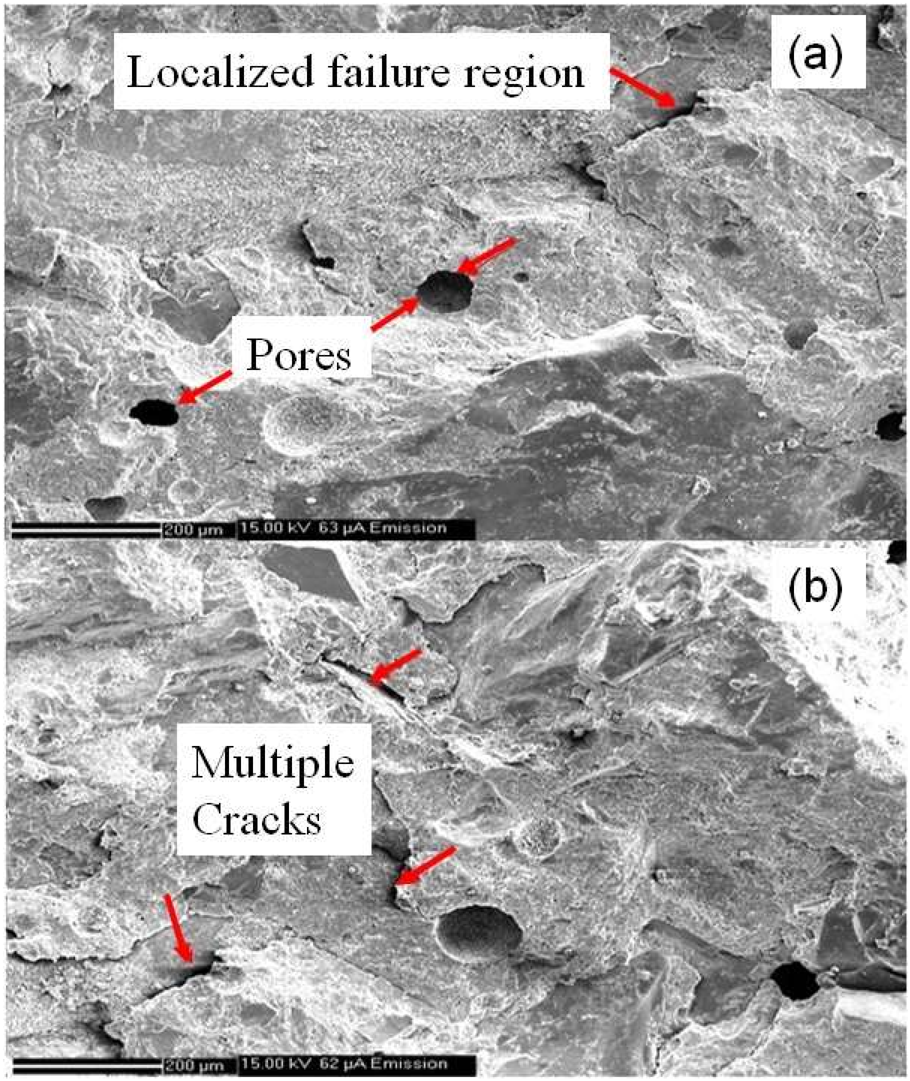

Figure 6.19 SEM images of the fracture surface of a concrete specimen.

6.4.4 Application of the wireless AE sensor system to concrete corrosion test

Rebar corrosion is one of the critical deterioration modes of reinforced concrete structures due to exposure to the saline environment. Acoustic emission monitoring of rebar corrosion has a significant role in the condition monitoring of concrete structures. For on-line corrosion damage monitoring, reinforced concrete beams having dimensions 350 mm x 100 mm x 100 mm is prepared, and rebar of 15 mm Diameter is embedded in the concrete beam. The test specimen is kept in NaCl solution on a copper plate, and 100 mA current is continuously charged between rebar and the copper plate to accelerate the corrosion. The photograph of the experimental test setup for the corrosion test in rebars is shown in **Figure 6.20**.

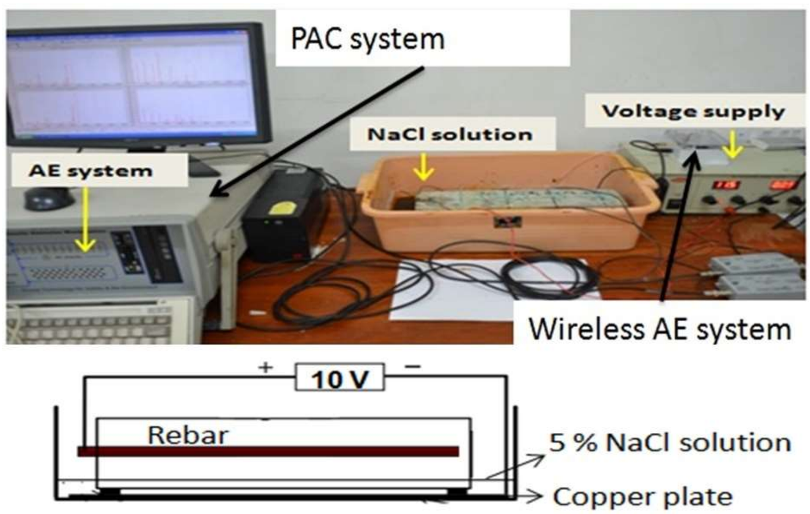

Figure 6.20 Photograph of an experimental setup for the concrete corrosion test in the Lab.

AE monitoring was done continuously for ten days using the developed wireless AE system and the commercially available PAC system. The similar test setup is used as in the compression test described earlier. The cumulative count represents the strong variation of AE activity. The result is shown by the variation of cumulative counts with time (no. of days) in **Figure 6.21**.

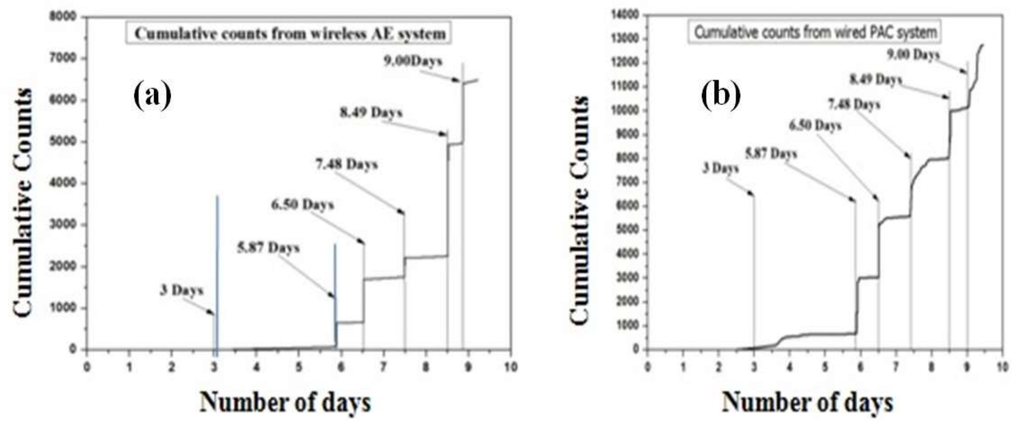

Figure 6.21 Cumulative count as a function of time in days from (a) developed wireless AE system and (b) wired PAC system.

It is seen from **Figure 6.21** that the generation of AE signals starts after three days from the starting of the test. This can be attributed to the onset of corrosion. From six days onwards, the volume of the corrosion product increases on rebar, leading to multiple cracking in the concrete, and turn to produce an AE signal. The volume of rust products is much bigger than the metallic Fe leading to cracking of the cover concrete when stress exceeds the tensile strength of the concrete. The AE results obtained by the developed system are in compliance with the results from the commercial system, thus validating the developed wireless AE sensor system. The occurrence of corrosion and cracks in the concrete beam has been confirmed by X-ray radiography. It is found that the result is in line with the reported result in the literature **[159]**.

X-ray radiography has been used to identify the rebar corrosion damage and the cracking process in the concrete. For X-ray radiography exposure, a 320 kV Balteau constant potential mini-focus X-ray unit was used with a focal spot size of 0.2 mm. Flash scan FS35

Thales flat panel detector with 127 µm pixels was used as an X-ray detector. The sample was mounted on a 7-axis manipulator stage. **Figures 6.22 (a) – (b)** show the X-ray radiography images of the concrete block before and after corrosion damage. It is seen that 12 mm thick mild steel rebar is corroded at the periphery of the rod. Grey-level intensity profile across the line segment L-M as indicated in **Figure 6.22 (b)** shows that the thickness of the rebar is reduced to 11.50 mm from the initial 12 mm, which is approximately 4% of the thickness loss at this location. It is also observed that the thickness loss due to corrosion is not uniform along the length of the rebar. After the accelerated corrosion, multiple cracks were observed, as indicated by the arrow in **Figure 6.22 (b)**.

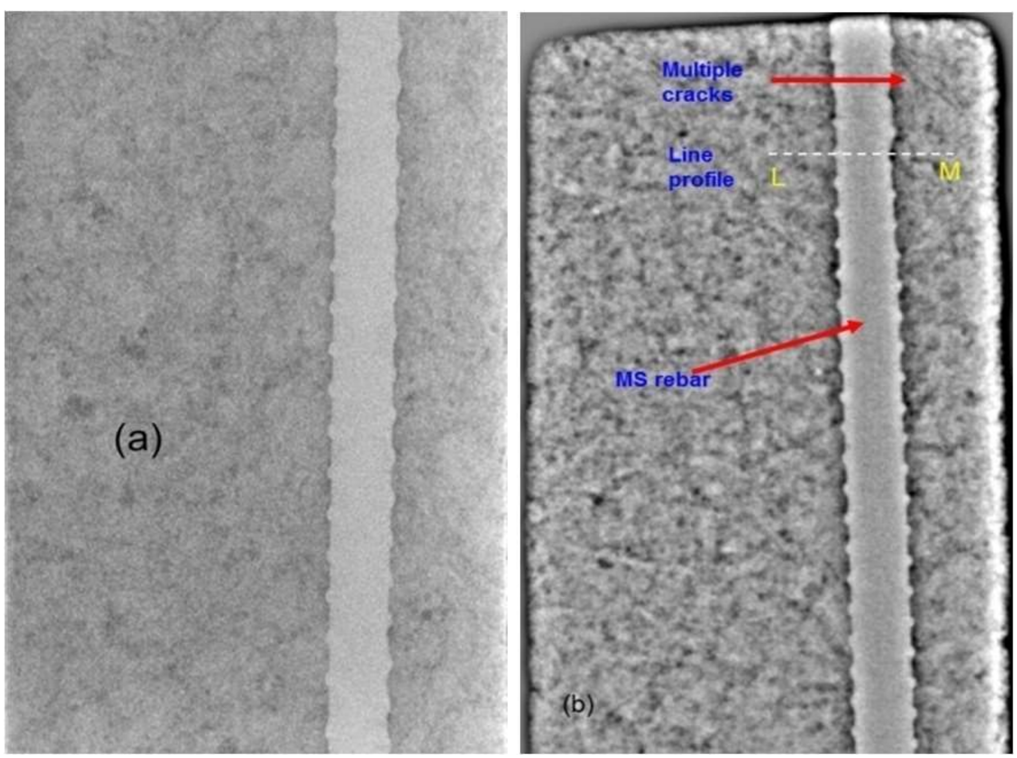

Figure 6.22 X-ray radiography image of concrete block (a) without corrosion (b) after accelerated corrosion

It can be concluded that the developed wireless system is able to detect the AE activity as shown by the characteristic curves from the compression test and corrosion test and are in compliance with the detected activity by the commercially available wired PAC system. The results of compression and corrosion tests have been verified with the SEM and X-ray radiography methods. Moreover, the developed system is the first of its kind, which has been designed and implemented on PSoC technology. The developed system can be effectively deployed for structural health monitoring of various critical concrete structures like nuclear power plant (NPP) containment, bridges, and tanks along with corrosion monitoring of rebar concrete structures in the petrochemical industry, where corrosion is a potential issue.

6.5 Summary

A real-time wireless AE-SS for structural health monitoring applications of concrete has been developed, and various design and developmental aspects have been discussed. The acquisition of burst type AE signals and extraction of various parameters of the signals is successfully implemented in real-time based on a programmable system on chip (PSoC). The wireless AE system developed has been validated by three different methods viz. signal validation using artificial AE signal along with pencil lead break test, concrete compression test and concrete corrosion test in the laboratory.

The developed wireless AE system has been successfully used for monitoring the compression test of concrete specimens. Three different regions of AE activity have been identified. The obtained results from the compression test by the developed system are in compliance with the results obtained by a commercially available system. The results of AE activity obtained by the developed system during the concrete corrosion test also match the activity obtained by the commercially available system. The results of compression and corrosion tests of concrete have been verified with the SEM and X-ray radiography methods.

7 Conclusion, contribution and scope for future work

7.1 Conclusion

The objective of the thesis is the development of a wireless acoustic emission sensor system (AE-SS) for structural health monitoring applications. A combination of hardware and software design approaches has been implemented in a programmable system on chip (PSoC) towards achieving the objective. There are different sub-modules in the design, such as signal conditioning unit (SCU), data acquisition (DAQ) device and computational core unit (CCU), for realizing a complete wireless AE sensor system.

The signal conditioning unit is developed and successfully validated by detecting artificial AE events through the piezoelectric sensor. The developed SCU is suitable for integration in the wireless sensor system and further processing of the signals. Fast Fourier Transform is used to assess the frequency characteristics of the AE signal conditioned by the SCU. The developed SCU has also been validated by comparing the signal with a commercially available AE system.

There are different parameters of burst type AE signals such as peak amplitude, RMS, counts, cumulative counts, rise time and event duration. The parameter analysis technique is found to be promising for wireless systems. The parameter-based technique solves the constraint of the embedded system over the signal-based technique with respect to a huge amount of physical memory data storage, high processing time, and large transmission bandwidth. A new and novel method for hardware-based parameters extraction from burst type AE signals has been presented. The designed and measured values of the parameters obtained from the simulation results are in good agreement with each other. Wireless transmission of AE parameters instead of the signal is advantageous in terms of the storage capacity of data, the processing load of the microcontroller, and transmission time.

A data acquisition device is developed based on an integrated hardware and software design approach in a programmable system on chip for acquiring burst type AE events. The developed DAQ is capable of capturing AE events at 1 mega samples per second (1 MSPS) rate with a 12-bit resolution, which is sufficient for the reliable representation of AE events.

The computational core hardware and software design is implemented in PSoC for parameter extraction from burst type AE events and transmission of the parameters wirelessly to a base station. ZigBee wireless communication protocol has been established to ensure reliable transmission of the signal parameters to the base station. Finally, the signal conditioning unit, computational core unit and the wireless unit is fabricated, assembled, and the complete wireless AE-SS is validated in the laboratory.

A number of experiments were carried out for validating the developed wireless acoustic emission sensor system. This involves signal validation using artificial AE signal along with pencil lead break test, concrete compression test and concrete corrosion test. The AE results from concrete compression test have confirmed three different regions of activity as envisaged and these are attributed to (a) closure of pre-existing cracks and formation of micro-cracks through weak boundaries of particles within the concrete specimen, (b) steady growth of the cracks resulting in continuous increase in AE counts and (c) unstable cracking near to ultimate strength of the concrete specimen resulting in drastic increase in AE counts. The results of monitoring of accelerated rebar corrosion by AE show the generation of AE signals from 3rd day onwards, which is attributed to the onset of corrosion. The increased AE activity from 6th day onwards is attributed to multiple cracking in concrete, and this could be understood by an increase in the volume of the corrosion products. The developed wireless AE-SS has been successfully employed for detecting damage in concrete materials. The additional advantages of the wireless AE sensor system are that it is cost-effective, compact in size, easy to install on structures, portable, low power consumption capability to ensure long term monitoring in a single charge battery supply and remote operational capability.

7.2 Contribution

In this thesis, a first of its kind, programmable system on chip (PSoC) based wireless acoustic emission sensor system has been designed and developed. The developed wireless acoustic emission sensor system has been successfully validated and applied for structural health monitoring applications. The developed wireless system offers unique advantages of its compactness in size (85 mm x 56 mm), low power consumption capability (50 mA), battery operated, portability, reduced wiring complexity, reduced cost and remote operational capability. This system can be effectively utilized for condition monitoring of structures and components such as NPP containments, bridges, tanks, and components in petrochemical industries where corrosion is a potential issue, with utmost ease and efficiency. The following contribution arises from the design and development process for the wireless acoustic emission sensor system, as listed below.

1. A signal conditioning unit has been designed, developed and validated for acoustic emission signal. The developed SCU provides a wide range of sensor signals, rail-to-rail input and output swings, and reduces the complexity of biasing, and provides an optimal level for further processing of AE signals.
2. The performance of the in-house developed SCU has been compared with a commercially available system through the pencil lead break test. The time-domain and power spectral density of AE events reproduced by the in-house developed SCU and a commercially available system has been found to agree with each other. The resonant frequency of AE signals at different locations is found to be the same and lies within the operating frequency range from 100 to 400 kHz for metallic material and 35 to 65 kHz for concrete, respectively.
3. A new and novel hardware design approach has been proposed towards extracting the parameters of AE signals. Combinations of analog and digital circuits were employed in this design and the simulation results were presented. Implementation of the hardware had resulted in reliable extraction of the parameters of AE signals and is found to be promising for wireless transmission for SHM applications.
4. A programmable system on chip based data acquisition (DAQ) has been designed and developed for AE signals. The developed DAQ has been successfully validated with artificial AE signals and can be applied for SHM of concrete.
5. A programmable system on chip based computational core unit has been designed and interfaced with the signal conditioning unit along with Zigbee based wireless communication unit for the development of the wireless acoustic emission sensor system in a single two-layer PCB. The developed wireless system has been successfully

validated with a commercially available wired PAC system through concrete compression and corrosion tests. The results of compression and corrosion tests of concrete have been verified with scanning electron microscopy and X-ray radiography methods.

7.3 Scope of future work

In this work signal conditioning unit has been developed for resonant type piezoelectric sensor. The development of a signal conditioning unit for wideband sensor is not covered. A study can be made to realize the frequency characteristics present in continuous type AE signals. An appropriate filter can be designed and implemented to avoid external noise within the operating frequency band of the wideband sensor. Low sampling and resolution are required for data acquisition devices for burst type AE signals in concrete compared to continuous type AE signals generated in metallic materials. Hence further steps can be taken to develop data acquisition with high sampling and high resolution for metallic materials. In the present work, the developed wireless AE-SS is restricted to wireless transmission of the AE parameters only. This development can be extended to wireless transmission of AE parameters along with the complete AE signal. In this work, a single wireless sensor unit has been realized by using peer to peer communication between the sensor unit and the base station. This work can be extended to the development of multiple sensor units, which can be synchronized with the base station for identifying the location of AE sources during SHM. The structural integrity of large structures such as pressure vessels, aircrafts and bridges can be realized using acoustic emission wireless sensor network.

Appendix

A

Embedded C Programming Code for data acquisition device

```
/*
===========================================================================

 *PROGRAMMING CODE FOR THE DATA ACQUISITION DEVICE IN PSoC CREATOR 4.0 IDE

===========================================================================
*/
#include<project.h>
#include<stdio.h>
#include<math.h>
#definesample_size 1024
unsignedintThresholdValue=2070;
unsignedint VDAC=2070;
uint16 signal[1024];
charbuf[4];
uint8 Gain;
unsignedint  samples;
uint8Flag_Run;
uint8Thr_Flag;

//Data Acquisition using interrupts
CY_ISR(T_crossing_ISR)
{
for(samples=0;samples<1024;samples++)
        {
             ADC_SAR_1_StartConvert();
             ADC_SAR_1_IsEndConversion(ADC_SAR_1_WAIT_FOR_RESULT);
             signal[samples]= ADC_SAR_1_GetResult16();
         }
```

```
or(samples=0;samples<1024;samples++)
        {
sprintf(buf,"%d\n",signal[samples]);
            UART_1_PutString(buf);
        }
 }

voidsysteminit(void)
{
ADC_SAR_1_Start();  // Initilaize ADC
    Opamp_1_Start();
    Comp_1_Start();//Initilaize COMP
    VDAC8_1_Start();//Initiliaze DAC
    ADC_SAR_1_SetPower(ADC_SAR_1__HIGHPOWER); //Normal power at 18 MHz
    ADC_SAR_1_SetResolution(ADC_SAR_1__BITS_12);//Sets resolution to 12  bits
    UART_1_Start();     /* Enabling the UART */
Interrupt_StartEx(T_crossing_ISR);
    VDAC8_1_SetValue(VDAC);
}
////////////////////////////////
    // HEX to NeumericConvertion //
///////////////////////////////
uint8 GetNeumeric8Bit(void)
{
char P1,P2;
    P1=UART_1_ReadRxData();
if ((P1 >= '0') && (P1 <= '9'))
    {
P1 -= '0';
    }
elseif ((P1 >= 'A') && (P1 <= 'F'))
    {
P1 -= 'A';
    }
    P2=UART_1_ReadRxData();
if ((P2 >= '0') && (P2 <= '9'))
    {
P2 -= '0';
    }

elseif ((P1 >= 'A') && (P2 <= 'F'))
    {
P2 -= 'A';
    }
P1 <<= 4;
P1 += P2;
return P1;
}
voidprocesscommand(void)
{
charch;
ch = UART_1_GetChar();
if(ch== 'S')
    {
```

```
Flag_Run = 1;
    }
if (ch=='R')
    {
Flag_Run = 0;
    }
if(ch=='T')
     {
ThresholdValue=GetNeumeric8Bit();
     }
if(ch=='I')
     {
      VDAC=GetNeumeric8Bit();
     }
if(ch=='G')
     {
      Gain=GetNeumeric8Bit();
     }
}
int main(void)
{
CyGlobalIntEnable; /* Enable global interrupts. */
systeminit();
while(1)
        {
processcommand();
if(Flag_Run == 1)
        {
Interrupt_Enable();

        }
if(Flag_Run == 0)
        {
Interrupt_Disable();
        }
        }
}
/* END OF PROGRAM */
```

B

Embedded C Programming Code for signal generator device

```
/*
============================================================================

 *PROGRAMMING CODE FOR THE SIGNAL GENERATOR DEVICE IN PSoC CREATOR 4.0 IDE

============================================================================
*/

#include "project.h"

int AE_Burst1024[]=
      {156, 156,  156,  156,  156,  157,  157,  157,  157,  156,  156,  155,
      155,  155,  154,  154,  155,  155,  156,  157,  159,  160,  161,  161,
      161,  160,  159,  157,  155,  152,  150,  148,  148,  148,  149,  152,
      155,  159,  162,  166,  168,  169,  169,  167,  163,  159,  153,  148,
      143,  140,  139,  139,  142,  146,  153,  159,  166,  172,  177,  179,
      178,  175,  169,  162,  153,  145,  137,  132,  129,  129,  133,  140,
      149,  159,  169,  178,  185,  188,  188,  184,  176,  166,  154,  142,
      132,  124,  120,  120,  125,  133,  144,  157,  171,  183,  192,  197,
      197,  192,  183,  171,  156,  142,  128,  118,  112,  112,  116,  126,
      139,  155,  171,  185,  197,  203,  204,  200,  190,  176,  159,  142,
      126,  114,  106,  105,  109,  119,  134,  151,  170,  186,  200,  208,
      211,  206,  196,  181,  163,  144,  126,  112,  102,  100,  103,  113,
      129,  147,  167,  186,  201,  211,  215,  212,  202,  186,  167,  147,
      127,  111,  100,  96,   99,   108,  124,  143,  164,  184,  201,  213,
      218,  215,  206,  191,  172,  150,  130,  112,  100,  94,   96,   104,
      119,  139,  160,  181,  199,  212,  219,  218,  210,  195,  176,  154,
      133,  114,  101,  94,   94,   102,  116,  135,  156,  178,  197,  211,
      218,  219,  212,  198,  180,  158,  137,  118,  103,  95,   94,   100,
      113,  131,  152,  174,  193,  208,  217,  219,  213,  200,  183,  162,
      141,  121,  106,
       97,  95,   100,  111,  128,  149,  170,  189,  205,  214,  217,  213,
      202,  185,  166,  145,  126,  110,  100,  96,   100,  110,  126,  145,
      166,  185,  201,  211,  215,  212,  203,  188,  169,  149,  130,  114,
```

103,	99,	101,	110,	124,	142,	162,	180,	196,	207,	212,	211,
203,	189,	172,	153,	134,	119,	107,	102,	103,	110,	123,	140,
158,	176,	192,	203,	209,	208,	202,	190,	174,	156,	139,	123,
112,	105,	105,	111,	122,	137,	155,	172,	187,	199,	205,	206,
201,	190,	176,	159,	143,	128,	116,	109,	108,	113,	122,	136,
152,	168,	183,	194,	201,	203,	199,	190,	177,	162,	146,	132,
120,	113,	111,	115,	123,	135,	149,	164,	179,	190,	197,	200,
197,	189,	178,	164,	150,	136,	125,	117,	115,	117,	124,	134,
147,	161,	175,	186,	193,	196,	194,	188,	178,	166,	153,	140,
129,	121,	118,	119,	125,	134,	146,	159,	171,	182,	189,	193,
192,	187,	178,	167,	155,	143,	133,	125,	122,	122,	126,	134,
145,	156,	168,	178,	185,	189,	189,	185,	178,	168,	157,	146,
136,	129,	125,	125,	128,	135,	144,	154,	165,	174,	182,	186,
187,	184,	178,	169,	159,	149,	140,	133,	128,	127,	130,	135,
143,	153,	162,	171,	178,	183,	184,	182,	177,	169,	160,	151,
143,	136,	131,	130,	132,	136,	143,	151,	160,	169,	175,	180,
181,	180,	176,	169,	162,	153,	145,	139,	134,	133,	134,	137,
143,	150,	158,	166,	172,	177,	179,	178,	175,	169,	162,	155,
148,	141,	137,	135,	135,	138,	143,	150,	157,	164,	170,	174,
176,	176,	174,	169,	163,	156,	150,	144,	140,	137,	137,	140,
144,	149,	156,	162,	168,	172,	174,	174,	172,	168,	163,	157,
151,	146,	142,	140,	139,	141,	144,	149,	155,	160,	166,	170,
172,	172,	171,	168,	163,	158,	153,	148,	144,	142,	141,	142,
145,	149,	154,	159,	164,	168,	170,	171,	170,	167,	163,	159,
154,	150,	146,	143,	143,	143,	146,	149,	153,	158,	162,	166,
168,	169,	169,	167,	163,	159,	155,	151,	148,	145,	144,	145,
146,	149,	153,	157,	161,	164,	167,	168,	167,	166,	163,	160,
156,	152,	149,	147,	146,	146,	147,	150,	153,	156,	160,	163,
165,	166,	166,	165,	163,	160,	157,	153,	150,	148,	147,	147,
148,	150,	153,	156,	159,	162,	164,	165,	165,	164,	162,	160,
157,	154,	151,	149,	148,	148,	149,	150,	153,	155,	158,	161,
163,	164,	164,	164,	162,	160,	157,	155,	152,	150,	149,	149,
149,	151,	153,	155,	157,	160,	162,	163,	163,	163,	162,	160,
158,	155,	153,	151,	150,	150,	150,	151,	153,	155,	157,	159,
161,	162,	162,	162,	161,	160,	158,	156,	154,	152,	151,	151,
151,	151,	153,	155,	156,	158,	160,	161,	162,	162,	161,	160,
158,	156,	154,	153,	152,	151,	151,	152,	153,	154,	156,	158,
159,	160,	161,	161,	160,	159,	158,	157,	155,	154,	153,	152,
152,	152,	153,	154,	156,	157,	159,	160,	160,	160,	160,	159,
158,	157,	155,	154,	153,	153,	152,	153,	153,	154,	156,	157,
158,	159,	160,	160,	160,	159,	158,	157,	156,	155,	154,	153,
153,	153,	154,	154,	156,	157,	158,	159,	159,	159,	159,	159,
158,	157,	156,	155,	154,	154,	153,	153,	154,	155,	155,	156,
157,	158,	159,	159,	159,	159,	158,	157,	156,	155,	154,	154,
154,	154,	154,	155,	155,	156,	157,	158,	158,	159,	159,	158,
158,	157,	156,	156,	155,	154,	154,	154,	154,	155,	155,	156,
157,	158,	158,	158,	158,	158,	158,	157,	156,	156,	155,	155,
154,	154,	154,	155,	155,	156,	157,	157,	158,	158,	158,	158,
158,	157,	157,	156,	155,	155,	155,	155,	155,	155,	155,	156,
157,	157,	157,	158,	158,	158,	157,	157,	157,	156,	156,	155,
155,	155,	155,	155,	155,	156,	156,	157,	157,	158,	158,	158,
157,	157,	157,	156,	156,	155,	155,	155,	155,	155,	155,	156,
156,	157,	157,	157,	157,	157,	157,	157,	157,	156,	156,	156,
155,	155,	155,	155,	156,	156,	156,	157,	157,	157,	157,	157,

```
      157,  157,  157,  156,  156,  156,  155,  155,  155,  155,  156,  156,
      156,  156,  157,  157,  157,  157,  157,  157,  157,  156,  156,  156,
      156,  155,  155,  155,  156,  156,  156,  156,  157,  157,  157,  157,
      157,  157,  157,  156,  156,  156,  156,  156,  156,  156,  156,  156,
      156,  156,  157,  157,  157,  157,  157,  157,  157,  156,  156,  156,
      156,  156,  156,  156,  156,  156,  156,  156,  156,  157,  157,  157,
      157,  157,  157,  156,  156,  156,  156,  156,  156,  156,  156,  156,
      156,  156,  156,  157,  157,  157,  157,  157,  157,  156,  156,  156,
      156,  156,  156,  156,  156,  156,  156,  156,  156,  157,  157,  157,

      157
};

inti;
int main(void)
{
    VDAC8_1_Start();
    Opamp_1_Start();
CyGlobalIntEnable; /* Enable global interrupts. */
while (1)
for(i=0;i<1023;i++)
    {
        VDAC8_1_SetValue (AE_Burst1024[i]);
    }
return 0;
}
/* END OF PROGRAM */
```

C

Embedded C Programming Code for the wireless sensor unit

```
/*
===========================================================================

  *PROGRAMMING CODE FOR THE wireless sensor unit IN PSoC CREATOR 4.0 IDE

===========================================================================
*/
#include<project.h>
#include<stdio.h>
#include<math.h>
#definesample_size 1024
#definesample_interval 1//in microseconds
//unsigned long int sample_size=1024;
unsignedintThresholdValue=2070;
unsignedint VDAC=2076;
unsignedintMidValue=2036;
uint8 Gain;
unsignedintz,event;
unsignedint
samples1[sample_size],samples2[sample_size],samples3[sample_size],samples
4[sample_size],samples5[sample_size],samples6[sample_size];
unsignedint
*a[6]={samples1,samples2,samples3,samples4,samples5,samples6};
unsignedintDPArray[sample_size];
unsignedint
sem_DA,sem_DP1,sem_DP2,sem_DP3,sem_DP4,sem_DP5,sem_DP6,array,parray,sampl
es,PeakAmplitude,RiseTime,EventDuration,ApproxAEcount,AEcount;
unsignedintsem_DP,refill=0;
unsignedlongintsquare,sumofsquares;
unsignedlongintCumulativeCount=0;
unsignedintSquareMean;
unsignedint RMS;
unsignedint Hit;
unsignedint sum;
unsignedint average=0;
unsignedintfirstthresholdcrossing;
unsignedintlastthresholdcrossing;
unsignedintpeaksamples;
```

```
uint32CapturedTime=0;
uint8Flag_Run;
uint8Thr_Flag;
void parameters(void)
{
ApproxAEcount=0;
sumofsquares=0;
AEcount=0;
    square=0;
SquareMean=0;
RMS=0;
    sum=0;
PeakAmplitude=0;
peaksamples=0;
firstthresholdcrossing=0;
lastthresholdcrossing=0;
      for(samples=0;samples<sample_size;samples++)
        {
            //to find peakamplitude and risetime
            PeakAmplitude=DPArray[0];
if(DPArray[0] <DPArray[samples])
                {
DPArray[0]= DPArray[samples];
PeakAmplitude=DPArray[0];
peaksamples=(sample_interval*samples);
                }
            //event duration
            if(DPArray[samples]>ThresholdValue)
                     {
lastthresholdcrossing=samples;
                     }
if(DPArray[lastthresholdcrossing-1]<ThresholdValue)
                     {
firstthresholdcrossing= samples;
                     }
            //to find AEcount and cumulativecount
if (DPArray[samples]<MidValue)
            {
Thr_Flag=0;
            }
            elseif(DPArray[samples]>ThresholdValue)
                {
if (Thr_Flag==0)
                        {
Thr_Flag=1;
AEcount++;
                        }
                }
            // to find rms
            square=((DPArray[samples]-2057)*(DPArray[samples]-2057));
sumofsquares=sumofsquares+square;
        sum=sum+DPArray[samples];
        }
      //AEcount and cumulativecount
EventDuration = lastthresholdcrossing - firstthresholdcrossing;
RiseTime= peaksamples-firstthresholdcrossing;
    Hit=Hit+1;
```

```
CumulativeCount=AEcount+CumulativeCount;
SquareMean=sumofsquares/sample_size;
    RMS=sqrt(SquareMean);
RMS=(RMS*5000)/4096;
    average=sum/sample_size;
PeakAmplitude=PeakAmplitude-average;
PeakAmplitude=(PeakAmplitude*5000)/4096;
sem_DP=1;
}
voidDataprocessing()
{
      sem_DA=0;
parray=parray+1;//variable to choose arrays for data processing.
      if(parray>6)
      {
            parray=1;
      }
      switch(parray)
        {
case 1:
for(samples=0;samples<sample_size;samples++)
                        {

                        DPArray[samples]=samples1[samples];
                              }
                  parameters();
                  break;
            case 2:
for(samples=0;samples<sample_size;samples++)
                        {
DPArray[samples]=samples2[samples];
                        }
                  parameters();
                  break;
case 3:
for(samples=0;samples<sample_size;samples++)
                        {
DPArray[samples]=samples3[samples];
                        }
                  parameters();
                  break;
case 4:
for(samples=0;samples<1024;samples++)
                        {

DPArray[samples]=samples4[samples];
                        }
                  parameters();
                  break;
            case 5:
for(samples=0;samples<sample_size;samples++)
                        {

DPArray[samples]=samples5[samples];
                              }
                  parameters();
                  break;
```

```
case 6:
for(samples=0;samples<sample_size;samples++)
                        {

DPArray[samples]=samples6[samples];
                        }
                  parameters();
                  break;
        }
}

//Data Acquisition using Interrupts
CY_ISR(T_crossing_ISR)
{
CapturedTime = Counter_1_ReadCapture();
      if(refill<=0)
      {
            for(samples=0;samples<sample_size;samples++)
            {
        ADC_SAR_1_StartConvert();
        ADC_SAR_1_IsEndConversion(ADC_SAR_1_WAIT_FOR_RESULT);
            a[event][samples]=ADC_SAR_1_GetResult16();
        }
            event=event+1;
            if(event>5)
            {
                  event=0;
                  refill=refill+1;
            }
            sem_DA=1;
      }
      else
      {
            if(sem_DP==1)
            {
                  sem_DP=0;
                  for(samples=0;samples<sample_size;samples++)
                  {
                ADC_SAR_1_StartConvert();
                ADC_SAR_1_IsEndConversion(ADC_SAR_1_WAIT_FOR_RESULT);
                        a[event][samples]=ADC_SAR_1_GetResult16();
                  }
                  event=event+1;
                  if(event>5)
                  {
                        event=0;
                        refill=refill+1;
                  }
                  sem_DA=1;
            }
      }
}

CY_ISR(counterInterrupt)
{
}
voidDatatransmission()
```

```
{
char buffer[80];
sprintf(buffer,sizeof(buffer),"  %u,%u,%u,%lu,%u,%u,%u,%u,%lu\n",PeakAmpli
tude,RMS,AEcount,CumulativeCount,Hit,RiseTime,EventDuration,average,Captu
redTime);
    UART_1_PutString(buffer);
}
voidsysteminit(void)
{
    Counter_1_Start();
    ADC_SAR_1_Start();  // Initilaize ADC
    Comp_1_Start();//Initilaize COMP
    VDAC8_1_Start();//Initiliaze DAC
    ADC_SAR_1_SetPower(ADC_SAR_1__HIGHPOWER); //Normal power at 18 MHz
    ADC_SAR_1_SetResolution(ADC_SAR_1__BITS_12);//Sets  resolution  to  12
bits
    UART_1_Start();     /* Enabling the UART */
    PGA_1_Start();
    isr_1_StartEx(T_crossing_ISR);
    PGA_1_SetGain(Gain);
    VDAC8_1_SetValue(VDAC);
}
////////////////////////////////
    // HEX to NeumericConvertion //
///////////////////////////////
uint8 GetNeumeric8Bit(void)
{
char P1,P2;
    P1=UART_1_ReadRxData();
if ((P1 >= '0') && (P1 <= '9'))
    {
P1 -= '0';
    }
elseif ((P1 >= 'A') && (P1 <= 'F'))
    {
P1 -= 'A';
    }
    P2=UART_1_ReadRxData();
if ((P2 >= '0') && (P2 <= '9'))
    {
P2 -= '0';
    }
elseif ((P1 >= 'A') && (P2 <= 'F'))
    {
P2 -= 'A';
    }
P1 <<= 4;
P1 += P2;
return P1;
}
voidprocesscommand(void)
{
charch;
ch = UART_1_GetChar();
if(ch== 'S')
    {
Flag_Run = 1;
```

```
    }
if (ch=='R')
    {
Flag_Run = 0;
    }
if(ch=='T')
     {
ThresholdValue=GetNeumeric8Bit();
     }
if(ch=='I')
     {
      VDAC=GetNeumeric8Bit();
     }
if(ch=='G')
     {
      Gain=GetNeumeric8Bit();
     }
}
int main(void)
{
CyGlobalIntEnable; /* Enable global interrupts. */
systeminit();
while(1)
        {
processcommand();
if(Flag_Run == 1)
        {
        isr_1_Enable();
if(sem_DA==1)
                    {
                  Dataprocessing();
                  Datatransmission();
                    }
        }
if(Flag_Run == 0)
        {
        isr_1_Disable();
        }
        }
}
/* END OF PROGRAM */
```

References

1. D. E. Bray and R. K. Stanley, "Non-destructive Evaluation", Revised edition, CRC Press, Florida, 1997.
2. Robert C. Memaster, "Non-destructive testing handbook", American Society for Nondestructive testing, 1st edition, 1959.
3. Jack Blitz, "Electrical and Magnetic Methods of Non-destructive Testing", Chapman & Hall, London, 2nd edition, 1997.
4. R. Prakash, "Non-destructive Testing of Composites", Composites, Vol.11, No. 4, pp. 217-224, 1980.
5. Harold Berger, "Non-destructive testing of railroad", Transportation Research Record, pp. 22-26, 1980.
6. D. C. Hollaby, "Ultrasonic flaw detection and characterization–an Australian view", Non-destructive Testing, Australia, Vol. 17, No.10, pp.9-13, 1980.
7. D. L. Parry, "Detection and analysis of vessel discontinuities by acoustic emission inspection", Ammonia Plane Safety (and related facilities), Vol. 33, pp. 140-145, 1980.
8. Yoseph Bar-Cohen, "Emerging NDE technologies and challenges at the beginning of the 3 rd millennium-Part1", NDT.net, Vol. 5, No.1, 2000.
9. G. Dobmann, R. Becker and M. Disque, "Life extension the contribution of a low and multi-frequency eddy current technique to assure the integrity of

cladding in nuclear power plant pressure vessels", Welding Research Abroad, Vol. 44, pp. 16-23, 1998.

10. Annual Book of ASTM Standards, Section Three, Metals Test and Analytical Procedures, Non-destructive Testing, ASTM International, Vol. 03, 2005.

11. Mohamed Ben Gharsallah and Ezzeddine Ben Braiek, "Weld inspection based on radiography image segmentation with level set active contour guided off-center saliency map", Journal of Advances in Materials Science and Engineering, Vol. 2015, pp 1-10, 2015.

12. A. A. Pollock, "Acoustic emission inspection", Metals Handbook, Vol. 17, pp. 278-294, 1989.

13. T. H. Loutas, G. Sotiriades, I. Kalaitzoglou, and V. Kostopoulos, "Condition monitoring of a single-stage gearbox with artificially induced gear cracks utilizing on-line vibration and acoustic emission measurements", Journal of Applied Acoustic, Vol. 70, pp. 1148-59, 2009.

14. T. H. Loutas, D. Roulias, E. Pauly, and V. Kostopoulos, "The combined use of vibration, acoustic emission and oil debris on-line monitoring towards a more effective condition monitoring of rotating machinery", Mechanical System Signal Process, Vol. 25, pp. 1339–1352, 2011.

15. D. M. McCann and M. C. Forde, "Review of NDT methods in the assessment of concrete and masonry structures", NDT & E International, Vol. 34, pp. 71-84, 2001.

16. J. M. Brownjohn, “Structural health monitoring of civil infrastructure”, Philosophical Transactions of the Royal Society A: Mathematical, Physical and Engineering Sciences, Vol. 365, pp. 589-622, 2007.

17. Z. Hou, A. Hera, and A. Shinde, “Wavelet-based structural health monitoring of earthquake excited structures”, Computer-Aided Civil and Infrastructure Engineering, Vol. 21, pp. 268-279, 2006.

18. Allen C. Estes, M Asce, Dan Frangopol and F Asce, “Updating bridge reliability based on bridge management systems visual inspection results”, Journal of Bridge Engineering, Vol.8, pp. 374-382, 2003.

19. Charles R. Farrar and Keith Worden, “An introduction to structural health monitoring”, Philosophical Transaction of the Royal Society A, Vol. 365, pp. 303–315, 2006.

20. A. Mahoon, “The role of non-destructive testing in the airworthiness certification of civil aircraft composite structures”, Composites, Vol.19, pp.229-235, 1988.

21. D. M. Frangopol, “New directions and research needs in life-cycle performance and cost of civil infrastructures”, Structural Health Monitoring 2003, From diagnostics & Prognostics to Structural Health Management, Proceedings of the 4th International Workshop on Structural Health Monitoring, Stanford, CA, Lancaster, PA, DEStech Publications, Inc, pp. 53-63, September 15-17, 2003.

22. M. M. Derriso, D. M. Pratt, D. B. Homan, J. B. Schroeder and R. A. Bortne, “Integrated vehicle health management: the key to future aerospace systems”,

Structural health monitoring from diagnostics & prognostics to structural health introduction to SHM management, proceedings of the 4th International workshop on structural health monitoring, Stanford, CA, Lancaster, PA, DEStech Publications, Inc, pp. 3-11, September 15-17, 2003.

23. S. M. Walsh "A requirements-based approach to Structural Health Monitoring research, development, and application", Structural Health Monitoring 2003, From diagnostics & Prognostics to Structural Health Management, Proceedings of the 4th International Workshop on Structural Health Monitoring, Stanford, CA, Lancaster, PA, DEStech Publications, Inc, pp. 79-87. September 15-17, 2003.

24. B. Beral and H. Speckmann, "Structure Health Monitoring (SHM) for aircraft structures: a challenge for system developers and aircraft manufacturers", Structural health monitoring from diagnostics & prognostics to structural health management, proceedings of the 4th international workshop on structural health monitoring, Stanford, CA, Lancaster, PA, DEStech Publications, Inc, pp. 12-29. September 15-17, 2003.

25. R. K. Miller, "Acoustic Emission Testing", Non-destructive Testing Handbook, 3rd ed. Vol. 6, Columbus, OH: Amer. Society for Non-Destructive Testing, 2006.

26. G. A. Washer, "Developments for the non-destructive evaluation of highway bridges in the USA", NDT& E International, Vol. 31, pp. 245-249, 1998.

27. V. M. Malhotra and N. J Carino, “Handbook on non-destructive testing of concrete”, CRC Press, LLC, Boca Raton, FL, 2004.

28. Boris Muravin, “Acoustic Emission Science and Technology”, Journal of Building and Infrastructure Engineering of the Israeli Association of Engineers and Architects, Vol. 1. pp. 4-5, 2009.

29. C. Boller, “Structural health monitoring — An introduction and definitions”, Encyclopedia of Structural Health Monitoring, 2009.

30. Raj Dharma, Dharma Raj Dhakal, Keshab Neupane, Chirayu Thapa and G. V. Ramanjaneyul, “Different techniques of structural health monitoring” International Journal of Civil, Structural, Environmental and Infrastructure Engineering Research and Development, Vol. 3, pp. 55-66, 2013.

31. Thodamra Kandy Haneef, Barid Baran Lahiri, Subramaniam Bagavathiappan, Chandan Kumar Mukhopadhyay, John Philip, Bhagi Purna Chandra Rao and Tamanna Jayakumar, “Study of the tensile behavior of AISI type 316 stainless steel using acoustic emission and infrared thermography techniques”, Journal of Materials Research and Technology, Vol. 4, pp. 241–253, 2015.

32. Gongtian Shen, Zhanwen Wu and Junjiao Zhang, “Advances in acoustic emission technology”, Springer Proceedings in Physics, Vol. 179, pp. 257-258, 2015.

33. M. Mondal and G. B. Kumbhar, “Detection, measurement, and classification of partial discharge in a power transformer: methods, trends and future research”, IETE Technical Review, Vol. 35, pp. 483-493, 2017.

34. Ozevin, Didem and James Harding "Novel leak localization in pressurized pipeline networks using acoustic emission and geometric connectivity", International Journal of Pressure Vessels and Piping, Vol. 92, pp. 63-69, 2012.

35. P. Mazal and J. Dvoracek, "Application of acoustic emission method in contact damage identification", International Journal Materials and Product Technology, Vol. 41, pp. 140-152, 2011.

36. David Crivelli and Stewart Bland, "Structural health monitoring via acoustic emission", Journal of Reinforced Plastics, Vol. 60, pp. 390-392, 2015.

37. Mohamed K. ElBatanouny, Paul H. Ziehl, Aaron Larosche, Jesé Mangual, Fabio Matta and Antonio Nanni, "Acoustic emission monitoring for assessment of pre-stressed concrete beams", Construction and Building Materials, Vol. 58, pp. 46-53, 2014.

38. A. Damgaard Jensen and S. Chatterji, "State of the art report on micro-cracking and lifetime of concrete - Part I", Matdriauxet Constructions Materials and Structures, Vol. 29, pp 3-8. 1996.

39. Mahindra Kaphle, "Analysis of acoustic emission data for accurate damage assessment for structural health monitoring applications", PhD Thesis, School of chemistry, Queensland University of Technology, Australia, 2012.

40. David Roylance, "Stress-strain curves", 2001. Available at http://web.mit.edu/course/3/3.11/www/modules/ss.pdf.

41. Jianan Hu Alan and C. F. Cocks, “A multi-scale self-consistent model describing the lattice deformation in austenitic stainless steels”, International Journal of Solids and Structures, Vol. 78–79, pp. 21-37, 2016.

42. Parag Tandaiya, R. Narasimhan and U. Ramamurty, “Mode I crack tip fields in amorphous materials with application to metallic glasses”, Acta Materialia, Vol. 55, pp. 6541–6552, 2007.

43. J. Pokluda “Brittle and ductile fracture”, Micromechanisms of Fracture and Fatigue, Chapter 2, Vol. 0, pp 69-123, 2010.

44. A. V. Lavrov, and V. L. Shkuratnik, “Deformation and fracture-induced acoustic emission in rocks”, Acoustical Physics, Vol. 51, pp. S2–S11, 2005.

45. The Collaboration for NDT Education. (n.d.). Theory - AE Sources. Retrieved August 10, 2010, Available from NDT Education Resource Center: http://www.ndt-ed.org/EducationResources/CommunityCollege/Other Methods/AE/AE_Theory-Sources.htm

46. M. Ohtsu, “The history and development of acoustic emission in concrete engineering”, Magazine of Concrete Research, Vol. 48, pp. 321-330, 1995.

47. M. Mondal and G. B. Kumbhar, “Detection, measurement, and classification of partial discharge in a power transformer: methods, trends and future research”, IETE Technical Review, pp. 483-493, 2017.

48. Christian U. Grosse and Masayasu Ohtsu, “Acoustic emission testing”, 1st Edn. SpringerVerlag Berlin Heidelberg, le-tex publishing services HG, Leipzig, Germany, 2008.

49. F. G. Baptista and J. V. Filho, “A new impedance measurement system for PZT-based structural health monitoring”, IEEE Transaction Instrument and Measurement, Vol. 58, pp. 3602–3608. 2009.

50. S. Gholizadeh, Z. Leman and B.T.H.T. Baharudin, “A review of the application of acoustic emission technique in engineering”, Structural Engineering and Mechanics, Vol. 54, pp. 1075-1095, 2015.

51. Kaita Ito and Manabu Enoki, “Acquisition and analysis of continuous acoustic emission waveform for classification of damage sources in ceramic fiber mat”, Materials Transactions, Vol. 48, No. 6, pp. 1221-1226, 2007.

52. N.N. Hsu and F.R. Breckenridge, “Characterization and calibration of acoustic emission sensors”, Materials Evaluation, Vol. 39, pp. 60-68, 1981.

53. C. A. Tatro, “Design criteria for acoustic emission experiment”, Acoustic Emission, ASTM STP 505, Hiladelphia, PA: American Society for Testing and Materials; 1972.

54. Lance E. Rewerts, Ron A. Roberts and M Amanda Clark, “Dispersion compensation in acoustic emission pipeline leak location”, Review of Progress in Quantitative Non-destructive Evaluation, no. 4, pp. 427-434, 1997.

55. Jun Zhou, “A study of acoustic emission technique for concrete damage detection”, Master’s report, Michigan Technological University, 2011. http://digitalcommons.mtu.edu/etds/726.

56. Horst Czichos, “Handbook of technical diagnostics: fundamentals and application to structures and systems,” Springer Science & Business Media, Chapter 8, pp. 137-154, 2013.

57. P. Kalyanasundaram, C. K. Mukhopadhyay and S. V. Subba Rao; Series editor: Baldev Raj, and B. Venkatraman, “Practical acoustic emission”, Pub. Narosa Publishing House, New Delhi, India, 2007.

58. D. O. Harris, A. S. Tetelman and F. A. Darwish, “Acoustic emission”, ASTM STP 505 (American Society for Testing and Marerials, Philadelphia, PA), pp. 243-246, 1972.

59. Masayasu Ohtsu, Manabu Enoki, Yoshihiro Mizutani, and Mitsuhiro Shigeishi, “Practical acoustic emission testing”, The Japanese Society for Non-Destructive Inspection (Springer Japan), Chapter 2, pp. 5-34, 2016

60. Paulo R. Aguiar, Cesar H.R. Martins, Marcelo Marchi and Eduardo C. Bianchi “Digital signal processing for acoustic emission”, IntechOpen, pp. 297-316, 2012.

61. Shaowei Hu, Jun Lu and Feipeng Xiao, “Evaluation of concrete fracture procedure based on acoustic emission parameters”, Construction and Building Materials, Vol. 47, pp. 1249–1256, 2013.

62. A. Nair and C. S. Cai “Acoustic emission monitoring of bridges: Review and case studies”, Engineering Structures, Vol. 32, pp. 1704-1714, 2010.

63. Farid A. K. M. Uddin, Mitsuhiro Shigeish and Masayasuohtsu. “Fracture mechanics of corrosion cracking in concrete by acoustic emission”, Meccanica, Vol. 41, pp. 425-442, 2006.

64. Carpinteri and G. Lacidogna, “Earthquakes and acoustic emission”, 2007.

65. A. Carpinteri, G. Lacidogna and N. Pugno, "Structural damage diagnosis and life-time assessment by acoustic emission monitoring", Engineering Fracture Mechanics, Vol. 74, pp. 273-289, 2007.

66. T. M. Morton, R. M. Harrington and J. G. Bjeletich, "Acoustic emissions of fatigue crack growth", Engineering Fracture Mechanics, Vol.5, pp. 691-697, 1973.

67. A. Berkovits and D. Fang, "Study of fatigue crack characteristics by acoustic emission," Engineering Fracture Mechanics, Vol. 51, pp. 401-409, 1995.

68. J. Labuz, S. Dai and K. Shah, "Identifying failure through locations of acoustic emission", Transportation Research Record, Vol. 1526, pp. 104-111, 1996.

69. W. Li, W. Sun and Jinyang Jiang, "Damage of concrete experiencing flexural fatigue load and closed freeze/thaw cycles simultaneously", Construction and Building Materials, Vol. 25, pp. 2604-2610, 2011.

70. Tetsuya Suzuki, Hidehiko Ogata, Ryuichi Takada, Masao Aoki and Masayasu Ohtsu, "Use of acoustic emission and X-ray computed tomography for damage evaluation of freeze-thawed concrete", Construction and Building Materials, Vol. 24, pp. 2347-2352, 2010.

71. A. K. M. Farid Uddin, Kenichiro Numata, Jun Shimasaki, Mitsuhiro Shigeishi and Masayasu Ohtsu, "Mechanisms of crack propagation due to corrosion of reinforcement in concrete by AE-SiGMA and BEM", Construction and Building Materials, Vol. 18, pp. 181-188, 2004.

72. C. Grosse, H. Reinhardt and T. Dahm, "Localization and classification of fracture types in concrete with quantitative acoustic emission measurement techniques", NDT & E International, Vol. 30, pp. 223-230, 1997.

73. K. Ohno and M. Ohtsu, "Crack classification in concrete based on acoustic emission", Construction and Building Materials, Vol. 24, pp. 2339-2346. 2010.

74. Ahmad Zaki, Hwa Kian Chai, Dimitrios G. Aggelis and Ninel Alver, "Non-destructive evaluation for corrosion monitoring in concrete: A review and capability of acoustic emission technique", Sensors, Vol. 15, pp. 19069-19101, 2015.

75. Sudhir Singh Bhadauria and Saleem Akhtar, "Review of nondestructive testing methods for condition monitoring of concrete structures", Journal of Construction Engineering, Vol. 2013, pp. 1-11, 2013.

76. D. Soulioti, N. M. Barkoula, A. Paipetis, T. E. Matikas, T. Shiotani and D. G. Aggelis, "Acoustic emission behavior of steel fiber reinforced concrete under bending", Construction and Building Materials, Vol. 23, pp. 3532-3536, 2009.

77. B. Chen and J. Liu, "Experimental study on AE characteristics of three-point bending concrete beams", Cement and Concrete Research, Vol. 34, pp. 391-397, 2004.

78. S. X. Bernd Weiler and Utz Mayer, "Acoustic emission analysis applied to concrete under different loading conditions", Otto Graf Journal, Vol. 8, pp. 255-269, 1997.

79. P. G. Leszek Golaski and Kanji Ono, "Diagnostics of reinforced bridges by acoustic emission", Journal of Acoustic Emission, Vol. 20, pp. 83-98, 2002.

80. M. Ohtsu and H. Watanabe, "Quantitative damage estimation of concrete by acoustic emission", Construction and Building Materials, Vol. 15, pp. 217-224, 2001.

81. T. Suzuki and M. Ohtsu, "Quantitative damage evaluation of structural concrete by a compression test based on AE rate process analysis", Construction and Building Materials, Vol. 18, pp. 197-202, 2004.

82. P. G. Ranjitha, D. Jasinge, J. Y. Song and S. K. Choi, "A study of the effect of displacement rate and moisture content on the mechanical properties of concrete: Use of acoustic emission", Mechanics of Materials, Vol.40, pp. 453-469, 2008.

83. T. K. Haneef, Kalpana Kumari, C. K. Mukhopadhyay, Venkatachalapathy, B. Purnachandra Rao and T. Jayakumar, "Influence of fly ash and curing on cracking behavior of concrete by acoustic emission technique", Construction and Building Materials, Vol. 44, pp. 342-350, 2013.

84. D. J. Pines and P. A. Lovell, "Conceptual framework of a remote wireless health monitoring system for large civil structure", Smart Material and Structures. Vol. 7, pp. 627–636, 1998.

85. Y. Yu, J. Ou and H. Li, "Design, calibration and application of wireless sensors for structural global and local monitoring of civil infrastructures" Smart Structures and Systems, Vol. 6, pp. 641–659. 2010.

86. Y. Yu, J. Ou, J. Zhang, C. Zhang and L. Li, “Development of wireless MEMS inclination sensor system for swing monitoring of large-scale hook structures”, IEEE Trans. Ind. Electron., Vol. 56, pp. 1072–1078, 2009.

87. Peng Li, Haichang Gu, Gangbing Song, Rong Zheng and Y. L. Mo, “Concrete structural health monitoring using piezoceramic based wireless sensor networks”, Smart Structures and Systems. Vol. 6, pp. 731–748, 2010.

88. A. N. Zagrai and V. Giurgiutiu, “Electro-mechanical impedance method for crack detection in thin plates”, Journal of Intelligent Material Systems and Structures, Vol. 12, pp. 709-718, 2001.

89. A. Raghavan and C. E. S. Cesnik, “Review of guided-wave structural health monitoring”, The Shock and Vibration Digest, Vol. 39, pp. 91-114, 2007.

90. K. M. Holford, “Acoustic emission in structural health monitoring”, Key Engineering Materials, Vol. 413-414, pp. 15-28, 2009.

91. Dong-Jin Yoon, Sang-I Lee, Chi-Yeop Kim and Dae-Cheol Seo, “Acoustic emission diagnosis system and wireless monitoring for damage assessment of concrete structures”, NDT for Safety, pp. 55-62, 2007.

92. Yang Wang, Jerome P. Lynch and Kincho H. Law, “A wireless structural health monitoring system with multithreaded sensing devices: design and validation”, Structure and Infrastructure Engineering, Vol. 3, No. 2, pp. 103-120, 2007.

93. Victoria J. Hodge, Simon O’Keefe, Michael Weeks and Anthony Moulds, “Wireless sensor networks for condition monitoring in the railway industry: A

survey", IEEE Transactions on Intelligent Transportation Systems, Vol. 16, pp. 1088 – 1106, 2015.

94. MA Shamshi, "Technologies convergence in recent instrumentation for natural disaster monitoring and mitigation", IETE Technical Review, Vol. 21, No. 4, pp. 277-290, 2004.

95. M. Bocca, A. Mahmood, L. M. Eriksson, J. Kullaa and R. Jäntti, "A synchronized wireless sensor network for experimental modal analysis in structural health monitoring", Computer-aided Civil & Infrastructure Engineering, Vol. 26, No. 7, pp. 483-499, 2011.

96. Ali M. Sadeghioon, Nicole Metje, David N. Chapman and Carl J. Anthony, "Smart wireless sensor networks for leak detection in water pipelines" Journal of Sensor and Actuator Networks, Vol. 3, pp. 64-78, 2014.

97. M. J. Chaea, H.S. Yoo, J.Y. Kim and M.Y. Cho, "Development of a wireless sensor network system for suspension bridge health monitoring", Automation in Construction, Vol. 21, pp. 237–252, 2012.

98. Dipanjan Bhattacharjee, Sourabh Kumar, Akash Kumar and Sushabhan Choudhury, "Design and development of wireless sensor node", International Journal of Computer Science and Engineering, Vol. 02, No.7, pp. 2431-2438, 2010.

99. B. P. Ladgaonkar and A. M. Pawar, "Design and implementation of sensor node for wireless sensors network to monitor humidity of high-tech poly house

environment", International Journal of Advance in Engineering and Technology, Vol.1, pp. 1-11, 2011.

100. ÁkosLédeczi, Thomas Hay, PéterVölgyesi, D. Robert Hay, AndrásNádas and Subash Jayaraman, "Wireless acoustic emission sensor network for structural monitoring", IEEE Sensor Journal, Vol.9, No. 11, pp. 1370-1377, 2009.

101. Damian Sala, Jerzy Motylewski and Przemysław Kołakowski, "Wireless transmission system for a railway bridge subject to structural health monitoring", Diagnostyka, Vol. 2, pp. 69-72, 2009.

102. Junmei Zhang, Yanyi Wang, Bowen Cheng and Shuai Wang, "Design of acoustic emission data acquisition system of wood damage", International Journal of Control and Automation, Vol. 8, No. 9, pp. 291-302, 2015.

103. Christian U. Grosse, Steven D. Glaser and Markus Krüger, "Initial development of wireless acoustic emission sensor motes for civil infrastructure state monitoring", Smart Structures and Systems, Vol. 6, No. 3, pp. 197-209, 2010.

104. Yin Wu, Wenbo Liu and Kaiyu Li, "A novel wireless acoustic emission sensor system for distributed wooden structural health monitoring", International Journal of Innovative Computing, Information and Control, Vol. 13, No. 4, pp. 1289–1306, August 2017.

105. A. Carpinteri, G. Lacidogna, A. Manuello and G. Niccolini, "Acoustic emission wireless transmission system for structural and infrastructural networks", VIII International Conference on Fracture Mechanics of Concrete and Concrete Structures, FraMCoS-8, pp. 1-12, 2013.

106. Jerome P. Lynch and Kenneth J. Loh, “A summary review of wireless sensors and sensor networks for structural health monitoring”, The Shock and Vibration Digest, Vol. 38, No. 2, pp. 91–128, 2006.

107. Alex Doboli and Edward H. Currie, “An Overview of Mixed-Signal, Embedded System Design”, Introduction to Mixed-Signal, Embedded Design, Springer, New York, NY, pp. 1-49, 2011.

108. Nordin Aranzabal, Adrián Suárez, José Torres, Raimundo García-Olcina, Julio Martos, Jesús Soret, Abraham Menéndez and Pedro A. Martínez, “Design of digital advanced systems based on programmable system on chip,” in Field-Programmable Gate Array Technology, InTech, pp. 124–157, 2017.

109. Chun-Ming Huang, Chien-Ming Wu, Chih-Chyau Yang , Shih-Lun Chen, Chi-Shi Chen, Jiann-Jenn Wang , Kuen-Jong Lee and Chin-Long Wey, “Programmable system-on-chip for silicon prototyping”, in IEEE Transactions on Industrial Electronics, Vol. 58 , pp. 830 – 838, May 2009.

110. Kester Walt, “Sensor signal conditioning”, S. Jon Wilson (Ed.), Sensor Technology Handbook, Elsevier Inc., pp. 31–108, 2005.

111. W. Kester, J. Bryant, W. Jung, Wurcer Scott and Kitchin Chuck, Sensor signal conditioning”, W. Jung (Ed.), Op Amp Applications Handbook J, Elsevier Inc., pp. 227–305, 2005.

112. B. Dobkin and Hamburger (Eds.), Signal Conditioning, Part 3 in Analog Circuit Design, Circuit Note Collection, Elsevier Inc., Vol. 3, pp. 869–1054, 2015.

113. W. Gao, S. Emamineja, H. Y. Y. Nyein, S. Challa, K. Chen, A. Peck, H. M. Fahad, H. Ota, H. Shiraki, D. Kiriya, D. H. Lien, G. A. Brooks, R. W. Davis and A. Javey, “Fully integrated wearable sensor arrays for multiplexed in situ perspiration analysis”, Nature, Vol. 529, pp. 509-514, 2016.

114. M. A. Carvajal, M. S. Martínez-García, D. Guirado, J. Banqueri and A. J. Palma, “Dose verification system based on MOS transistor for real-time measurement”, Sensors and Actuators A, Vol. 238, pp. 240–248, 2016.

115. Jose Pelegri Sebastia, Jorge Alberola Lluch and J. Rafael Lajara Vizcaino, “Signal conditioning for GMR magnetic sensors applied to traffic speed monitoring GMR sensors”, Sensors and Actuators A, Vol. 137, pp. 230–235, 2007.

116. Christian Falconia, Corrado Di Natalea, Arnaldo D’Amicoa and Marco Facciob, “An electronic interface for theaccurate read-out of resistive sensors in low voltage-low power integrated systems”, Sensors and Actuators A, Vol. 117 pp.121–126, 2005.

117. Naveen Kumar Vaegae, Venkata Lakshmi, Narayana Komanapalli and Srikanth Malla, “Development of an intelligentpressure measuring technique for bellows using radial basis function neural network” Sensors and Actuators A, Vol. 238, pp. 240–248, 2016

118. Luis Armando Carvajal Ahumada, Nuria Peña Pérez, Oscar Leonardo Herrera Sandoval, Franciscodel Pozo Guerrero and José Javier Serrano Olmedo, “A new

way to fine dielectric properties of liquidsample using the quartz crystal resonator (QCR)", Sensor and Actuators A, Vol. 239, pp. 153–160, 2016.

119. Ferran Reverter and Oscar Casas, "Direct interface circuit for capacitive humidity sensors", Sensor and Actuators A, Vol. 143, pp. 315-322, 2008.

120. An. Sang Hou and Susan Xiao-Ping Su, "Design of acapacitive-sensor signal processing systemwith high accuracy and short conversion time", Sensor and Actuators A, Vol. 119, pp. 113–119, 2005.

121. K. Vairamani, N. Mathivanan, K. A. Venkatesh and U. D. Kumar, "Environmental parameter monitoring using wireless sensor network", Instruments and Experimental Techniques, Vol. 56, pp. 468-471, 2013.

122. Gioacchino. Fertitta, Antonio Di. Stefano, Giuseppe. Fiscelli and Giuseppe C Giaconia, "A low power and high-resolution data loggerfor submarine seismic monitoring, Smart sensors and MEMS", Microprocess. Microsyst. Vol. 34, pp. 63-72, 2010.

123. B. Baker, "Real analog solutions for digital designers", Elsevier Science & Technology, 2005.

124. B. Murmann, "Digitally assisted analog circuits" IEEE Micro, Vol. 26, pp. 38–47, 2006.

125. R Frank, Understanding Smart Sensors, 2nd ed., Artech House, 2000.

126. Edward A. Lee, "What are the Key Challenges in Embedded Software? (Guest Editorial)", System Design Frontier, Volume 2, No. 1, 2005.

127. Giorgio Buttazzo, "Research trends in real-time computing for embedded systems", ACM Sigbed Review - Special issue on major international initiatives on real-time and embedded systems, Vol. 3, pp. 1-10, 2006.

128. Philip Garcia, Katherine Compton, Michael Schulte, Emily Blem and Wenyin Fu, "An Overview of Reconfigurable Hardware in Embedded Systems", Eurasip Journal on Embedded Systems, Vol. 2006, pp. 1-19, 2006.

129. Li Zhou, Tao Sun, Yuanzhi Zhan and Jia Wang, "Software and hardware implementation of stereo matching", International Journal of Signal Processing, Image Processing and Pattern Recognition, Vol. 7, No. 4, pp. 37-55, 2014.

130. Rainer Leupers, "Code Optimization Techniques for Embedded Processors: Methods, Algorithms and Tools" Springer US, Chapter 1, pp. 1-28, 2000.

131. D. Zivkov, I. Papp, D. Kurtjak, M. Grumic, M. Ivanovic, "Application engine for resource-constrained embedded platforms" IEEE 1st International Workshop on Consumer Electronics (CE WS), 2015, doi:10.1109/cews.2015.7867153.

132. Thomas A. Intisar Ibrahim, Rosmah Ali, Mohamad Zulkefli and Nazar El Fadil, "Embedded systems pedagogical issue: Teaching approaches, students readiness, and design challenges", American Journal of Embedded Systems and Applications, Vol. 3, No. 1, pp. 1-10, 2015.

133. Thomas A. Henzinger and Joseph Sifakis, "The embedded systems design challenge", International Symposium on Formal Methods, Vol. 4085, pp. 1-15, 2006.

134. Sunil R. Das, Jun-Feng Li, Amiya R. Nayak, Mansour H. Assaf, Emil M. Petriu and Satyendra N. Biswas, "Circuit architecture test verification based on hardware software co-design with model sim", IETE Journal of Research, Vol. 59, pp. 132-140, 2013.

135. Vilas V. Deotare, Dinesh V. Padole and S. Ashok. "Performance evaluation of AES using hardware and software co-design", International Journal on Recent and Innovation Trends in Computing and Communication, Vol. 2, pp. 1638-1643, 2014.

136. Hans Petter Halvorsen, "Data Acquisition in LabVIEW", Telemark University College Department of Electrical Engineering. Information Technology and Cybernetics, 2016.

137. Prattana Lopin and Kyle V. Lopin, "PSoC-Stat: A single chip open source potentiostat based on a Programmable System on a Chip" in PLOS ONE, Vol. 3, pp. 1-21, 2018. Available from: https://doi.org/10.1371/journal.pone.020135

138. Abhay Raj Kansal, "A study on programmable system on chip", IOSR Journal of VLSI and Signal Processing (IOSR-JVSP), Vol. 4, Issue 5, Ver. I, pp. 31-37, 2014.

139. PSoC Mixed Signal Array, Technical Reference Manual, Document No. PSoC TRM 1.21, Cypress Semiconductor Corporation, 2005.

140. Carlos J. G. Aguilera, Cristiano P. Chenet and Tiago R. Balen, "Fault injection on a mixed-signal programmable SOC with design diversity mitigation", in Journal of Integrated Circuits and System, Vol.11, pp. 185-191, 2016.

141. Fernando Manzano Rubio, M.Tech Thesis on Programmable-System-on-Chip based data acquisition for educational purposes, Universitatpolitecnica De Catalunya, Spain, 2012.

142. J. Guevara, A. Fatecha, E. Vargas and F. Barrero, “A reconfigurable WSN node based on ISO/IEC/IEEE 21451 standard”, IEEE International Conference on Instrumentation and Measurement Technology (I2MTC) Proceedings, pp. 873-877, 2014.

143. Hyejung Kim, Sunyoung Kim, N. Van Helleputte, A. Artes, M. Konijnenburg, J. Huisken, C. Van Hoof and R. F. Yazicioglu, “A configurable and low-power mixed signal SoC for portable ECG monitoring applications, Biomedical Circuits and Systems”, IEEE Transaction on Bio Medical Circuits and system, Vol 8, pp. 257-267, 2014

144. J. J. Cabrera-Lopez and C. A. Romero-Beltran, “Auto-adjustable low-signal processing technique based on programmable mixed-signal SoCs”, IEEE 9th Ibero-American Congress on Sensors (Fiber Sensor), pp. 1- 4, 2014.

145. Arturo Fatecha, Jean Guevara and Enrique A. Vargas Cabral, “Reconfigurable architecture for smart sensor node based on IEEE 1451 standard”, IEEE Sensors, Vol. 1, pp. 1- 4, 2013.

146. Vallen Systeme GmbH, “Acoustic Emission Sensors Specification”, 2015. Available from: http://www.vallen.de/zdownload/pdf/sov1507.pdf.

147. Perry Miller and Richard Cesari, "Op Amp for everyone", Wireless Communication: Signal Conditioning for IF Sampling, 3rd Ed., Chapter 16, Pages 271-293, 2009.

148. Analog Devices, Data sheet, available from: http://www.analog.com/media/en/technicaldocumentation/datasheets/AD8628_8629_8630.pdf.

149. Analog Devices, Data sheet, available from: http://www.analog.com/media/en/technical-documentation/datasheets/AD8369.pdf.

150. Randy White, "Blocking out the noise means selecting the right filter", Electronic Design, 2009. Available from:https://www.electronicdesign.com/displays/blocking-out-noise-meansselecting-right-filter.

151. Janet Heath, "Basics of bandpass filters" Analogictips, May 2017. available from: https://www.analogictips.com/basics-of-bandpass-filters/

152. Markus G. R. Sause, "Investigation of pencil-lead breaks as acoustic emission sources", Journal of Acoustic Emission, vol. 29, pp. 29-184, 2011.

153. H. M. Ledbetter, "Sound velocities and elastic constants of steels 304, 310, and 316", Journal of Metal Science, Vol. 14, pp. 595-596, 1980.

154. Francisco Sagasta, Yoshihiro Mizutani, Ignacio Valverde, Elisabet Suarez, Francisco J. Rescalvo and Antolino Gallego, "Influence of attenuation on the acoustic emission b-value for damage evaluation of reinforced concrete

specimens", 32nd European Conference on Acoustic Emission Testing Prague, Czech Republic, pp. 433-440, September 07-09, 2016.

155. B. K. Sharma, Amod Kumar and V. M. Murthy, "Evaluation of seismic events detection algorithms", Journal of the Geological Society of India, Vol. 75, pp. 533-538, March 2010.

156. Tony R. Kuphaldt, "Lessons in electric circuits", Sixth Edition, pp. 16-17, 2007. Available from: https://www.ibiblio.org/kuphaldt/electricCircuits/AC/AC.pdf.

157. Steve Arar, "Understanding the dynamic range specification of an ADC", All about circuit, Technical Article, June 2018.

158. Anders Brandt and Kjell Ahlin, "Sampling and time-domain analysis", Sound & Vibration, pp. 13-16, May 2010. Available at: http://www.sandv.com/downloads/1005bran.pdf.

159. Shilpa Patil, Bilavari Karkare and Shweta Goyal, "Acoustic emission vis-Ã-vis electrochemical techniques for corrosion monitoring of reinforced concrete element", Construction and Building Materials, Vol. 68, pp.326–332, 2014.